11-8-2013 12:00 AM

Spatial Heterogeneities in a Simple Earthquake Fault Model

Javad Kazemian, *The University of Western Ontario*

Supervisor: Dr. Kristy Tiampo, *The University of Western Ontario*

A thesis submitted in partial fulfillment of the requirements for the Doctor of Philosophy degree in Geophysics

SPATIAL HETEROGENEITIES IN A SIMPLE EARTHQUAKE FAULT MODEL

(Thesis format: Integrated Article)

by

Javad Kazemian

Graduate Program in Geophysics

A thesis submitted in partial fulfillment
of the requirements for the degree of
Doctor of Philosophy

The School of Graduate and Postdoctoral Studies
The University of Western Ontario
London, Ontario, Canada

Abstract

Natural earthquake fault systems are composed of a variety of materials with different spatial configurations a complicated, inhomogeneous fault surface. The associated inhomogeneities with their physical properties can result in a variety of spatial and temporal behaviors. As a result, understanding the dynamics of seismic activity in an inhomogeneous environment is fundamental to the investigation of the earthquakes processes.

This study presents the results from an inhomogeneous earthquake fault model based on the Olami-Feder-Christensen (OFC) and Rundle-Jackson-Brown (RJB) cellular automata models with long-range interactions that incorporates a fixed percentage of stronger sites, or 'asperity cells', into the lattice. These asperity cells are significantly stronger than the surrounding lattice sites but eventually rupture when the applied stress reaches their higher threshold stress.

The introduction of these spatial heterogeneities results in temporal clustering in the model that mimics that seen in natural fault systems. Sequences of activity that start with a gradually accelerating number of larger events (foreshocks) prior to a mainshock that is followed by a tail of decreasing activity (aftershocks) are observed for the first time in simple models of this type. These recurrent large events occur at regular intervals, similar to characteristic earthquakes frequently observed in historic seismicity, and the time between events and their magnitude are a function of the stress dissipation parameter. The relative length of the foreshock to aftershock sequences can vary and also depends on the amount of stress dissipation in the system.

The magnitude-frequency distribution of events for various amounts of inhomogeneities (asperity sites) in the lattice is investigated in order to provide a better understanding of Gutenberg-Richter (GR) scaling. The spatiotemporal clustering of events in systems with different spatial distribution of asperities and the Thirumalai and Mountain (TM) metric behaviour, an indicator of changes in activity before the main event in the sequence, also are investigated. Accelerating Moment Release (AMR) is observed before the mainshock. The Omori law behaviour for foreshocks and aftershocks is quantified for the model in this study.

Finally, a fixed percentage of randomly distributed asperity sites were aggregated into bigger asperity blocks in order to investigate the effect of changing the spatial configuration of stronger sites. The results show that the larger block of asperities generally increases the capability of the fault system to generate larger events, but the total percentage of asperities is important as well. The increasing number of larger events is also associated with an increase in the total number of asperities in the lattice.

This work provides further evidence that the spatial and temporal patterns observed in natural seismicity may be controlled by the underlying physical properties and are not solely the result of a simple cascade mechanism and, as a result, may not be inherently unpredictable.

Keywords

Earthquake simulation; heterogeneities; spatiotemporal clustering; extreme events; magnitude frequency scaling;

Co-Authorship Statement

This thesis is prepared in integrated-article format and the following manuscripts were written by Javad Kazemian. This thesis contains only the original results of research conducted by the candidate under supervision of his supervisor.

1. Kazemian, J., Tiampo, K.F., Klein W. and Dominguez, R. (2013), Foreshock and aftershocks in simple earthquake models. Physical Review Letters. (in review)

2. Kazemian, J., Dominguez, R., Tiampo, K.F. and Klein W. (2013), spatial heterogeneity in earthquake fault-like systems. Pure and Applied Geophysics. (in review)

3. Kazemian, J., Tiampo, K.F., Klein, W., Dominguez, R. and Serino, C.A. (2013), Spatiotemporal clustering in simple earthquake fault models. Journal of Geophysical Research. (in review)

The candidate developed the new model, investigated and analyzed the results of the model and developed all the codes that are needed to produce and analyze the results.

The work for these projects was completed under supervision and financial support of Dr. Kristy Tiampo.

Dr. Kristy Tiampo provided the analysis of the swarm event at the north Iceland, southern Eyjafjarðaráll graben.

Dr. Rachele Dominguez provided some of her results for comparison to the results of our model in the third paper.

Dr. William Klein, Dr. Rachele Domingez and Dr. Chris Serino assisted with interpretation and suggestions, reviewing all the above papers.

Acknowledgments

"*In the name of God, the most Beneficent, the most Merciful*"

I would like to express my sincere appreciation to those who have contributed to this thesis and supported me during this amazing journey.

First of all, I am extremely grateful to my supervisor, Professor Kristy Tiampo, for her continuous encouragement, support, and advice throughout the various stages of my research.

I would also like to extend my gratitude to Prof. William Klein, Dr. Rachele Dominguez and Dr. Christopher Serino for following my progress with their helpful suggestions reviewing my articles.

I am also very thankful for the most important person in my life, my wife Maryam. She has been a constant source of strength and inspiration. There were times during the past four years when everything seemed hopeless, but I can honestly say that it was only her determination and constant encouragement that ultimately made it possible for me to see this project through to the end.

Finally, I would last, but not least, thank my parents, my brother, my sisters and my friends for their encouragement, and constant support in one way or the other throughout every adventure, including graduate school.

Table of Content

List of Tables

List of Figures

List of Appendices

Glossary

OFC	Olami, Feder and Christensen model
RJB	Rundle, Jackson and Brown model
L	Linear size of the lattice
z	Number of predefined neighbors in the range of interaction
R	Range of interaction
σ^r	Residual stress
σ^f	Failure threshold
α	Stress dissipation parameter
η	Random noise
$\Delta\sigma^f$	Difference between the regular sites failure threshold and asperity sites failure thresholds
$\sigma^F_{(asperity)}$	Failure threshold for stronger asperity sites
σ_i	Internal stress variable
pu	Plate update time step
Δt	Course-grained time bin
q	fraction of dead sites in the damaged OFC model
AMR	Accelerated Moment Release
ETAS	Epidemic Type Aftershock Sequences
AT	Aftershock Time

FT	Foreshock Time
TM	Thirumalai and Mountain metric
b	linear size of the asperity block
γ_i	stress dissipation at the site
$\bar{\gamma}$	average dissipation for each lattice
φ_i	percentage of dead sites in a given neighborhood
M_0	scalar moment release
μ	shear modulus of the medium
Δu	average scalar displacement of the fault
A	rupture surface
M_w	moment magnitude
n_M	number of events per unit time
R_a	rate of aftershocks
t_M	time of the mainshock
p_a	decay rate for aftershocks
R_f	rate of foreshocks
t_M	time of the mainshock
p_f	reverse decay (growth) rate for foreshocks
$\varepsilon(t)$	accumulated seismic moment
t	time

u_i	displacement of the i^{th} block
v_{db}	speed of the driving block
θ_i	friction force
p_i	externally applied force
T_{ij}	interaction between squares
Φ_i (t)	order parameter
s_i	total distance square i has slipped
$dx_{i,j}$	displacement of each block in OFC model
K_1, K_2 and K_L	elastic constant of the springs
GR	Guttenberg-Richter scaling
MGR	Modified Guttenberg-Richter scaling

Chapter 1

1 Introduction and Background

The spatial inhomogeneities of a fault play an important role in the seismicity of an earthquake fault system. The complicated spatial arrangements of inhomogeneities on the surface of a fault are dependent on the geologic history of the fault, which is typically quite complex. Understanding the dynamics of seismic activity in an inhomogeneous medium is fundamental to the investigation of earthquakes processes. In addition, the fact that nonlinearity is a significant aspect of earthquake physics (Kanamori, 1981; Main, 1996; Turcotte, 1997; Rundle et al., 1999; Scholz, 2002) and the rare occurrence of extreme events means that computational simulations are a critical tool in understanding the dynamics of the earthquake systems (Schorlemmer and Gerstenberger, 2007; Vere-Jones, 1995, 2006; Zechar et al., 2010). There are several numerical models that have been proposed to test hypotheses regarding the complicated dynamics of earthquake fault systems and the controlling parameters and their relative variability (Burridge and Knopoff, 1967; Otsuka, 1972; Rundle and Jackson, 1977; Rundle, 1988; Carlson and Langer, 1989; Nakanishi, 1990; Rundle and Brown, 1991; Olami et al., 1992; Alava et al. 2006). Although inhomogeneity plays an important role in the spatial and temporal behavior of an earthquake fault (Dominguez et al., 2013), most of the numerical models of earthquake faults simulate a spatially homogeneous fault in a short stress transfer range (Nakanishi, 1990; Olami et al., 1992; Alava et al. 2006). Those OFC models that have been expanded to include inhomogeneity by varying individual parameters along the fault plane are limited to short range stress transfer (Janosi and Kertesz, 1994; Torvund and Froyland; 1995; Ceva, 1995; Mousseau, 1996; Ramos et al., 2006; Bach et al. 2008; Jagla, 2010).

In this dissertation, the macroscopic behaviour of an earthquake fault-like system with microscopic spatial heterogeneities is studied. The model is a variation of the RJB (Rundle, Jackson and Brown) and OFC (Olami, Feder and Christensen) models with long-range stress transfer, where particular parameters of the model vary from site to site.

In particular, a stress driven system with a variety of imposed localized stress accumulators is investigated in order to improve our understanding of the dynamics of faulting and seismic activity. This proposed earthquake fault model is a driven, dissipative, cellular automaton model originally introduced by Rundle, Jackson, and Brown (Rundle and Jackson, 1977; Rundle and Brown, 1991) and reintroduced by Olami, Feder, and Christensen (Olami et al., 1992). The inhomogeneities are imposed by converting a percentage of either organized or randomly selected locations of the lattice into sites that have the ability to accumulate higher levels of stress, similar to asperities on natural faults.

In the first chapter, some general properties of this earthquake fault model are discussed. Section 1.1 introduces physical concepts relevant to this study. This is followed by a discussion of some of the pioneering numerical models for earthquake fault systems which are used as the foundation to this cellular automata model in section 1.2. The important properties of the spring-block Burridge-Knopoff (BK) model (1972) are presented in Section 1.2.1. The Rundle-Jackson-Brown (RJB) model is discussed Section 1.2.2. The RJB model is a cellular automata version of a two-dimensional BK spring block model, introduced by Rundle and Jackson in 1991 and based an earlier model of Rundle and Jackson (1977). The Olami-Feder-Christensen (OFC) cellular automata model (1992) is reviewed in Section 1.2.3. The OFC model is generalized from the Bak, Tang and Wiesenfeld sand-pile model (1987), designed to investigate self-organized criticality (SOC) behaviour in earthquakes.

1.1 Earthquake phenomenology

This section presents those fundamental concepts of seismology related to earthquake fault systems that are necessary to describe physical properties such as the magnitude of an event in terms of the output of the model. Basic ideas are introduced in order to better understand the behavior of an earthquake fault. In particular, internal parameters such as the stress dissipation or the amount and configuration of inhomogeneities are shown to affect the well-studied characteristics of real earthquake fault systems, such as the magnitude-frequency distribution of events known as Gutenberg-Richter (GR) scaling.

1.1.1 Magnitude and scaling of earthquakes

Earthquakes are the result of the brittle failure of materials. Initially, a fracture starts with the arbitrary appearance of damage in the form of microcracks, followed by nucleation and propagation of the microcracks (Alava, 2006; Herrmann, 1990). The increase of microcracks and their spatial localization creates a macroscale discontinuity in the material which is designated a "fault" in geological terms. An earthquake is an abrupt release of energy inside a volume in the earth as a result of sudden motion on that surface. The associated displacement of the fault is the result of a stick-slip dynamical instability across a fault plane, ultimately caused by plate tectonic motion (Scholz 1968; 2002). The stick-slip instability is an expression of a so-called "locking-up" phenomenon, in which the loaded stress is stored and abruptly released at the critical stress threshold. The energy during an earthquake can be represented by the seismic moment tensor, **M** (a symmetric tensor of rank two). The description of the moment tensor can be simplified by introducing the *scalar* moment, which is one measure of the size of an earthquake based on the area of fault rupture, the average amount of slip, and the force that was required to overcome the friction sticking the rocks together that were offset by faulting (Aki, 1966; Hanks and Kanamori, 1979).

$$M_0 = \mu \Delta u A, \tag{1.1}$$

where μ is the shear modulus of the medium, Δu is the average scalar displacement and A is the entire surface that slips during the earthquake event is called the rupture surface.

Seismic moment can also be calculated from the amplitude spectra of seismic waves (Brune, 1970, 1971; Allen and Kanamori, 2003; Wu and Kanamori, 2008).

The first quantitative method for the comparison of earthquakes was introduced by Richter in the mid-1930's (Richter, 1935). Using a seismograph, the released energy of an earthquake was quantified based on the amplitude of the seismic waves. He defined the local, or Richter, magnitude, M_L,

$$M_L \equiv \log_{10} A - \log_{10} A_0, \tag{1.2}$$

where A is the maximum amplitude recorded by a Wood-Anderson torsion seismograph and A_0 is a reference magnitude that is adjusted based on the distance between the epicentre of the event and the location of the instrumentation (Richter, 1935).

Subsequently, different magnitude scales were introduced to overcome the limitations of the previous techniques, including the surface-wave magnitude, M_s, the body-wave magnitude, M_b, and the moment magnitude, M_W (Aki, 1972; Kanamori, 1977, 1978; Kanks and Kanamori, 1979). The moment magnitude can be calculated by an empirical equation, based the scalar moment, as

$$M_W \equiv \frac{2}{3}\log_{10} M_0 - 10.7, \tag{1.3}$$

where the scalar moment, M_0, is expressed in *cgs* units, that is, *dyne-cm* (Hanks and Kanamori, 1979). Note that log M_0 is effectively $\log(M_0/\tilde{M}_0)$ where $\tilde{M}_0 \equiv 1$ *dyne-cm* is a reference magnitude.

With the magnitude of an earthquake properly quantified, it is possible to study the features of earthquakes with different magnitudes. One of the most studied properties of earthquake fault systems is the magnitude-frequency distribution of events, or Gutenberg-Richter (GR) scaling (Gutenberg and Richter, 1954). This empirical equation relates the frequency of earthquakes to their magnitudes in a cumulative distribution

$$\log_{10} N_M = a - bM, \tag{1.4}$$

where M is the Richter magnitude (Gutenberg and Richter, 1954). If n_M is defined as the number of events per unit time with a magnitude $M \in [M, M+\mathrm{d}M]$, then

$$N_M = \int_M^\infty n_\xi d\xi. \tag{1.5}$$

It is interesting to note that $b \sim 1$ for the worldwide distribution of earthquakes (Gulia and Weiner, 2010). If we substitute the scalar moment with the magnitude from Equation 1.3,

the exponential distribution of magnitudes can be written as a power-law distribution of scalar moments where

$$N_{M_0} \propto \frac{1}{M_0^{2b/3}}, \tag{1.6}$$

This scaling relationship and its b-value exponent has been of great interest (e.g. Gutenberg and Richter, 1954; Mogi, 1962; Scholz, 1968; Mori and Abercombie, 1997; Sornette, D. and Sornette, A. 1999; Main, 1996, 2000; Kagan, 1997, 1999; Schorlemmer et al., 2005) and will be investigated further here.

Klein et al. (2007) and Serino (2011) argued that the magnitude-frequency of events on individual faults does not, in general, scale as a power law. However, they also showed that the aggregate distribution of different faults with various parameters is well-described by the GR scaling relation. Klein et al. (2007) studied GR scaling of the mean-field limit of an OFC model and found that the number of events of size s for a noncumulative distribution is associated with a spinodal critical point and obeys the scaling

$$n(s) \sim \frac{e^{-\Delta h\, s^{\sigma}}}{s^{\tau}}, \tag{1.7}$$

where $n(s)$ is the number of events of size s, $\tau = 3/2$, $\sigma = 1$, and Δh is a measure of the distance from the spinodal which is the limit of stability of the metastable state. The above distribution approaches a power law distribution as the dissipation parameter goes to zero ($\Delta h \rightarrow 0$ *if* $\alpha \rightarrow 0$). It should be noted that $n(s)$ is the number of events of size s, which is the noncumulative distribution, rather than the number of events of size s or smaller, which is the cumulative distribution often discussed in relation to the Gutenberg-Richter law.

1.1.2 Clustering of earthquakes

The clustering of seismic events in space-time is an essential aspect of earthquake sequences on both global and regional scales. In general, there are two classes of

earthquake clusters: Foreshocks, mainshock and aftershocks, or earthquakes belonging to what are generally known as swarms. Swarms are a localized surge of earthquakes where no one shock is conspicuously larger than all other shocks of the swarm. These occur in a variety of geologic environments and have not been proven to be indicative of any change in the long-term seismic risk of the region (Hill, 1975b; Klein et al., 1977; Waite, 2002; Govoni et al., 2013). Various types of spatiotemporal clustering have been identified in historic earthquake catalogues, briefly described below (Kanamori, 1981).

Schwartz et al. (1981) and Schwartz and Coppersmith (1984) originally introduced the concept of recurrent large events, or characteristic earthquakes based on Reid's Elastic Rebound Theory (1910), which states that the crust of the earth gradually stores elastic stress over time that is released suddenly during an earthquake. The characteristic earthquake theory hypothesizes that earthquakes repeatedly rupture the same fault segments with the similar magnitude and slip distribution (Ellsworth and Cole, 1997; Parsons and Geist, 2009; Schwartz and Coppersmith, 1984; Schwartz et al., 1981; Wesnousky, 1994).

Many researchers have concentrated on identifying earthquakes that occur in the vicinity of the mainshock as either foreshocks which occur immediately before the mainshock or aftershocks which occurs subsequent to the mainshock (Bath, 1965; Kanamori, 1981; Ogata, 1983; Utsu et al., 1995; Dodge et al., 1996 and Shcherbakov et al., 2004).

Occurrence of an earthquake produces a spatially localized series of generally smaller events in which their frequency and magnitude decreases with time (aftershocks). Omori (1894) and Utsu (1961) were the first to quantify this decrease in the frequency of aftershocks. The modified Omori law for aftershocks (Utsu, 1961) states that the rate of aftershocks is proportional to the inverse of time since the mainshock,

$$R_a \sim (\mathrm{t}_M - \mathrm{t})^{-p_a} \tag{1.8}$$

where R_a is the rate of aftershocks, t_M is the time of the mainshock, and p_a is the decay rate for aftershocks.

Similarly, it has been suggested (Papazachos, 1975; Jones and Molnar 1979; Kagan and Knopoff, 1976) that there is an inverse Omori distribution for foreshocks with different exponents:

$$R_f \sim (t - t_M)^{-p_f} \tag{1.9}$$

where R_f is the rate of foreshocks, t_M is the time of the mainshock, and p_f is the reverse decay (growth) rate for foreshocks.

There is also another empirical constraint on the behaviour of the aftershocks (Båth, 1965). Bath's law states that difference in magnitude between a main shock and its largest aftershock is approximately constant and the largest aftershock is, on average, 1.2 magnitude units smaller than the main shock. McGuire et al. (2005) studied foreshocks on East Pacific Rise transform faults and showed that the transform faults in that region have a relatively low number of aftershocks and higher foreshock rates when compared to continental strike-slip faults. Their findings support the idea that the underlying physics links the foreshocks and mainshocks through stress changes. Recently, Shearer (2012) studied foreshock and aftershock behaviour in southern California and in numerical simulations and demonstrated that aftershock b-values are significantly lower than that of the complete catalogue. He also studied the foreshock-to-aftershock ratio and concluded that the ratio is too large to be consistent with Båth's law. Their observations also demonstrated that triggering self-similarity in southern California does not hold for small main shocks, and the associated spatiotemporal clustering is not caused primarily by earthquake-to-earthquake triggering.

1.1.3 Accelerating moment release (AMR)

Mogi (1981) observed a regional increase in seismicity rates before great earthquakes. This included an increase in the overall level of seismicity in the crust surrounding the future rupture zone, in conjunction with a relative shortage of events, or quiescence, along or near the fault. Ellsworth et al (1981) also observed an increase in the rate of M5 events over a broad region in the years preceding the 1906 San Francisco earthquake. This precursory regional increase in the seismicity (AMR) has been documented in a

variety of papers (Bowman and King, 2001, Bowman et al, 1998, Sornette and Sammis, 1995, Bufe and Varnes, 1993, and Skyes and Jaumé, 1990). It is defined by the equation

$$\varepsilon(t) = A - B(t_f - t)^m \tag{1.10}$$

where $\varepsilon(t)$ has been interpreted as the accumulated seismic moment, the energy release or the Benioff strain release within a specified region, from some origin time t_0, up to time t.

$$\varepsilon(t) = \sum_{1}^{N(t)} E_i^k, \tag{1.11}$$

where N(t) is the number of events in the region between t_0 and t, E_i is the energy release from the ith event, and k=0, 1/2, or 1. The remaining quantities, A, B, t_f and m, are parameters characterizing the seismic episode under study. In 2002, Ben-Zion and Lyakhovsky analyzed the deformation preceding large earthquakes and obtained a 1-D analytical power-law time-to-failure relation for accelerating moment release before big events. They found that phases of accelerating moment release exist when the seismicity occurring immediately before a large event has broad magnitude-frequency statistics. These and similar results are consistent with observed seismic activation before some large earthquakes (Turcotte et al., 2003; Zoller et al., 2006).

1.1.4 Thirumalai–Mountain (TM) metric

The TM metric was introduced in the field of statistical physics in order to study the time scales necessary to achieve effective ergodicity in models of liquids and supercooled liquids (Thirumalai and Mountain, 1989). In statistical mechanics, the ergodic theory is justified by replacing the time averages with ensemble averages. It is an important measure that quantifies equilibrium in a system. In seismology, the TM metric has been used to quantify whether an earthquake system can be considered effectively ergodic for some period of time which is interrupted by large events (Timapo et al. 2003, 2006). This is important because equilibrium-like systems may be treated as statistically stationary over long periods of time, which justifies using statistical methods inherent in some forecasting techniques (Tiampo et al., 2007). In addition, application of the TM metric

also has been used to demonstrate that numerical models of earthquakes exhibit the property of effective ergodicity (Tiampo et al., 2003).

In a lattice system (or a system of many particles), the time average for some interval t of a phase variable $x_j(t)$ for lattice site (or particle) j is

$$f_j(t) = \frac{1}{t}\int_0^t x_j(\mathrm{t}')\,\mathrm{dt}', \tag{1.12}$$

and the space average of this time average is

$$\overline{f}(\mathrm{t}) = \frac{1}{N}\sum_{j=1}^{N} f_j(\mathrm{t}), \tag{1.13}$$

where N is the total number of sites (or identical particles).

The TM metric is a fluctuation metric used to test if a self-averaging system with statistical symmetry is effectively ergodic on some timescale of interest. It is defined as

$$\Omega_x(t) \equiv \frac{1}{N}\sum_{j=1}^{N}\left(f_j(t) - \overline{f}(t)\right)^2, \tag{1.14}$$

and can be understood as the spatial variance of the temporal mean. Recently, the TM metric was used to measure whether or not the earthquake fault models are in equilibrium (Ferguson et al., 1999; Klein et al., 2000 and Serino et al., 2011). These systems are defined as effectively ergodic if

$$\Omega(t) \sim \frac{1}{t}, t \to \infty, \tag{1.15}$$

and effective ergodicity is used to determine whether or not a spatially uniform system is in statistical equilibrium (Thirumalai et al. 1989, 1993).

1.2 Pioneering Earthquake Fault Models

In this section, three models of earthquake faults are described that are the foundation of the model studied in this dissertation. These include the well-known Burridge and Knopoff (BK), the Rundle, Brown and Jackson (RJB) (1991) and the Olami, Feder and Christensen (OFC) models.

1.2.1 Burridge and Knopoff (BK) Model

Burridge and Knopoff (1967) introduced one of the first simple models of an earthquake fault. This model has been applied to the fields of geology, seismology, mechanical and materials engineering, mathematics, and physics (Vasconcelos, 1996, 1992; Clancy and Corcoran, 2005, 2006; Carlson and Langer, 1989; Carlson et al., 1991; Carlson et al. 1994; Langer, 1992; Xia et al. 2005, 2008; Mori and Kawamora, 2005, 2006).

Burridge and Knopoff (BK) (1967) formulated their initial model of a one-dimensional continuum by studying the motion of an elastic string in contact with a frictional surface which retards the motion and then expanded it to a one-dimensional (1D) system of springs and blocks which was originally established to study the role of friction along a fault in the propagation of an earthquake.

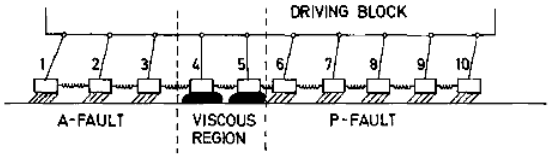

Figure 1-1 *Schematic diagram of the BK numerical model (Burridge and Knopoff, 1967). A chain of ten connected blocks where the dashed lines separate the chain into three parts with markedly different properties; all particles are coupled through the springs with constants μ. Particles 6-10 form the analog of a strongly seismic fault. Particles 4 and 5 form a viscous region adjacent to the large fault and Particles 1-3 form the analog of a second seismic fault weaker than the one represented by particles 6-10.*

In order to model this concept, BK considered a chain of ten particles connected as shown in Figure 1-1, with specified parameters. They divided the ten particles into three parts with clearly different properties, as shown in Figure 1-1. Particles 6 through 10 form the analog of a strongly seismic fault, while particles 4 and 5 represent a viscous region adjacent to the large fault. Particles 1 through 3 form the analog of a second seismic fault, weaker than that represented by particles 6 through 10. Hence the seismic energies released by shocks in the region of particles 1 through 3 will be generally less than those released by shocks in the region of particles 6 through 10.

BK solved the nonlinear differential equations of this system by numerical integration using a Runge-Kutta procedure and computed the potential energy as a function of time in the quiet intervals between shocks, as well as during the shocks themselves. They also computed the loss of potential energy and the total energy radiated for each shock, along with a detailed description of the coordinates, velocities and accelerations of the particles during each shock. Figure 1-2 shows the detailed motion of the system when a major shock occurred in the region of particles 6 through 10. The motion is initiated with particle 6, the particle adjacent to region 4 and 5; the latter is the viscous region. Since particle 6 is defined to have the largest value of static friction, when large motions of this particle take place, large energies are released.

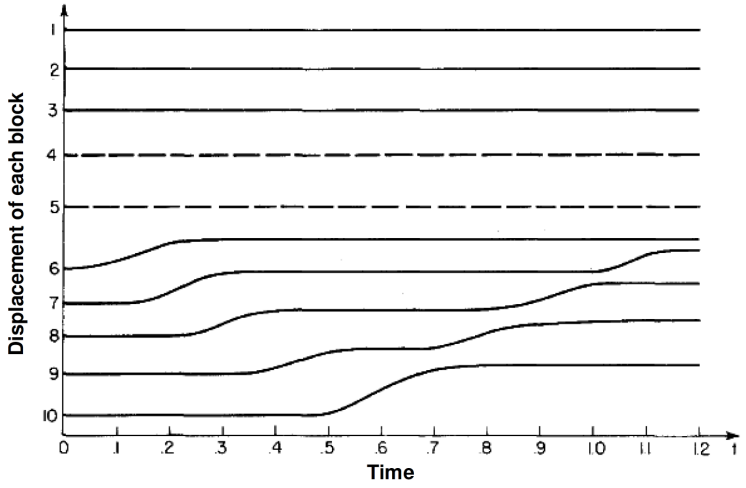

Figure 1-2 *Detailed motion of the lattice during a major shock occurred in the region of particles 6-10. (Burridge and Knopoff, 1967).*

Following the major shock of Figure 1-2, a large number of aftershocks were observed. Figure 1-3 is the plot of potential energy against time for this aftershock sequence. (Burridge and Knopoff, 1967).

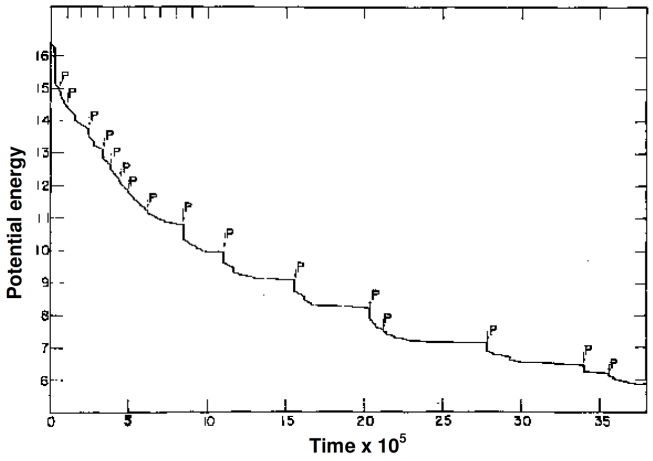

Figure 1-3 *Potential energy as a function of time for the aftershock sequence following the main shock. Shocks occurring on the principal segment of the fault are identified by the symbol P (Burridge and Knopoff, 1967).*

In a generalized one-dimensional BK model, there is an array of N identical blocks in a row. The blocks are connected to their two adjacent neighbors via springs with the elastic constant of k_c. Each block also is attached to the driving plate via some other springs with the elastic constant of k_p. All blocks are subjected to the friction force θ_i, which is the only source of nonlinearity in the model. Based on the described configuration, the equation of motion for the i^{th} block can be written as:

$$m\ddot{u}_i = k_p(v_{db}t - u_i) + k_c(u_{i+1} - 2u_i + u_{i-1}) - \theta_i, \tag{1.16}$$

where t is the time, u_i is the displacement of the i^{th} block, $\underline{v_{db}}$ is the speed of the driving block, and θ_i is the friction force at the i^{th} block (Burridge and Knopoff, 1967).

After the initial BK studies, many other researchers investigated similar dynamical models of many-body systems with friction, ranging from propagation and rupture in earthquakes to the fracture of over layers on a rough substrate. A deterministic version of

the 1D Burridge-Knopoff model was analyzed by Carlson and Langer (1989) and the same model but in a quasi-static limit was studied by Nakanishi (1990). Otsuka (1972) simulated a two-dimensional (2D) version of Burridge-Knopoff model. In this model, today known as a Burridge-Knopoff spring-block model, the particles on opposite sides of the fault are reduced to a 2D network of masses interconnected by springs. Here the usual elastic elements are further coupled by frictional elements interconnecting the elements on opposite sides of the fault. A network of masses (blocks) is constructed and each of them is connected to the four nearest neighbors by identical springs. These blocks also are frictionally connected to a fixed rigid block with the different maximal static friction. Each block is connected to another rigid plate by a set of springs and used this plate as the driving plate for the system. The blocks are driven by the relative movement of the two rigid plates (Figure 1-4). When the force on one of the blocks exceeds its threshold value, the block starts to slip. The movement of one block will redistribute the forces on its nearest neighbors and can result in further slips and a chain of reaction can evolve.

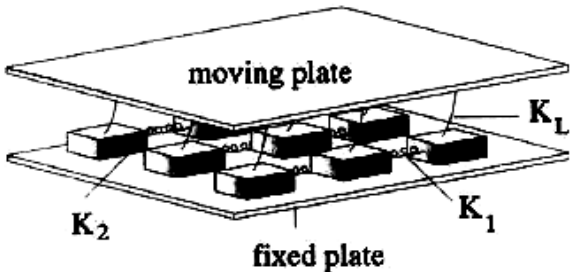

Figure 1-4 *The geometry of a 2D spring block model. K_1, K_2 represents the elastic constants of the springs between the blocks and K_L is the elastic constant of the spring between each block and the moving plate. (Olami et al., 1992).*

Later Rundle and Brown (1991) introduced a discrete version based on the Rundle and Jackson (1977) model, which was formulated as a cellular automaton and is described in the next section.

1.2.2 Rundle, Jackson and Brown Model (RJB)

Rundle and Brown (1991) presented the first cellular automaton model for frictional sliding using the Mohr-Coulomb friction law. Their model was a lattice automaton generalized from earlier model of Rundle and Jackson (1977) which was based on the well-known models described by Burridge and Knopoff (1967) and Dieterich (1972a). Rundle and Brown (1991) studied a microscopic system based upon the macroscopic velocity-dependent friction force.

In this model the contacting surface is idealized as a lattice of microscopic contact points, called "*asperities*". Each cell (or block in BK model) represents an asperity along the fault to manifest the "locking-up" process in the stick-slip dynamical instability across a fault plane. As the stress on an asperity increases, it will break (slip), and therefore decrease its own stress but raise the stress on surrounding asperities. Upon successive application of a shearing force at a series of discrete times, contact points fail and slip relative to each other. This model is based on a lattice dividing the surface below a macroscopic block into an $M \times M$ lattice of adjoining microscopic squares. The force σ_i on the i^{th} square is

$$\sigma_i = p_i(\mathrm{t}) + \sum_j T_{ij}\Phi_j(\mathrm{t}), \tag{1.17}$$

where p_i is an externally applied force, and T_{ij} is an interaction between squares. The spring constants are encoded in the stress tensor, T, which is, in principle, derived from a continuum elastic theory and is the Green's function for a given boundary value problem. Theoretically, a Green's function is the impulse response of the elastic medium and is used to describe the propagation of seismic waves in the medium. Here, it is used as a function to describe the stress interaction between the lattice sites or the propagation of stress in the system. The order parameter $\Phi_i(\mathrm{t}) = s_i - vt$ is the "slip deficit", with s_i being the total distance square i has slipped. A failure envelope σ_i^F is specified, so that slip occurs if $\sigma_i^F > \sigma_i$. In the BK model, the driving plate moves with a constant velocity (v). Here, since the blocks rearrange themselves immediately after a failure, the driving plate can move a fixed distance ($v\Delta T$), with ΔT much smaller than the mean time for an event

to stop in the BK model. Therefore, the plate does not move while an event occurs. Then it moves some fixed distance and waits for the event to stop, provided one was triggered. In a system such as this, the fracture dynamics are slow, so that in spite of potentially rapid local developments, the sample can be considered to be in equilibrium during most of the increments. The dynamics are generated by incrementing t by $\delta t = \Delta$, producing a force increment $\delta\sigma_i = -\sum_i T_{ij}\, v\Delta > 0$ at site i at regular intervals δt. As these sites fail by sliding, a chain reaction, or an avalanche of failed sites, may occur by the triggering of neighboring sites. Another addition of Rundle and Brown was to introduce a "jump function", J, to determine the new position of a block after the slip that occurs when a site decays from the active to the passive state (Rundle and Jackson, 1977; Rundle, 1988). Site i is in an active state for $\sigma_i > \sigma_i^F$ and in a passive state when $\sigma_i^F \geq \sigma_i$.

1.2.3 Olami, Feder and Christensen Model (OFC)

Olami, Feder, and Christensen (OFC) introduced a cellular automata (Olami et al. 1992) based on the Burridge and Knopoff slider bock model which is very similar to the RJB model (Rundle and Jackson, 1977). Inspired by the Bak, Tang, and Wiesenfeld's sandpile model (Bak et al., 1987), Olami et al. (1992) presented evidence that a nonconservative cellular automata without added external noise can display SOC behaviour (Olami et al., 1992).

Bak et al. (1987) introduced the concept of self-organized criticality: a dynamical many-body system reaches a critical state without the need to fine-tune the system parameters (Olami et al., 1992). Olami, Feder and Christensen (1992) generalized the BTW model (Bak et al., 1987) based on a 2D version of the Burridge-Knopoff spring block model. They mapped the 2D spring-block model into a cellular automaton model by defining an $L \times L$ array of blocks by (i,j), where i, j were integers between 1 and L. They calculated the total force on a specific block by (i,j)

$$F_{i,j} = K_1[2dx_{i,j} - dx_{i-1,j} - dx_{i+1,j}] + K_2[2dx_{i,j} - dx_{i,j-1} - dx_{i,j+1}] + K_L dx_{i,j}, \tag{1.18}$$

where $dx_{i,j}$ is the displacement of each block from its relaxed position and K_1, K_2 and K_L denote the elastic constant. When the driving plate begins to move, the total force on all

the blocks increases until one site reaches the threshold value and the process of relaxation begins (an earthquake is triggered). To summarize, the OFC model is a lattice of cells which interact by redistributing a proportion of their strain to neighboring cells once they reach a failure threshold (Olami et.al, 1992). OFC argued that this dependence explains the variance of the exponent in the Gutenberg-Richter (1956) law observed in real earthquakes.

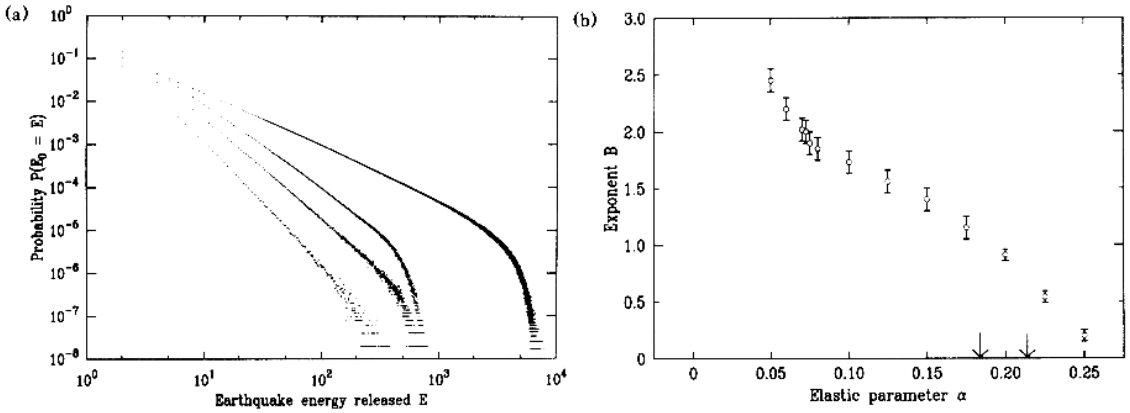

Figure 1-5 *a) Simulation results for the probability density of an earthquake of energy E as a function of E for a 35 by 35 system. The curves correspond to different elastic ratios. The slope of the curve becomes steeper as the elastic ratio is decreased. b) The power-law exponent B as a function of the elastic parameter (α). The level of conservation is 4α. Notice the sudden change of the B value around α=0.07. Below α=0.05 there is a transition to exponential decay. The arrows indicate the actual measured B values for earthquakes. (Olami et al., 1992).*

Olami et al., (1992) demonstrated that their continuous, non-conservative cellular automaton model exhibits SOC behaviour for a wide range of elastic ratios (Figure 1-5a). The level of conservation in this nearest neighbour model is dependent on the elastic parameter of α. Because each cell in the model is connected to four adjacent neighbours (nearest neighbours), the level of conservation is $4*\alpha$. They also increased the system size for a constant elastic ratio to verify the criticality in the model and observed that the exponent stays the same while the cutoff in the energy distribution scales with system size (Figure 1-6).

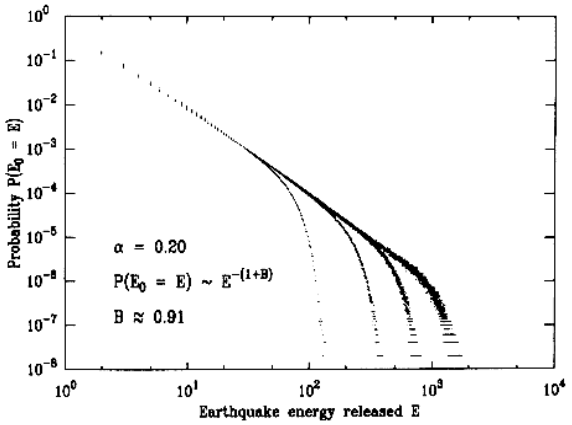

Figure 1-6 *The probability density function for an earthquake of energy E as a function of E for a constant elastic ratio. The different curves refer to different system sizes L=15, 25, 35 and 50. The cutoff in energy distribution scales with* $L^{2.2}$ *(Olami et al., 1992).*

The approach of these studies generally examines various metrics averaged over the model evolution. These include testing the presence of *1/f* pink noise (Bak et al., 1987), quantifying branching ratios (Carvalho and Prado, 2000), or the examination of the behaviour in more analytically tractable regimes (Kinouchi et al., 1998). Naylor and Main (2008) also investigated the occurrence of spatial organisation and quantified the strain distributions and their dependency on the lattice geometry. As noted above, there has been considerable investigation into the scaling properties of rupture modeling. Bak et al. (1987) and Feder and Feder (1991) showed that GR scaling is a form of self-organized criticality.

The OFC model is important as it provides insight into the statistical behaviour of rupturing in heterogeneous materials that do not fail through a single crack mechanism. In such materials rupture statistics are a product of complex interactions. However, formal comparison with data, especially at high magnitude, remains difficult due to the short duration of earthquake catalogues (Leonard and Papasouliotis, 2001). In the OFC model, nucleation always occurs when a single cell slips by a fixed amount. However variation of the conservation parameter, α, as shown in Figure 1-5b, leads to a wide variety of rupture propagation behaviour (Olami et al., 1992).

Klein et al. (1997, 2000, and 2007) also studied earthquake behaviour in long-range OFC and found that the earthquake fault systems relieve stress via long-range elastic interactions within the Earth's crust (Klein et al., 2000). They showed that, for nearest neighbor stress transfer, there is no apparent GR scaling (Grassberger, 1994; Klein et al., 1997, 2000, 2007). However, in long-range interaction models (R>>1), the system becomes near mean-field (Klein et al., 2000) and there appears to be GR or cluster scaling associated with a spinodal critical point (Klein et al., 1997, 2000). In models of this type, the number of events obeys the equation 1-7. Recently, several cellular automata models of earthquake fault system based on the RJB and OFC models have been expanded to include different aspect of inhomogeneity. Most of these studies have tried to integrate inhomogeneity into OFC models by changing the individual parameters along the fault plane, but only for the short-range stress transfer system (Janosi and Kertesz, 1994; Torvund and Froyland, 1995; Ceva, 1995; Mousseau, 1996; Ramos et al. 2006; Bach et al., 2008; Jagla, 2010). Serino et al. (2011) and Dominguez et al. (2012, 2013) incorporated inhomogeneities in terms of damage into a long-range OFC model. Their findings illustrate that the interaction between structures has an important effect on the earthquake fault process and this interaction affects how close the fault is to the critical point.

We have noted in section 1.1.1 that the cumulative magnitude-frequency distribution for earthquakes obeys the GR relation (equation 1-2). However, this distribution is not accurate enough for larger earthquakes. There are some physical limitations that suggest an upper bound or taper and a maximum size for extreme events (Main, 1996; Kagan and Jackson, 2000; Bell et al., 2013). Turcotte (1999) proposed a modified GR relation (MGR) that adds an exponential tail to the cumulative form, with an exponential cutoff at the corner moment or magnitude. However, because of the statistical limitations of the available data, the debate continues as to the true nature of this distribution (Main 2000; Zoller et al., 2006).

Serino et al. (2011) introduced a physical basis for the MGR form of the magnitude-frequency distribution that depends on the level of damage in each fault network, denoted by a damage parameter q. They showed that the corner magnitude is dependent on the

amount of damage and the scaling exponent depends on the relative frequency of the faults with a particular amount of damage. Dominguez et al., (2012, 2013) expanded the previous study by altering the spatial configuration of inhomogeneities into the lattice. They showed that the frequency of events depends on the amount of damage but also on the spatial configurations of the damage.

As noted above, a variety of models for earthquake fault have been established to provide further insights into the complex dynamics of the earthquakes. Although significant improvement has been made in our knowledge and understanding of the statistical properties of earthquakes, none of them are able to reproduce one of the most crucial characteristics of natural seismicity: temporal clustering. Based on the known structure of natural faults and the fact that long-range interactions model are able to reproduce more realistic representations of earthquake seismicity (Fisher et al., 1997; Ben Zion et al., 2008; Serino et al., 2011) this dissertation introduces spatial heterogeneity in the form of asperities into the OFC model with long-range stress transfer. The results of the model illustrates that while this long-range heterogeneous earthquake fault model leaves the GR scaling intact while it also produces, for the first time, temporal clustering similar to that seen in natural faults, including aftershocks, foreshocks and quasi-periodic large events (characteristic earthquakes).

1.3 Thesis structure

This integrated thesis is presented in five chapters. The introductory chapter (Chapter 1) outlines the background information and earlier important models.

Chapter 2 presents results related specifically to foreshock and aftershock statistics, submitted to *Physical Review Letters*. This chapter illustrates the initial results and shows that, for the first time in these models, the occurrence of characteristic earthquake sequences associated with a gradually accelerating number of larger events (foreshocks) prior to a mainshock and is followed by a tail of decreasing activity (aftershocks). The relative length of the foreshock to aftershock sequences can vary and depends on the amount of stress dissipation in the system.

In the next chapter, the investigation is expanded by increasing the number of stronger asperity sites. In Chapter 3, the focus is on the spatiotemporal clusters of events and the scaling behavior of the magnitude-frequency distribution of earthquakes. The effect of different asperity percentages for a range of values of the stress dissipation parameter is studied. It is concluded that the spatial heterogeneities are responsible for the primary features of the higher activity sequences, including the size of the largest events and the upper bound or taper, of the modified GR relation. The sensitivity of the spatial and temporal clusters and their activity rates to the initial parameters of the model such as stress dissipation and the number and configuration of asperity sites in the model is discussed. Included is a thorough investigation of the presence of Accelerating Moment Release (AMR) before the mainshock, along with the Omori and reverse Omori law for foreshocks and aftershocks. The TM metric analysis is applied to the higher periods of activity prior to the main event in the sequence. The results of this chapter have been submitted to the *Journal of Geophysical Research*.

In Chapter 4, additional properties of this OFC model are outlined. This chapter has been submitted to the journal *Pure and Applied Geophysics*. It discusses the different spatial configurations and amount of inhomogeneities in the model. Changing the spatial configuration of inhomogeneities increases the ability of the fault system to generate larger events, but results show that the total percentage of asperities is important as well.

Chapter 5 concludes with a summary and discussion of the results and suggestions for future work.

1.4 References

Aki, K. (1972). Earthquake Mechanism; Tectonophysics; Elsevier B.V.; Vol 13, pages 423-446.

Aki, K. (1966). "Generation and propagation of G waves from the Niigata earthquake of June 14, 1964. Part 2. Estimation of earthquake moment, released energy and stress-strain drop from G wave spectrum". Bulletin of the Earthquake Research Institute 44: 73–88.

Aki, K., Richards, P.G. (2002). Quantitative seismology (2 ed.). University Science Books. ISBN 0-935702-96-2.

Alava, M. J., Nukala, P., and Zapperi, S. (2006). Statistical models of fracture, Adv. Phys. 55, 349.

Allen, R. M., and Kanamori (2003). The potential for Earthquake Early Warning Southern california, Sciences, 300, 786-789.

Bach, M., Wissel F. and Dressel, B. (2008). Olami-Feder-Christensen model with quenched disorder. Phys. Rev. E77, 067101.

Bak, P., Tang, C. and Wiesenfeld K. (1987). Self-organized criticality: an explanation of 1/f noise. Phys. Rev. Lett., 59:381-384.

Båth, M. (1965). Lateral inhomogeneities of the upper mantle, Tectonophysics, 2, 483–514.

Bell, A.F., Mark Naylor, M., Main, I.G. (2013). Convergence of the frequency-size distribution of global earthquakes, GRL, 40, 2585–2589, doi:10.1002/grl.50416.

Ben-Zion, Y. (2008). Collective Behavior of Earthquakes and Faults: Continuum-Discrete Transitions, Progressive Evolutionary Changes and Different Dynamic Regimes, Rev. Geophysics, 46, RG4006, doi:10.1029/2008RG000260.

Ben-Zion, Y., Lyakhovsky, V., (2002). Accelerated seismic release and related aspects of seismicity patterns on earthquake faults. Pure and Applied Geophysics 159, 2385–2412.

Bowman, D.D., Ouillon, G., Sammis, C.G., Sornette, A., Sornette, D., (1998). An observational test of the critical earthquake concept. Journal of Geophysical Research 103, 24,359–24,372.

Bowman, D.D., King, G.C.P., (2001). Accelerating seismicity and stress accumulation before large earthquakes. Geophysical Research Letters 28, 4039–4042.

Brune, J. N. (1970). Tectonic stress and spectra of seismic shear waves of earthquakes, J. Geophys. Res., 75 (26), 4997-5009.

Brune, J. N. (1971). Corrction, J. Geophys. Res., 76 (20), 5002.

Bufe, C.G., Varnes, D.J., (1993). Predictive modeling of the seismic cycle of the greater San Francisco Bay region. Journal of Geophysical Research 98, 9871–9883.

Burridge, R., Knopoff, L. (1967). Model and theoretical seismicity, Bull. Seismol. Soc. Am. 57. 341–371.

Carlson, J. M., Langer, J. S. and Shaw, B. E. (1994). "Dynamics of earthquake faults". Rev. Mod. Phys. 66, 657.

Carlson J.M., Langer, J., Shaw, B., Tang, C. (1991). "Intrinsic properties of a Burridge-Knopoff model of an earthquake fault". Phys. Rev. A 40, 884.

Carlson, J. M. and Langer, J. S. (1989). Mechanical model of an earthquake fault. Phys. Rev. Lett. 62, 2632; Phys. Rev. A 40, 6470.

Ceva, H. (1995). Inhuence of defects in a coupled map lattice modeling earthquakes. Phys. Rev, E52, 154.

Clancy, I. and Corcoran, D. (2005). "Criticality in the Burridge-Knopoff model". Phys. Rev. E 71, 046124.

Clancy, I. and Corcoran, D. (2006). "Burridge-Knopoff model: Exploration of dynamic phases". Phys. Rev. E 73, 046115.

de Carvalho, J.X., Prado, C.P.C., (2000). Self-Organized Criticality in the Olami-Feder-Christensen Model, Phys. Rev. Lett. 84, 4006.

Dieterich, J. H. (1972a). Time dependent friction as a possible mechanism for aftershocks, J. Geophys. Res. 77, 3771-3781.

Dodge, D.A., Beroza, G.C., Ellsworth, W.L., (1996). Detailed observations of California foreshock sequences: implications for the earthquake initiation process. Journal of Geophysical Research 101, 22,371–22,392.

Dominguez, R., Tiampo, K.F., Serino, C.A. and Klein W. (2013). Scaling of earthquake models with inhomogeneous stress dissipation. Phys. Rev. E 87, 022809.

Ellsworth, W.L., Lindh, A.G., Prescott, W.H., Herd, D.J., (1981). The 1906 San Francisco Earthquake and the seismic cycle. In: Simpson, D.W., Richards, P.G. (Eds.), Earthquake Prediction: An Internation Review. Maurice Ewing Ser., vol. 44. AGU, Washington, D.C.

Feder H. J. S. and Feder, J. (1991). Self-organized criticality in a stick-slip process Phys. Rev. Lett. 66, 2669.

Ferguson, C. D., Klein, W., and Rundle, J. B. (1999). Spinodals, scaling, and ergodicity in a threshold model with long-range stress transfer, Phys. Rev. E, 60, 1359–1373.

Fisher, D.S., Dahmen, K., Ramanathan, S. and Ben-Zion, Y. (1997). Statistics of Earthquakes in Simple Models of Heterogeneous Faults. Phys. Rev. Lett. 78, 4885.

Grassberger, P., (1994). Efficient large-scale simulations of a uniformly driven system. Phys. Rev. E 49, 2436 (1994).

Gulia, L. and Wiener, S. (2010). “Statistical physics approach to understanding the multiscale dynamics of earthquake fault systems”. Geophys. Res. Lett. 37, L10305.

Gutenberg, B. and Richter, C. F. (1954). “Seismicity of the earth and associated phenomena”, 2nd ed. Princeton University Press, Princeton, NJ.

Hanks, T. C. and Kanamori, H. (1979). “A moment magnitude scale”. J. Geophys. Res. 84, 02348.

Herrmann H. J. and Roux S. (1990). Statistical Models for the Fracture of Disordered Media (Amsterdam: North-Holland)

Hill, D. P., Mowinckel, P., Lahr, K. M. (1975b). Catalog of earthquakes in the Imperial Valley, California, June 1973-May 1974Open File Rep. 75-101, 25U.S. Geol. Surv., Menlo Park, Calif..

Jagla, E.A. (2010). Realistic spatial and temporal earthquake distributions in a modified Olami-Feder-Christensen model. Phys. Rev, E81, 046117.

Janosi, I.M. and Kertesz, J. (1994), Self-organized criticality with and without conservation. Physica A200, 0378.

Jones L. M. and Molnar. P. (1979). Some characteristics of foreshocks and their possible relationship to earthquake prediction and premonitory slip on faults. J. Geophys. Res. 84 (1979), 3596.

Kagan Y Y. (1997). Statistical aspects of Parkfield earthquake sequence and Parkfield prediction experiment. Tectonophysics, 1997, 270: 207~219.

Kagan Y Y. (1999). Universality of the seismic momnet-frequency relation. Pure Appl. Geophys, 1999, 155: 537~573.

Kagan, Y. Y. and Jackson, D.D (2000). Probabilistic forecasting of earthquakes, Geophys. J. Int., 143, 438-453.

Kagan, Y. Y. and Knopoff, L. (1976). Statistical search for non-random features of the seismicity of strong earthquakes. Phys. Earth Planet. Inter. 12, 291.

Kanamori, H. (1981). The nature of seismicity patterns before large earthquakes, in Earthquake Prediction, Maurice Ewing Series, IV, 1–19, AGU, Washington

Kanamori, H. (1978). Quantification of Earthquakes, Nature 271, 411-414 doi:10.1038/271411a0.

Kanamori, H. (1977). The energy release in great earthquakes. J. Geophys. Res., v. 82, p. 2981-2987.

Kinouchi, O., Pinho, S.T.R., Prado, C.P.C., (1998). Random-neighbour Olami-Feder-Christensen slip-stick model, Phys. Rev. E 58, 3997.

Klein, W., Anghel, M., Ferguson, C. D., Rundle, J. B. and Martins J. S. S. (2000). Geocomplexity and the Physics of Earthquakes (American Geophysical Union, Washington, DC), AGU Monograph 120.

Klein W., Rundle J. B., and Ferguson C. D. (1997). Scaling and Nucleation in Models of Earthquake Faults. Phys. Rev. Lett. 78, 3793 (1997).

Klein, F. W., Einarsson, P., Wyss, M. (1977). The Reykjanes Peninsula, Iceland, earthquake swarm of September 1972 and its tectonic significance, J. Geophys. Res., 82, 865–889.

Langer, J.S. (1992). “Models of crack prorogation”. Phys. Rev. A 46, 3123.

Leonard, T., Papasouliotis, O., Main, I.G., (2001). A Poisson model for identifying characteristic size effects in frequency data: Application to frequency-size distributions for global earthquakes, "starquakes", and fault lengths, J. Geophys. Res. 106, 13473.

Main I. (2000). Apparent breaks in scaling in the earthquake cumulative frequency-magnitude distribution: fact or artifact? Bull. Seis. Soc. Am. 90(1): 86~97.

Main I G. (1996). Statistical physics, seismogenesis, and seismic hazard. Rev. Geophys., 34:433~462.

McGuire, J. J., Boettcher, M. S. and Jordan, T. H. (2005), Foreshock sequences and short-term earthquake predictability on East Pacific Rise transform faults, Nature, 434(7032), 457–461; Correction – Nature 435(7041), 528.

Mogi, K. (1981). Seismicity in western Japan and long term earthquake forecasting, in Earthquake Prediction: An International Review, Maurice Ewing Ser., vol. 4, edited by D. W. Simpson, and P. G. Richards, pp. 43 – 51, AGU, Washington, D. C.

Mogi, K. (1962), Magnitude frequency relations for elastic shocks accompanying fractures of various materials and some related problems in earthquakes, Bull. Earthquake Res. Inst. Univ. Tokyo, 40, 831–853.

Mori T. and Kawamura, H. (2006). "Simulation study of the one-dimensional Burridge-Knopoff model of earthquakes". J. Geophys. Res. 111, B07302.

Mori T. and Kawamura, H. (2005). "Simulation study of spatiotemporal correlations of earthquakes as a stick-slip frictional instability". Phys. Rev. Lett. 94, 058501.

Mori, J., et R. E. Abercombie (1997). Depth dependence of earthquake frequency-magnitude distributions in California: Implication for rupture initiation, Journal of Geophysical Research, 102(B7), 15081–15090.

Mousseau, N. (1996). Synchronization by Disorder in Coupled Systems. Phys. Rev. Lett. 77, 968.

Nakanishi, H. (1990). Cellular-automaton model of earthquakes with deterministic dynamics. Phys. Rev. A 41, 7086.

Naylor M. and Main I. G., (2008). Cell scale self-organisation in the OFC model: painting by numbers, re-rupturing and memory loss. Eur. J. Phys. B 64:139–146.

Ogata, Y. (1983). Estimation of the parameters in the modified Omori formula for aftershock frequencies by the maximum likelihood procedure, Journal of Physics of the Earth, Vol.31, 115-124.

Omori. F. (1984). On the aftershocks of earthquakes. J. Coll. Sci. Imp. Univ. Tokyo 7, 111.

Olami, Z., Feder, HJS., Christensen, K. (1992). Self-organized criticality in a continuous, nonconservative cellular automaton modelling earthquakes. Phys Rev Lett 68(8):1244–1247.

Otsuka, M. (1972). A Simulation of earthquake occurrence. Phys Earth Planet Inter. 6-311.

Papazachos, B. C. (1975). Foreshocks and earthquake prediction. Tectonophysics 28 213.

Ramos, O., Altshuler, E. and Maloy K.J. (2006), Quasiperiodic Events in an Earthquake Model. Phys. Rev. Lett. 96, 098501.

Reid, H.F. (1910). The Mechanics of the Earthquake, The California Earthquake of April 18, 1906, Report of the State Investigation Commission, Vol.2, Carnegie Institution of Washington, Washington, D.C. 1910

Richter C.F. (1935). An instrumental earthquake magnitude scale Bull. Seismol. Soc. Am. 25, 1.

Rundle, J. B. (1988). A physical model for earthquakes, J. Geophys. Res. 93-6237.

Rundle, JB, Klein W. and Gross S. (1999). Physical basis for statistical patterns in complex earthquake populations: Models, predictions, and tests, PAGEOPH, 155, 575-607.

Rundle, J. B. and Jackson, D. D. (1977). Numerical simulation of earthquake sequences, Bull. Seismol. Soc. Am. 67.

Rundle, J. B. and Brown, S. R. (1991). Origin of Rate Dependence in Frictional Sliding, J. Stat. Phys. 65, 403.

Scholz, C.H. (2002). The mechanics of earthquakes and faulting, Cambridge University Press, p. 471.

Scholz, C. H. (1968). The frequency-magnitude relation of microfracturing in rock and its relation to earthquakes, Bull. Seis. Soc. Am., 58(1), 399–415.

Serino, C. A., Tiampo, K. F. and Klein W. (2011). New Approach to Gutenberg-Richter Scaling, Phys. Rev. Lett. 106, 108501.

Shcherbakov R. and Turcotte D.L. (2004). "A modified form of Bath's law", Bull. Seism. Soc. Am., 94(5) 1968-1975, doi:10.1785/012003162.

Shearer, P. M. (2012), Self-similar earthquake triggering, Båth's law, and foreshock/aftershock magnitudes: Simulations, theory, and results for southern California, J. Geophys. Res., 117, B06310, doi:10.1029/2011JB008957.

Schorlemmer, D., and Gerstenberger, M. C. (2007). RELM testing center, Seismol. Res. Lett. 78, 1, 30-36.

Sykes, L.R., Jaumé, S.C., (1990). Seismic activity on neighbouring faults as a long-term precursor to large earthquakes in the San Francisco Bay area. Nature 348, 595–599.

Sornette, D. (2004), Critical Phenomena in Natural Sciences: Chaos Fractals, Self Organization and Disorder: Concepts and Tools, Springer, Heidelberg, Germany.

Sornette D. and Sammis, C. G. (1995). Complex critical exponents from renormalization group theory of earthquakes: Implications for earthquake predictions, J.Phys.I France 5, 607-619.

Sornette D, Sornette A. (1999). General theory of the modified Gutenberg-Richter law for large seismic moments. Bull. Seis. Soc. Am., 89(4): 1 121-1130.

Sornette, A., Sornette, D., (1990). Earthquake rupture as a critical-point-consequences for telluric precursors, Tectonophysics 179, 327.

Sornette, A., Sornette, D., (1989). Self-organized criticality and earthquakes, Europhys.Lett. 9, 197.

Thirumalai, D., Mountain, R.D., Kirkpatrick, T.R., (1989). Ergodic behavior in supercooled liquids and in glasses. Physical Review A 39, 3563–3574.

Tiampo, K. F., Rundle, J. B., Klein, W., Holliday, J., S´aMartins, J. S. and Ferguson, C. D. (2007). Ergodicity in natural earthquake fault networks. Phys. Rev. E 75, 066107.

Tiampo, K.F., Rundle, J.B., Klein, W, Holliday, J. (2006). Forecasting rupture dimension using the Pattern Informatics technique, Tectonophysics, 424/3-4, pp. 367–376.

Tiampo, K.F., Rundle J.B., Klein, W. Sá Martins, J.S. and Ferguson C.D. (2003). Ergodic dynamics in a natural threshold system. Phys. Rev. Lett., 91, p. 238501

Turcotte, D.L., Newman, W.I., Shcherbakov, R. (2003). Micro and macroscopic models of rock fracture. Geophysical Journal International 152, 718–728.

Turcotte, D. L. (1999), Self-organized criticality, Rep. Prog. Phys., 62, 1377–1429, doi:10.1088/0034-4885/62/10/201.

Turcotte, D. L. (1997). Fractals and chaos in geology and geophysics, 2nd edn. Cambridge, UK: Cambridge University Press.

Torvund F., and Froyland, J. (1995). Strong ordering by non-uniformity of thresholds in a coupled map lattice. Physica Scripta 52, 624.

Utsu, T., Ogata, Y. and Matsu'ura, R. S. (1995). The centenary of the Omori formula for a decay law of aftershock activity, Journal of Physics of the Earth, Vol.43, pp.1-33.

Utsu, T. (1961). A statistical study on the occurrence of aftershocks. Geophys. Mag. 30, 521.

Vasconcelos, G. L., (1996). "First-order phase transition in a model for earthquakes". Phys. Rev. Lett. 76, 4865.

Vasconcelos, G. L., (1992). "Phase transitions in a spring-block model of earthquakes". Physica A 191, 69.

Vere-Jones, D. (2006). The development of statistical seismology, A personal experience. Tectonophysics 413, 5–12.

Vere-Jones, D. (1995), Forecasting earthquakes and earthquake risk. International Journal of Forecasting 11, 503–538.

Waite, G. R. and R. B. Smith, (2002). Seismic evidence for fluid migration accompanying subsidence of the Yellowstone Caldera, J. Geophysical Res., 107(B9), 2177, doi:10.1029/2001JB000586.

Wu, Y. M. and Kanamori, H., (2008). Development of an Earthquake Early Warning System Using Real-Time Strong Motion Signals, Sensors, 8, 1-9.

Xia, J., Gould, H., Klein, W., Rundle J. B. (2008). "Near-mean-field behavior in the generalized Burridge-Knopoff earthquake model with variable-range stress transfer". Phys. Rev. E 77 (2008), 031132.

Xia, J., Gould, H., Klein, W., Rundle J. B. (2005). "Simulation of the Burridge-Knopoff model of earthquakes with variable range stress transfer". Phys. Rev. Lett. 95, 248501.

Zechar, J.D., Jordan, T.H. (2010), Simple smoothed seismicity earthquake forecasts for Italy. Annals of Geophysics 53.

Zoller, G., Hainzl, S., Ben-Zion Y., and Holschneider, M. (2006). Earthquake activity related to seismic cycles in a model for a heterogeneous strike-slip fault, Tectonophys., 423, 137–145.

Chapter 2

2 Foreshock and aftershocks in simple earthquake models

This chapter presents the cellular automata earthquake fault model with long-range interactions and a fixed percentage of randomly distributed stronger sites, or 'asperity cells'. The introduction of these spatial heterogeneities results in temporal clustering in the model that mimics those seen in natural fault systems. Sequences of activity are observed that start with a gradually accelerating number of larger events (foreshocks) prior to a mainshock that is followed by a tail of decreasing activity (aftershocks). These recurrent large events occur at regular intervals, similar to characteristic earthquakes described in historic seismicity, and the time between events and their magnitude are a function of the stress dissipation parameter. The relative length of the foreshock sequences to the aftershock sequences can vary and also depends on the amount of stress dissipation in the system. This work provides further evidence that the spatial and temporal patterns observed in natural seismicity may be controlled by the underlying physical properties and are not solely the result of a simple cascade mechanism and, as a result, may not be inherently unpredictable.

2.1 Introduction

Understanding the dynamics of seismic activity is fundamental to the investigation of the earthquake process. Simple models of statistical fracture have been used in the past to test many of the typical assumptions and effective parameters inherent in the complicated dynamics of the earthquake fault system and their relative variability (Burridge and Knopoff, 1967; Otsuka, 1972; Rundle and Jackson, 1977; Rundle, 1988; Carlson and Langer, 1989; Nakanishi, 1990; Rundle and Brown, 1991; Olami et al., 1992; Alava et al. 2006). Most of these models assume a spatially homogeneous fault and short range stress transfer. However, inhomogeneity plays an important role in the spatial and temporal behavior of an earthquake fault (Dominguez et al., 2013). A number of OFC models with nearest neighbor stress transfer have been expanded to include inhomogeneity, generally by varying individual parameters along the fault plane (Janosi and Kertesz, 1993; Torvund and Froyland; 1995; Ceva, 1995; Mousseau, 1996; Ramos et al., 2006; Bach et al. 2008; Jagla, 2010).

Stress transfer in natural earthquake faults is elastic and, as a result, OFC models with long-range interactions produce more realistic representations (Ben-Zion, 2008; Serino et al., 2011). Inhomogeneities in the form of stress relieving micro-cracks have been incorporated into long-range OFC models, resulting in a better understanding of Gutenberg-Richter (GR) scaling (Richter, 1935; Dominguez et al., 2013; Serino et al., 2011). However, to date, none of these models have been able to reproduce the temporal clustering that is a primary feature of natural seismicity and a critical component in the assessment of earthquake hazard. Motivated by the structure of natural faults, we introduce heterogeneity in the form of asperities into the OFC model with long-range stress transfer. The introduction of these spatial heterogeneities produces, for the first time, temporal clustering similar to that seen in natural faults, including aftershocks, foreshocks and quasi-periodic large events (characteristic earthquakes).

2.2 Model dynamics

Our model is a two-dimensional cellular automaton with periodic boundary conditions based on the OFC (Olami et al., 1992) and RJB (Rundle and Jackson, 1977; Rundle and Brwon, 1991) models. Every site in the lattice is connected to z neighbors which are defined as sites within a certain distance or stress interaction range, R. A homogeneous residual stress σ^r is assigned to all the sites in the lattice. To impose spatial inhomogeneity on the lattice, two sets of failure thresholds are introduced; 'regular sites' with a failure threshold of σ^F and 'asperity sites' with a significantly higher failure threshold ($\sigma^F_{(asperity)}=\sigma^F+\Delta\sigma^F$) in order to incorporate stronger sites which can support higher stress prior to failure.

Initially, an internal stress variable, σ_i(t), is randomly distributed to each site in such way that the stress on all sites falls between the residual stress and failure stress thresholds ($\sigma^r<\sigma_i(t=0)<\sigma^F$). Given the initializing procedure, it is clear that at t=0 no sites will have $\sigma_i > \sigma^F$. Here we use the so-called zero velocity limit to simulate the increase in stress associated with the dynamics of plate tectonics (Olami et al., 1992). The lattice is searched for the site that minimizes (σ^F - σ_i). Then (σ^F - σ_i) stress is added to each site such that the stress on at least one site is now equal to its failure threshold. One site fails and some fraction of its stress, given by α*[σ^F–($\sigma^r\pm\eta$)], is dissipated from the system. α is a dissipation parameter ($0 < \alpha \leq 1$) which quantifies the portion of stress dissipated from the failed site and η is a randomly distributed noise. Stress on the failed site is lowered to ($\sigma^r\pm\eta$) and the remaining stress is distributed to its predefined z neighbors. After the first site failure, all neighbors are searched to determine if the stress added to those neighbors caused additional failures. If so, the procedure is repeated. If not, the time step, known as the plate update (pu), increases by unity and the lattice is searched again for the next site which minimizes (σ^F - σ_i). The size of each event is calculated from the total number of failures that result from the initial failure. Stress is dissipated from the system both at the regular lattice sites (temporarily) and through the asperity sites which are placed randomly throughout the system. However, the asperity sites fail less frequently than the regular sites, providing a time-dependent source and sink of stress: storing "dissipated" stress until asperity failure releases it back into the system. The addition of these large

failure threshold heterogeneities, or localized stress accumulators, results in a rich pattern of temporal clustering, including the occurrence of large events with constant return period (characteristic events), foreshocks and aftershocks.

2.3 Foreshocks and aftershocks

Spatial and temporal clustering has long been recognized in seismicity data, and significant research efforts have focused on that which occurs in the same general region as the mainshock as well as both immediately before (foreshocks) or immediately after (aftershocks) its occurrence (Båth, 1965; Kanamori, 1981; Ogata, 1983; Utsu et al. 1995; Dodge et al., 1996; Shcherbakov and Turcotte, 2006). For example, aftershocks occur close to their triggering mainshocks and the aftershock rate generally decays with time, following the power law relation known as the modified Omori law (Ogata, 1983; Utsu et al. 1995). On the other hand, while precursory seismic activity, or foreshocks, have been recorded before a number of large events around the world, their signal is much more difficult to observe (Bakun et al., 2005; Ellsworth et al. 1981; Jordan and Jones, 2010; Shearer, 2012).

One particular foreshock pattern, accelerating moment release (AMR) (Ellsworth et al. 1981; Sykes and Jaumé, 1990; Bowman and King, 2001; Bowman et al., 1998; Sornette and Sammis, 1995; Bufe and Varnes; 1993) is defined by the equation $\varepsilon(t) = A + B(tf - t)m$. $\varepsilon(t)$ has been interpreted as either the accumulated seismic moment, energy release or Benioff strain release within a specified region, from some origin time t_0 to time t. A is a constant that depends on the background level of activity, t_f is the time of the mainshock, B is negative and m is a value between 0.3 and 0.7. For example, Ben-Zion et al. (2002) analyzed the deformation preceding large earthquakes and obtained a 1-D analytical power-law time-to-failure AMR relationship before large events when the seismicity occurring immediately before a large event had broad frequency-size statistics, consistent with observed seismic activation before some large earthquakes (Turcotte et al., 2003; Zoller et al., 2006).

The ETAS (Epidemic Type Aftershock Sequences) model (Ogata, 1999; Helmstetter and Sornette, 2002) is a triggering model based on the concept that every event, regardless of its size, increases the probability of later events. In ETAS, not only do mainshocks trigger aftershocks, they can trigger aftershocks with magnitudes larger than themselves. If the largest event is triggered by earlier, smaller events, these are classified as foreshocks. While ETAS can replicate many features of earthquake clustering seen in natural seismicity, recent work suggests that these triggering models may not fully explain the foreshock-mainshock-aftershock process and that other mechanisms may be important (Sykes and Jaumé, 1990; Dodge and G. C. Beroza, 1997; Enescu et al., 2009). For example, Chen and Shearer (2013) studied foreshock sequences for M > 7 earthquakes in California and determined that they behaved more like swarms initiated by aseismic transients rather than triggered cascades or a nucleation process. These foreshock sequences occurred in areas of significant fault zone complexity, highlighting the importance of heterogeneity in the clustering process.

2.4 The model behavior

Here we investigate a system with 1% of randomly distributed asperity sites in a two-dimensional lattice of linear size L=256 with periodic boundary conditions. We set a homogeneous failure threshold for the regular sites at σ^F=2.0, homogeneous residual stress for the entire lattice as σ^r=1.0, and random distribution of noise η=[-0.1,+0.1]. The failure threshold for asperity sites is designated $\sigma^F_{(asperity)}=\sigma^F+10$. The system has a stress transfer range R=16 and every failed site directly transfers stress to z=1088 neighbors.

We compare our inhomogeneous model and a standard homogeneous model with no asperity sites in Figure 2-1. This figure shows time series ($6*10^5$ pu) and distribution of events (collected during 10^7 *pu*) for three different values of stress dissipation parameters α (Figures. 2-1a, b, and c). The first diagram (*i*) in each set is the time series of events for the heterogeneous model with 1% of asperity sites. The time steps in which an asperity site breaks are shown with a grey background shade. The second diagram (*ii*) in each set is the time series for the homogeneous model with no asperity sites. Figure 2-1d is the comparison between the frequency distributions for different values of α with and

without asperity sites. For the 1% asperity model the lattice does not break randomly in the time domain, despite the random spatial distribution of asperity sites.

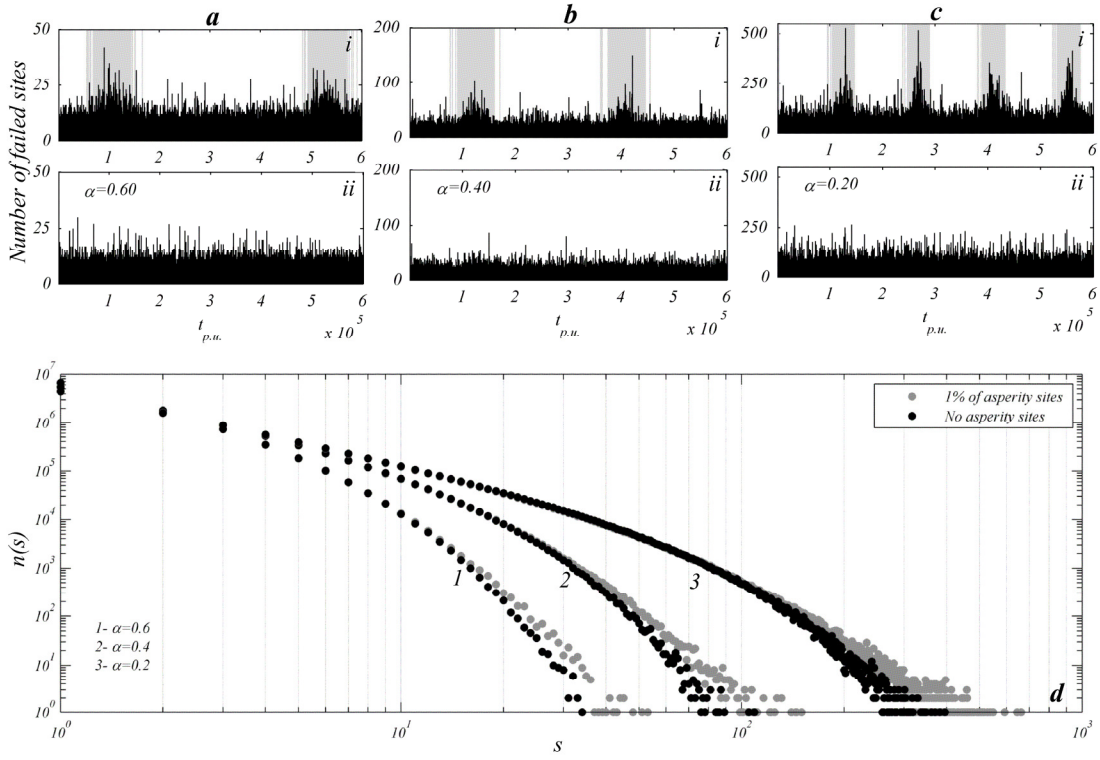

Figure 2-1. *Time series of events during a period of 6*10^5 pu for three different values of stress dissipation parameters (a) α = 0.6, (b) α = 0.4 and (c) α = 0.2; (i) are results for the model with 1% asperities (shaded background are those steps in which an asperity site breaks); (ii) are results for the homogeneous model. (d) Comparison between the distribution of events for two different scenarios (with and without 1% of spatially random distributed asperity sites) for three values of stress dissipation parameter.*

The asperity model produces large, characteristic events that recur at constant intervals. Those characteristic events occur less frequently as α, or stress dissipation, increases. The distributions also confirm that, as stress dissipation increases, the largest events become smaller, as higher stress dissipation works to suppress large events (Serino et al., 2011). The frequency distributions also show that the model with 1% of asperities generates larger events compared to the homogeneous model.

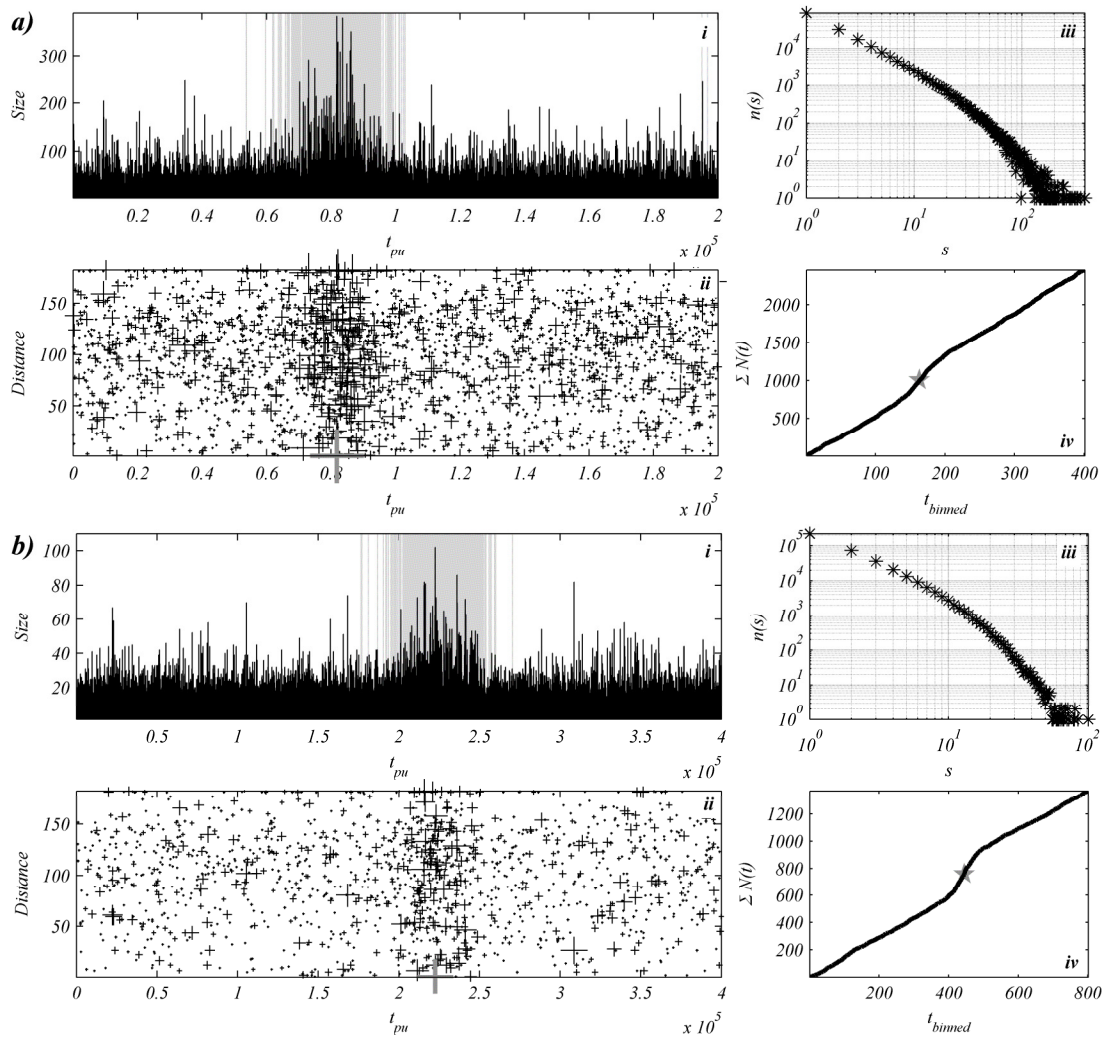

Figure 2-2 *(a-i) Time series of events (shaded areas indicate the steps where an asperity site breaks) for =0.2. (a-ii) The distance of each event from the biggest event (mainshock, shown by the larger grey cross). (a-iii) Distribution of events during the time period of (a-i). (a-iv) The accumulated number of events bigger than the defined threshold versus coarse-grained time. (b-i, ii, iii, iv) as in (a) for =0.4.*

In Figure 2-2, we bin time into coarse-grained units of Δt=500 *pu* and count the number of events greater than a predefined threshold in each bin. Figures 2-2a and 2-2b show one of the activation periods for α=0.2 and α=0.4, respectively. The first subfigure in each set (i) shows the time series of events and isolates, in gray, those time steps where an asperity breaks. The second subfigure of each set (ii) plots distance versus time for each

event (foreshock or aftershock) relative to the biggest event in the series (mainshock). In the third subfigure (iii) is shown the frequency distribution for the selected period and the fourth subfigure (iv) is the cumulative number of events greater than the chosen threshold versus coarse-grained (binned) time. Temporal clustering is clearly visible (i,ii), starting with a gradually increasing number of bigger events (foreshocks) and ending with a tail of decreasing activity (aftershocks). The increasing number of large events prior to the mainshock in Figures 2-2(a-iv) and 2-2(b-iv) produces an increasing rate of activity similar to AMR behavior before large events. This is the first time this complete set of phenomena has been observed in OFC models.

While most theoretical models of earthquake seismicity such as ETAS presuppose that all events are governed by the same physics, recent careful analysis has suggested that variation in foreshock-aftershock rates may be dependent on the local or regional rheology. Enescu et al. (2009) demonstrated that swarm-type seismic activity with higher foreshock rates occurred in areas of California with relatively high surface heat flow while more typical sequences occurred in regions with lower heat flow. McGuire et al. (2005) analyzed hydroacoustic data to mainshock along East Pacific Rise faults and identified sequences with higher foreshock rates and lower aftershock rates than previously observed in continental transform faults. The result is a relatively high ratio of foreshocks to aftershocks, similar to what is observed in the asperity-α combinations in Figure 2-2.

2.5 Real swarm events

We performed a similar analysis for a swarm that began in the southern Eyjafjarðaráll graben off the north coast of Iceland in the late summer of 2012 (Figure 2-3a). Data collected by the 55-station SIL seismic network was provided by the Icelandic Met Office (en.vedur.is). The bulk of the activity occurred between the Eyjafjarðaráll graben and the Húsavík-Flatey fault. Figure 2-3a shows a seismicity map of the events that occurred between Aug 20, 2012 and March 25, 2013, 66 and 66.75 degrees north latitude and -18 and -19.25 degrees longitude. We identified the fifteen largest events ($M \geq 2.5$) in the sequence. Eight of those events were associated with foreshock and/or aftershock

clusters that could be distinguished from the background swarm activity. The spatial and temporal distribution of those foreshock and aftershock events, relative to their respective mainshocks, is plotted in Figure 2-3b. Although here there is spatial clustering in addition to the temporal clustering evident in Figure 2-2, the similarity to Figures 2-2a(ii) and 2.2b(ii) provides further evidence for natural cases in which foreshock abundance is of the same order of magnitude and duration as aftershock sequences.

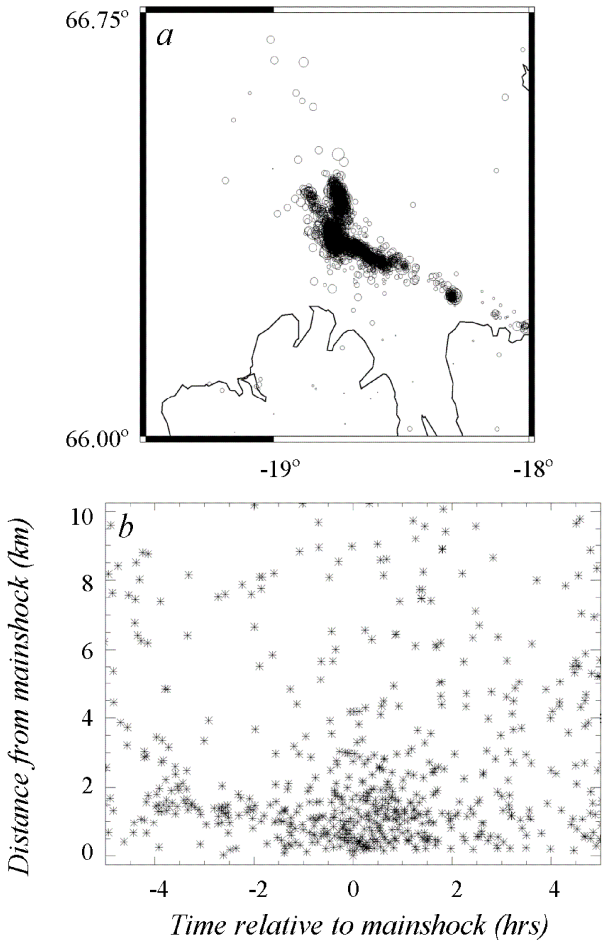

Figure 2-3 *(a) Swarm event, north Iceland, southern Eyjafjarðaráll graben, Aug 20, 2012 through March 25, 2013. (b) Spatiotemporal distribution of the seismicity associated with the twelve largest events in the sequence shown in (a).*

In order to better understand how the relative production of foreshocks and aftershocks is governed by the model parameters, we investigated the length of the average foreshock

and aftershock activation periods for different values of stress dissipation in our model. In general, lower dissipation models favor more frequent, larger events and higher dissipation suppresses the large events (Domiguez et al., 2013; Serino et al., 2011). This is also true for the asperity model, as shown in Figure 2-1d. However, stress dissipation appears to have an effect on the relative length of those foreshock sequences, as shown in Figure 2-4, where we plot the relative length of the foreshock and aftershock sequences, normalized by the total time period of each sequence. For low α values, the energy, or stress, available for foreshock activity is greater and initially results in an increased number of foreshocks, breaking more asperities. Once the mainshock occurs, there are fewer unbroken sites available for the occurrence of aftershocks. As a result, the aftershock sequence is shorter. On the other hand, in the higher dissipation systems, it is not until the occurrence of the largest event, the mainshock, that enough stress is injected into the surrounding sites to initiate the failure of large numbers of additional sites as aftershocks. High dissipation results in shorter foreshock sequences and relatively longer aftershock sequences (Figure 2-4).

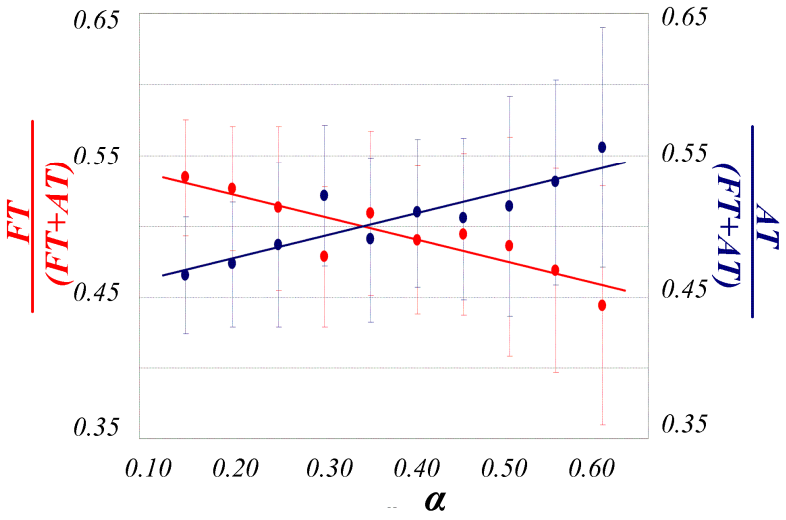

Figure 2-4 *The average time period associated with foreshocks and aftershocks as a function of stress dissipation, for a model with 1% asperities. FT: Foreshock time; AT = Aftershock time; Red = FT/(FT + AT); Blue = AT/(FT + AT); (FT + AT) = total time in the sequence.*

Again, as expected, the average number of all events is lower in models with higher stress dissipation, but the length of the total activity period also appears to be related to the stress dissipation parameter. Again, lower values of dissipation favor more frequent, larger events and higher dissipation values suppress large events. As a result, more plate updates are required to fail all of the asperities in the higher dissipation models.

2.6 Discussions

In summary, we present a long-range OFC model in which we have included randomly distributed asperities. While the asperities do not change the GR relation proposed in (Serino et al., 2011), this type of heterogeneity introduces temporal clustering similar to that seen in natural fault systems. For the first time in these models, we observe characteristic earthquake sequences associated with periods of activity which start with gradually increasing numbers of larger events, or foreshocks, that display AMR behavior, and end with a tail of decreasing activity, or aftershocks (Figure 2-2). The relative length of the foreshock and aftershock sequences varies, as observed in different tectonic regions (Figure 2-3). The length of the foreshock and aftershock activation is shown to be related to one or more controlling parameters of the model, including the stress dissipation (Figure 2-4), providing a potential explanation for the observation that certain tectonic regimes, such as mid-ocean ridges, produce measurable foreshock sequences, while others, such as crustal transform faults, produce very few foreshocks.. The results from this simple model also suggest that asperities are responsible for the time-dependent behavior observed in natural earthquake fault systems and support the hypothesis that spatial and temporal patterns observed in natural seismicity may be controlled by the underlying physical properties, rather than simple triggering alone. If the spatial and temporal patterns observed in natural seismicity are controlled by the underlying physical properties, this has broad implications for earthquake fault networks and other natural driven threshold systems in metastable equilibrium, suggesting that they may not be inherently unpredictable.

2.7 References

Alava, M. J., Nukala, P. and Zapperi S. (2006), Statistical models of fracture, Adv. Phys. 55, 349.

Bach, M., Wissel F. and Dressel, B. (2008). Olami-Feder-Christensen model with quenched disorder. Phys. Rev. E 77, 067101.

Bakun, W.H., Aagaard, B., Dost, B., Ellsworth, W.L., Hardebeck, J.L., Harris, R.A., Ji, C., Johnston, M.J.S., Langbein, J., Lienkaemper, J.J., Michael, A.J., Murray, J.R., Nadeau, R.M., Reasenberg, P.A., Reichle, M.S., Roeloffs, E.A., Shakal, A., Simpson R.W. and Waldhauser F. (2005). Implications for prediction and hazard assessment from the 2004 Parkfield earthquake. Nature 437, 969–974.

Båth M. (1965). Lateral inhomogeneities of the upper mantle, Tectonophysics, 2, 483–514.

Ben-Zion Y. and Lyakhovsky V. (2002). Accelerating seismic release and related aspects of seismicity patterns on earthquake faults, Pure Appl. Geophys., 159, 2385–2412.

Ben-Zion, Y. (2008). Collective Behavior of Earthquakes and Faults: Continuum-Discrete Transitions, Progressive Evolutionary Changes and Different Dynamic Regimes, Rev. Geophysics, 46, RG4006, doi:10.1029/2008RG000260.

Bowman D. D. and King G. C. (2001). Accelerating seismicity and stress accumulation before large earthquakes. Geophys. Res. Letters. 28: 4039-4042.

Bowman D. D., Ouillon G., Sammis C. G., Sornette A. and Sornette D. (1998). An observational test of the critical earthquake concept. J. Geophys. Res.103 (B10): 24,359 24,372.

Bufe C. G. and Varnes D. J. (1993). Predictive modeling of the seismic cycle for the greater San Francisco Bay region. J. Geophys. Res. 98: 9871-9883.

Burridge R. and Knopoff L. (1967). Model and theoretical seismicity, Bull. Seismol. Soc. Am. 57. 341–371.

Carlson J. M. and Langer J. S. (1989). Mechanical model of an earthquake fault. Phys. Rev. Lett. 62, 2632; Phys. Rev. A 40, 6470.

Ceva H. (1995). Inhuence of defects in a coupled map lattice modeling earthquakes. Phys. Rev, E52, 154.

Chen X. and Shearer P. M. (2013). California foreshock sequences suggest aseismic triggering process, doi: 10.1002/grl.50444.

Dodge, D.A., Beroza G.C. and Ellsworth, W.L. (1996). Detailed observations of California foreshock sequences: Implications for the earthquake initiation process. J. Geophys. Res., 101 (B10), pp. 22371–22392.

Dodge D.A. and Beroza G. C. (1997). Source array analysis of coda waves near the 1989 Loma Prieta, California, mainshock: Implications for the mechanism of coseismic velocity changes. J. Geophys. Res. 102, 24437–24458, (1997).

Dominguez, R., Tiampo, K.F., Serino C.A. and Klein W. (2013) Scaling of earthquake models with inhomogeneous stress dissipation. Phys. Rev. E 87, 022809.

Ellsworth, W. L., Lindh A.G., Prescott W.H. and Herd D.J. (1981). The 1906 San Francisco earthquake and the seismic cycle, in Earthquake Prediction: An Internation Review, Maurice Ewing Ser. Edited by D.W. Simpson and P. G. Richards. 4: 126-140.

Enescu B., Hainzl S. and Ben-Zion Y. (2009). Correlations of seismicity patterns in southern California with surface heat flow data. BSSA, 99(6): 3114-3123.

Helmstetter A. and Sornette D. (2002). Diffusion of epicenters of earthquake aftershocks, Omori's law, and generalized continuous-time random walk models, Phys. Rev. E., 66, 061104.

Jagla, E.A. (2010). Realistic spatial and temporal earthquake distributions in a modified Olami-Feder-Christensen model. Phys. Rev E 81, 046117.

Janosi I.M. and Kertesz J. (1993). Self-organized criticality with and without conservation. Physica A, 200, 0378.

Jordan T.H. and Jones L.M. (2010). Operational earthquake forecasting: some thoughts on why and how. Seismological Research Letters 81.

Kanamori H. (1981). The nature of seismicity patterns before large earthquakes, in Earthquake Prediction, Maurice Ewing Series, IV, 1–19, AGU, Washington D.C..

McGuire J. J., Boettcher M. S. and Jordan T. H. (2005). Foreshock sequences and short-term earthquake predictability on East Pacific Rise transform faults, Nature, 434.

Mousseau N. (1996). Synchronization by Disorder in Coupled Systems. Phys. Rev. Lett. 77, 968.

Nakanishi H. (1990). Cellular-automaton model of earthquakes with deterministic dynamics. Phys. Rev. A 41, 7086.

Ogata Y. (1983). Estimation of the Parameters in the Modified Omori Formula for Aftershock Frequencies by the Maximum Likelihood Procedure. Journal of Physics of the Earth 31, 115–124.

Ogata Y. (1999). Seismicity analysis through point-process modeling: A review, Pure Appl. Geophys., 155, 471–507.

Olami, Z., Feder, HJS. and Christensen K. (1992). Self-organized criticality in a continuous, nonconservative cellular automaton modeling earthquakes. Phys Rev Lett 68(8):1244–1247.

Otsuka M. (1972). A Simulation of earthquake occurrence, Phys. Earth Planetary Interior. 6-311.

Ramos O., Altshuler E. and Maloy, K.J. (2006). Quasiperiodic Events in an Earthquake Model. Phys. Rev. Lett. 96, 098501.

Richter, C. F. (1935). An instrumental earthquake magnitude scale. Bull. Seismol. Soc. Am. 25, 1-32.

Rundle J. B. and Jackson D. D. (1977). Numerical simulation of earthquake sequences, Bull. Seismol. Soc. Am. 67.

Rundle J. B. (1988). A physical model for earthquakes, J. Geophys. Res. 93-6237.

Rundle J. B. and Brown S. R. (1991). Origin of Rate Dependence in Frictional Sliding, J. Stat. Phys. 65, 403.

Serino, C.A., Tiampo, K. F. and Klein W. (2011.) New Approach to Gutenberg-Richter Scaling, Phys. Rev. Lett. 106, 108501.

Shcherbakov R. and Turcotte, D. L. (2004) A modified form of Båth's law, Bull. Seismol. Soc. Am., 94, 1968–1975.

Shearer P. M. (2012). Self-similar earthquake triggering, Båth's law, and foreshock/aftershock magnitudes: Simulations, theory, and results for southern California, J. Geophys. Res., 117, B06310.

Sornette D. and Sammis C. G. (1995). Complex critical exponents from renormalization group theory of earthquakes: Implications for earthquake predictions, J.Phys.I France 5, 607-619.

Sykes L.R. and Jaumé S.C. (1990). Seismic activity on neighboring faults as a long term precursor to large earthquakes in the San Francisco Bay area. Nature. 348: 595-599.

Torvund F. and Froyland J. (1995). Strong ordering by non-uniformity of thresholds in a coupled map lattice. Physica Scripta 52, 624.

Turcotte D. L., Newman W. I. and Shcherbakov R. (2003). Micro and macroscopic models of rock fracture. Geophys. J. Int., 152, 718–728.

Utsu T., Ogata Y. and Matsu'ura, R.S. (1995). The centenary of the Omori formula for a decay law of aftershock activity. Journal of Physics of the Earth 43, 1–33.

Zoller, G., Hainzl, S., Ben-Zion Y. and Holschneider M. (2006). Earthquake activity related to seismic cycles in a model for a heterogeneous strike-slip fault, Tectonophys., 423, 137–145.

Chapter 3

3 Spatiotemporal clustering in simple earthquake fault models

The work in this chapter extends the findings from the previous chapter on the simple, long-range cellular automata model for earthquake fault systems by increasing the number and configuration of randomly distributed asperity sites. We observe a rich array of spatial and temporal clustering, including large, recurrent events with foreshock and aftershock sequences and accelerating seismic moment release. From this simple model we conclude that the spatial heterogeneity is responsible for the primary features of those sequences, including the size of the largest events and the upper bound or taper, of the modified GR relation. Those are modulated by the amplitude of the stress dissipation of the system. In addition, this study shows that the relative activation rate of the foreshock and aftershock sequences can be modulated by the stress dissipation, which may help to explain similar variations in the observations of earthquake sequences in different tectonic regimes. This work provides support for the hypothesis that the spatial and temporal patterns observed in natural seismicity are, at least in part, controlled by the underlying physical properties, which is significantly different from the interpretation, based on self-organized criticality (SOC), that a simple cascade mechanism is the basis for these sequences. This interpretation has important implications for understanding large earthquakes, suggesting that they may not be inherently unpredictable.

3.1 Introduction

While understanding the dynamics of seismic activity is fundamental to the investigation of the earthquake process, detailed studies of the earthquake fault system are difficult because the underlying dynamics of the system are not observable (Herz and Hopfield, 1995; Rundle et al., 2000). In addition, the fact that nonlinear earthquake dynamics are coupled across a broad range of spatial and temporal scales (Kanamori, 1981; Main, 1996; Turcotte, 1997; Rundle et al., 1999; Scholz, 2002), combined with the occurrence of rare, extreme events and the associated patterns in seismic data (Schorlemmer and Gerstenberger, 2007; Vere-Jones, 1995, 2006; Zechar et al., 2010), means that computational simulations are critical to our understanding of the dynamics of the earthquake systems (see, e.g., Rundle et al., 2003).

The mechanisms governing the fracture evolution of a fault can vary significantly, depending on the associated materials, the nature and rate of applied load, and the amount of disorder in the system. Numerical and experimental models of both rock fracture and the earthquake process suggest that spatial inhomogeneities in the fault network play an important role in the occurrence of large events (Dahmen et al., 1998; Turcotte et al., 2003; Lyakhovsky and Ben-Zion, 2009; Serino et al., 2011, Dominguez et al., 2012, 2013). The nature of these fault inhomogeneities is dependent on the geologic history of the fault, and because this history is typically quite complex, the distribution of these inhomogeneities occurs on many length scales. The inhomogeneous nature of the fault system manifests itself in the spatial and temporal patterns in the network seismicity (Tiampo et al., 2002, 2007; Tiampo and Shcherbakov, 2012).

Simple models of statistical fracture have been employed effectively to test many of the typical assumptions and effective parameters inherent in the complicated dynamics of the earthquake fault system and their relative variability. These models have been employed with remarkable success to advance our understanding of the statistical properties of earthquakes (Burridge and Knopoff, 1967; Otsuka, 1972; Rundle and Jackson, 1977; Rundle, 1988; Carlson and Langer, 1989; Nakanishi, 1990; Rundle and Brown, 1991; Olami et al., 1992; Klein et al., 1997; Klein et al., 2000; Alava et al. 2006; Mori and

Kawamura, 2008a, b). Burridge and Knopoff (1967) introduced a one-dimensional (1D) system of spring and blocks to study the role of friction along a fault in the propagation of an earthquake. Later Rundle and Brown (1991) presented a version with frictional sliding using the Mohr-Coulomb friction law that ignored inertial effects. Olami, Feder and Christensen (1992) generalized Bak, Tang and Wiesenfeld (1987) sand-pile model and introduced a lattice version of the continuous, nonconservative cellular automata model (OFC) to investigate SOC behaviour in earthquakes. However, most of these models included only short-range stress transfer. None incorporated spatial heterogeneity into these earthquake-like fault models.

Because inhomogeneity plays an important role in the spatial and temporal behaviour of an earthquake fault (Serino et al., 2011; Dominguez et al., 2012, 2013), these models recently have been expanded to include different types of inhomogeneity, generally by varying individual parameters along the fault plane. Several studies incorporated inhomogeneity into OFC models, although only for those with short-range or nearest neighbor stress transfer (Janosi and Kertesz, 1993; Torvund and Froyland, 1995; Ceva, 1995; Mousseau, 1996; Ramos et al. 2006; Bach et al., 2008; Jagla, 2010). However, stress transfer in natural earthquake faults is elastic and, as a result, models with long-range interactions produce more realistic representations (Fisher et al., 1997; Ben Zion et al., 2008; Serino et al., 2011). OFC models with long-range stress transfer produce mean-field systems in stable or quasi-stable equilibrium, unlike short-range OFC models, and the existence and range of GR scaling is related to those periods of equilibrium (Gulbace et al., 2004; Klein et al., 2000, 2006; Rundle et al., 1995, 2000; Serino et al., 2011). In these mean-field systems near spinodal critical points, large events drive the system away from the critical point while small events bring it closer, resulting in GR scaling over several orders of magnitude.

Over the past few years, the incorporation of damage into long-range OFC models have provided insights into the nature of GR scaling, its relation to the critical point and the earthquake cycle, and the interaction between structure and the critical point process (Serino et al., 2011; Dominguez et al., 2012, 2013). Results suggest that the interaction between structure, or geometry, has an important effect on the critical point process.

Spatial features impact the earthquake fault process – the interplay between geometry and the critical point process affects how close the fault is to the critical point.

Serino et al. (2011) incorporated damage inhomogeneities into the long-range OFC model in the form of stress relieving micro-cracks, resulting in a better understanding of the earthquake frequency-size distribution. The Gutenberg-Richter (GR) distribution (Richter, 1935; Gutenberg and Richter, 1956) usually is expressed as $\log(N) = a - bM$, where N is the total number of earthquakes of magnitude M or greater, and a and b are model parameters (Turcotte, 1997). However, the form of this distribution is more uncertain for large events. Physical limitations suggest that there is an upper bound or taper and a maximum size for extreme events (Main, 1996; Kagan and Jackson, 2000; Bell et al., 2013). A modified GR relation (MGR) has been proposed that adds an exponential tail to the cumulative form, with an exponential cutoff at the corner moment or magnitude (Turcotte, 1997). A global catalog with GR scaling then is composed of many superimposed regional catalogs, each with different upper bounds. However, controversy remains as to the statistical limitations inherent in the data. For example, Zöller (2013) maintained that convergence to a specific distribution, if it ever occurs, requires approximately 200 years of homogeneous recording of global seismicity.

The model of Serino et al. (2011) introduced a physical basis for the MGR form of the magnitude-frequency distribution that depends on the level of damage in each fault network, denoted by a damage parameter q. The introduction of damage into the system results in an MGR distribution for individual faults and the corner magnitude is dependent on the amount of damage. The scaling exponent depends on the relative frequency with which faults with a particular amount of damage occur in the fault system. In aggregate, these non-interacting simple lattice models with different levels of damage produce GR scaling over much larger orders of magnitude, although the individual damaged models do not necessarily have well-defined scaling at the large event sizes. This paradigm results in an explanation for regional GR scaling as a result of the aggregation of varying amounts of damage in families of individual faults.

In subsequent work, Dominguez et al., (2012, 2013) incorporated spatial inhomogeneity into the lattice by clustering the dead sites in various patterns. They found that the scaling depends not only on the amount of damage but also on the spatial distribution of that damage. However, to date, none of the short or long-range models have been able to reproduce the variety of temporal clustering that is a primary feature of natural seismicity and a critical component in the assessment of earthquake hazard. In this work, motivated by the structure of natural faults, we incorporate damage in the form of asperities into a simple cellular automata model for earthquake fault systems with long-range stress transfer. These asperity sites fail less frequently than the regular sites, providing a time-dependent source and sink of stress, storing dissipated stress until asperity failure releases it back into the system. The addition of structural asperities leaves the MGR scaling intact but produces clustering of foreshocks and aftershocks as well as large quasi-periodic events.

The model is a cellular automata version of earthquake faults based on the OFC (Olami et al., 1992) and RJB (Rundle and Jackson, 1977; Rundle and Brown, 1991) models with some minor variations. Inhomogeneities are imposed on the model by inserting a percentage of either organized or randomly selected locations that accumulate higher levels of stress, similar to asperities on natural faults. These sites are incorporated by varying the ability of these individual sites to support much higher levels of stress. We observe a rich array of spatial and temporal clustering for the first time in these models, including large, recurrent events, seismic sequences consisting of foreshocks, mainshock and aftershocks, and accelerating moment release (AMR). In addition, we investigate the relationship between the spatial and temporal properties of the seismic sequences and the various parameters of the model, such as the overall stress dissipation and the percentage of asperities. These statistics include the magnitude-frequency distribution scaling regime for the largest events, the relative activation of the foreshock and aftershock sequences, AMR and Thirumalai-Mountain (TM) metric fluctuations prior to the sequence mainshock and the Omori law for foreshocks and aftershocks.

This paper is organized as follows. In Section 2, the model dynamics and details of the simulations are introduced. The magnitude-frequency distribution of events for various

amounts of inhomogeneities (asperity sites) in the lattice as well as the scaling behavior of the model is investigated in Section 3. Section 4 discusses various types of spatiotemporal clustering of events which are observed by imposing different spatial configuration of asperities in the model. These include AMR signals observed before the mainshocks and the Omori law behaviour for foreshocks and aftershocks. Also, an analysis of the TM metric behaviour (Thirumalai et al. 1989; Tiampo et al. 2003, 2007, 2010), here an indicator of increased activity before the main event, is introduced in Section 4. Finally, Section 5 presents a summary and discussion.

3.2 The model

The model is a two-dimensional cellular automaton model with periodic boundary conditions. In this model every site in the lattice is connected to z neighbors, which are defined as sites within a certain distance or stress interaction range, R. A homogeneous residual stress σ^r is assigned to all the sites in the lattice. To impose spatial inhomogeneity on the lattice, two sets of failure thresholds are introduced; 'regular sites' with a constant failure threshold of σ^f and 'asperity sites' with a much higher failure threshold ($\sigma^f_{(asperity)} = \sigma^f + \Delta\sigma^f$). These asperity sites incorporate a percentage of stronger sites into the lattice that will support higher stress before failure.

Initially, the internal stress variable, $\sigma_j(t)$, is randomly distributed on each site in such a way that the stress on all sites lies between the residual and failure stress thresholds ($\sigma^r < \sigma_i(t=0) < \sigma^f$). At $t=0$ no sites will have $\sigma_i > \sigma^f$. There are several ways to simulate the increase in stress associated with the dynamics of plate tectonics. Here we use the so-called zero velocity limit (Olami et al., 1992). The entire lattice is searched for the site that minimizes ($\sigma^f - \sigma_i$) and that amount of stress is added to each site such that the stress on at least one site is now equal to its failure threshold. That site fails and some fraction of its stress, given by $\alpha\ [\sigma^f - (\sigma^r \pm \eta)]$, is dissipated from the system. α is a dissipation parameter ($0 < \alpha \leq 1$) which describes the portion of stress dissipated from the failed site and η is randomly distributed noise. Stress on the failed site is lowered to ($\sigma^r \pm \eta$) and the remaining stress is distributed to its neighbors.

After the first site failure, all neighbors, including asperity sites, are searched to determine if the stress change from the failed site caused any of others to reach their failure stress. If so, the described procedure repeats for those neighbors and if not, the time step (known as the plate update) increases by unity and the lattice is searched again for the next site which minimizes (σ^f - σ_i). The size of each event is calculated from the total number of failures that expand from the first failed site during that plate update, or time step. Unlike the original model, stress is dissipated from the system both at the regular lattice sites and through asperity sites which are placed inhomogeneously throughout the lattice. The asperity sites fail less frequently than the regular sites and release much higher stress at the time of their failure resulting in inhomogeneous, time-dependent stress dissipation in this model.

Initial results for two different, organized spatial distributions of asperities are shown in Figure 3-1. In Figure 3-1a, 5% of the sites are designated as asperities and grouped in one large asperity. In Figure 3-1b, 10% of the total lattice sites are selected as asperity sites and grouped together. The associated magnitude-frequency relations are plotted for varying values of α. Both plots support previous results that increasing the stress dissipation decreases the length of the scaling regime (Serino et al., 2011; Dominguez et al., 2012, 2013).

3.3 Event Size Scaling

The magnitude-frequency scaling of the long-range OFC model introduced in Section 2 is studied in greater detail in order to investigate the effect of spatial inhomogeneities in earthquake fault-like systems with long-range stress transfer. Serino et al. (2011) studied an inhomogeneous version of OFC models with long-range stress transfer by adding random damage into the lattice and Dominguez et al., (2013) extended it by imposing various spatial configurations of damage into the model. They studied various amounts of stress dissipation, α ($0<\alpha\leq 1$) and showed that both stress dissipation and damage dissipation reduce the length of the scaling regime in the resulting magnitude-frequency distributions and reduce the size of the largest events.

Here, we study the magnitude-frequency distribution of events in our inhomogeneous model for different percentages of asperity sites by changing the number of stronger sites in the lattice. We find that the scaling relationship for the heterogeneous systems depends on the total amount of the asperity sites. We begin this study with the two different large size asperity blocks shown in Figure 3-1 and their associated magnitude-frequency relation plotted for varying values of stress dissipation.

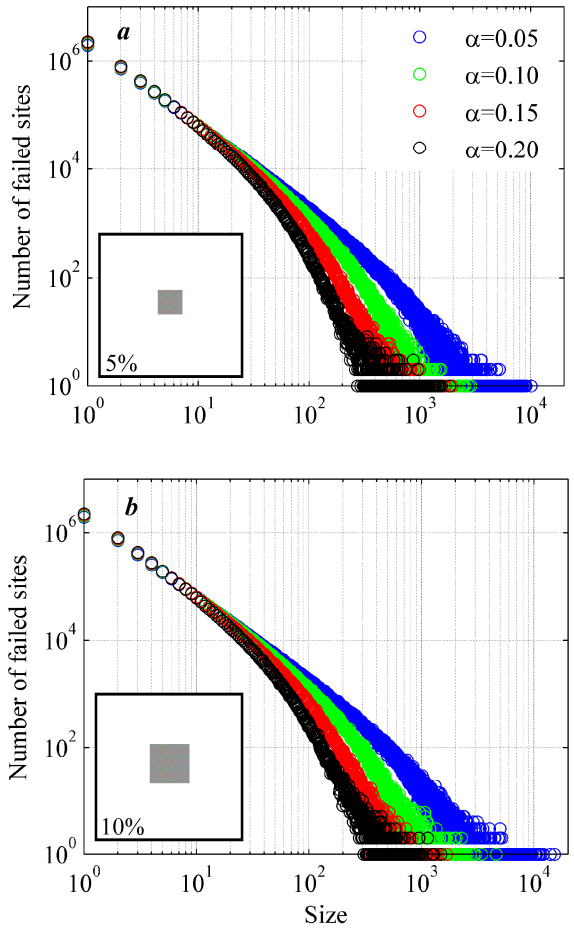

Figure 3-1 *Numerical distribution of event sizes for varying values of stress dissipation, α, for the asperity grouping as shown in the inset. a) 5% asperity sites, small block; b) 10% asperity sites, large block.*

The results confirm previous findings that higher values of stress dissipation in the system decrease the length of the region in which the event sizes follow a scaling form. However, it also shows that the larger asperity region (Figure 3-1b) promotes the

occurrence of larger events for lower values of dissipation (α = 0.05 and 0.10), while previous work (Serino et al., 2011; Dominguez et al., 2012, 2013) showed that increasing the number of damaged sites results in fewer extreme events.This distinction is a result of the different functionality of a dead site and an asperity site. As detailed above, a dead site in the lattice is a source of inhomogeneous stress dissipation in the model. Therefore, increasing the number of dead (damaged) sites increases the total overall amount of stress dissipation in the system. On the other hand, a stronger asperity site has a dual role. They act as a dead site while the applied stress has not reached their higher failure threshold, but when they break they input a higher amount of released stress back into the system. This large amount of released stress, relative to the background stress release occurring between the large characteristic-type events, has a greater effect on those sites within its interaction range for systems with lower dissipation. The result is the failure of a large number of neighboring asperity sites and larger mainshock events.

To better understand this relationship, we extend this study by imposing a percentage of *randomly* distributed asperity sites into the lattice. As expected from the results seen in Figure 3-1, the magnitude-frequency event distribution confirms that as the percentage of asperities increases, the system produces significantly larger events (Figure 3-2a). However, the region in which the event sizes follow a scaling form becomes shorter and the relative number of moderate-sized events decreases as the number of asperities in the lattice is increased (Figure 3-2b). By increasing the number of asperities in the lattice, some of the moderate events appear to grow into a larger event. This migration from the moderate to large sizes is the consequence of two effects. When an asperity site breaks, a greater amount of stress is released into the system and that amount of released stress can cause the failure of more sites, especially in a system with long range stress transfer. In addition, a greater number of randomly distributed asperity sites in the lattice increases the probability of asperity sites triggering each other. A system with a higher density of asperities increases the chance that asperity blocks are inside the stress transfer range of a failing asperity. That failure can result in a cascade behavior and a greater likelihood for a moderate-sized event to grow and become an extreme event.

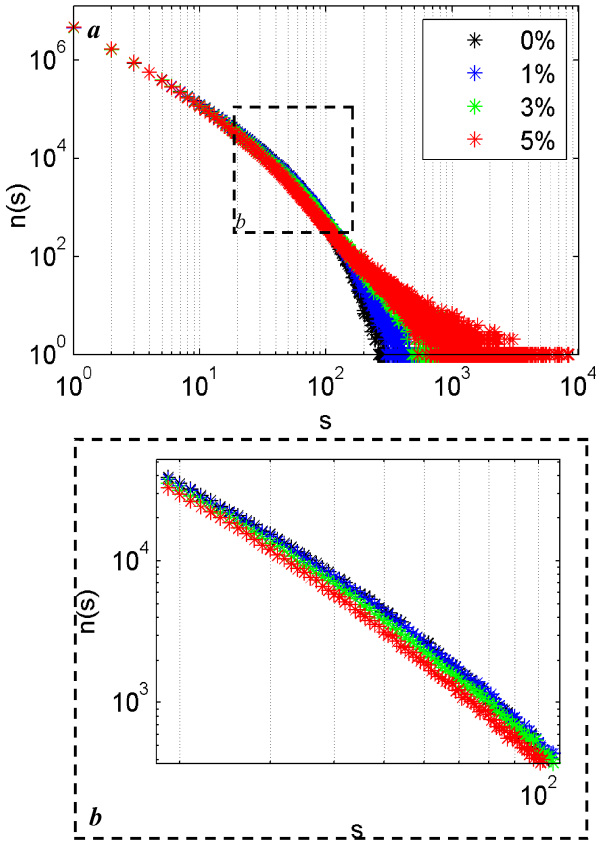

Figure 3-2 *a) Magnitude-frequency distribution of events of size "s" for various amounts of randomly distributed asperity sites in a system with low stress dissipation, α=0.2; b) a closer view of the dashed box in a.*

We compare the effect of stress dissipation parameters in a model with different amount of asperity sites and long-range stress transfer, R=16. As discussed earlier, some fraction of stress on a site, given by α $[\sigma^F-(\sigma^r\pm\eta)]$, is dissipated from the system at failure ($0<\alpha\leq 1$). In general, lower stress dissipation models produce larger events and higher stress dissipation suppresses large events. This also should be true in a system with asperity sites. In higher dissipation models, less stress is transferred to neighboring sites, even when asperities fail. As a result, there is a lower probability of an asperity triggering in the model. This implies that more plate update steps and a greater number of smaller events in general are required to trigger failure of all of the asperities,

In Figure 3-3, the event distribution for three different stress dissipation parameters, α=0.2, 0.4 and 0.6, is compared for three different percentages of asperity sites (1%, 3% and 5%). 20%, 40% and 60% of the failed site stress dissipates at the time of failure and the remaining stress is distributed to z=1088 neighbors.

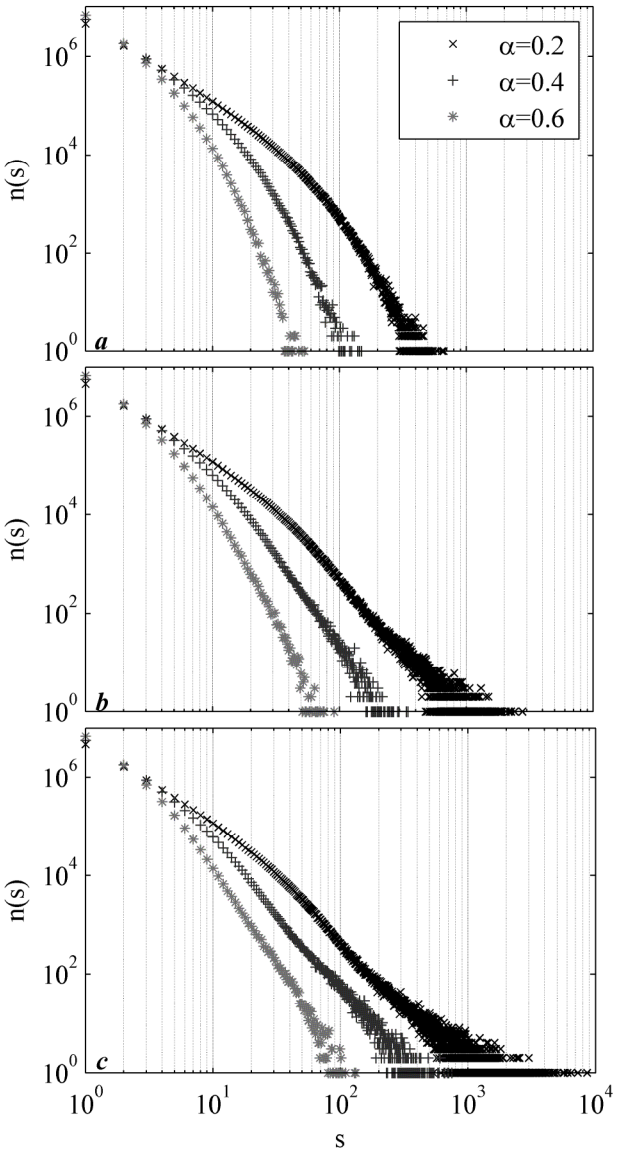

Figure 3-3 *Magnitude-frequency distribution of events of size "s" for three different stress dissipation parameters, α=0.2, 0.4 and 0.6, in a system with randomly distributed asperity sites and a) 1%, b) 3%, and c) 5% of asperity sites.*

For all three different percentages of asperities (Figure 3-3a, b and c), lower values of stress dissipation leads to a higher number of large events. On the other hand, in systems with a high amount of stress dissipation, the released stress from a less dense asperity site distribution (1%) is not enough to offset the greater dissipation and does not trigger any of the neighboring asperities. As a result, since asperities are not able to trigger each other, the system does not produce large events even in the case of distribution of 5% of asperity sites (Figure 3-3a, b and c).

We also compared the scaling in our system with the scaling of regular OFC with no asperity sites. Klein et al. (2007) studied the mean-field limit of OFC models with no damage and found that the number of events of size s for a noncumulative distribution is associated with a spinodal critical point and obeys the scaling

$$n(s) \sim \frac{e^{-\Delta h\, s^{\sigma}}}{s^{\tau}}, \tag{3.1}$$

where $n(s)$ is the number of events of size s, $\tau = 3/2$, $\sigma = 1$, and Δh is a measure of the distance from the spinodal. The distribution approaches a power law distribution as the dissipation parameter goes to zero. We apply the above scaling form to a system with no asperity sites for a range of stress dissipation parameters (0.05, 0.2, 0.4 and 0.6). Figure 3-4a shows the result of fitting Equation 1 to the magnitude-frequency event sized distribution. The best fit parameters for Equation 1 are listed in Table 3-1.

Table 3-1 Exponents of the model for magnitude frequency distributions in Figure 3-4.

Dissipation	$n_0 * 10^6$	Δh	σ	τ	*RMSE*
α=0.05	3.93	0.001	1.007	1.48	1.001
α=0.20	4.68	0.026	0.988	1.47	1.006
α=0.40	6.19	0.116	0.996	1.45	1.024
α=0.60	9.70	0.372	0.963	1.38	1.065

In order to further investigate the scaling behavior of the model, we investigated the data collapse of the magnitude-frequency distribution. Data-collapse is a method for establishing scaling in complex systems that show self-similar behavior and extracting the associated exponents. Data collapse is based on the hypothesis which predicts that all the curves for many simple systems with scaling can be ‘‘collapsed’’ onto a single curve, given that the correct renormalization values are chosen to scale the variable for each system (Stanley, 1999). Serino et al. (2011) showed that lattices with a spatially uniform distribution of damage follow the above scaling form (Equation 1) and the magnitude-frequency distributions collapse to a single curve in the form of Equation 1. They rescaled their data to $n_z\,(1\text{-}q)\,/\,q^3$ versus $z = q^2 s$, where q is the fraction of dead sites for uniform, randomly distributed damage. In their model, dead sites are spatially distributed sources of stress dissipation in addition to the regular stress dissipation parameter (α) of the system. Therefore the fraction of the dead sites (q) is the representative of the total damage in the model. In other words, higher values of q means higher dissipation in the system with constant stress dissipation parameter (α=constant).

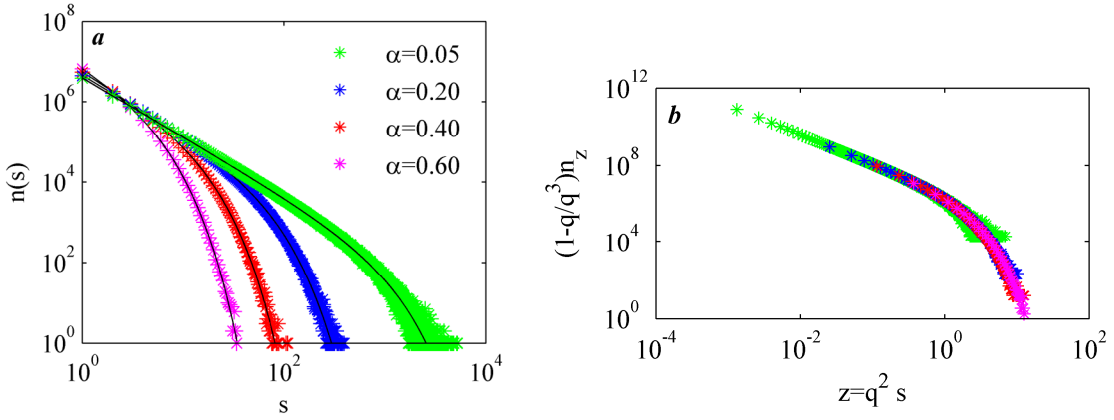

Figure 3-4 *a) Magnitude-frequency distribution of events of size “s” for a system without asperity cells for three different stress dissipation parameters α=0.05, 0.20, 0.40 and 0.60, the parameters of the model are listed in Table 1. b) The distribution of event sizes, n(s), weighted by $(1 - q)/q^3$ versus the scaling variable $z = q^2 s$. The data collapses to a single curve as in Serino et al. (2011).*

Because the initial values of α are changing in our model, we tested different scaling parameters and determined the best fit to be $q = (\Delta h)^{0.5}$ for the exponents in Table 1. It appears that Δh is representative of the total stress dissipation of the system, which is an aggregation of different parameters, including α and the total amount of inhomogeneity, in terms of dead sites. In Figure 3-4b, we plot the number of events of size s, scaled by $(1\text{-}q) \,/\, q^3$, versus the scaling variable $z = q^2 s$, with $q = (\Delta h)^{0.5}$, for a model without asperities and four different stress dissipation parameters (5%, 20%, 40% and 60%). The successful collapse into one curve in Figure 3-4b further confirms the validity of the scaling form of Equation 1 (Klein et al., 2007).

Table 3-2 Exponents of the model for magnitude frequency distributions in Figure 3-5.

	$n(s) = n_0 \frac{e^{-\Delta h s^{\sigma}}}{s^{\tau}}$						
Asperity Percentage	Dissipation	Model	$n_0 * 10^6$	Δh	σ	τ	RMSE
1 %	*α=0.05*	*red*	4.03	0.004	0.838	1.48	1.004
		blue	2.75	0.003	0.838	1.48	1.000
	α=0.20	*red*	4.78	0.053	0.840	1.43	1.021
		blue	1.80	0.039	0.840	1.43	1.003
	α=0.40	*red*	7.01	0.244	0.809	1.33	1.074
		blue	4.33	0.219	0809	1.33	1.012
	α=0.60	*red*	10.3	0.428	0.919	1.35	1.168
		blue	1.83	0.296	0.919	1.35	1.036
3 %	*α=0.05*	*red*	4.11	0.010	0.784	1.48	1.004
		blue	0.50	0.0001	0.784	1.48	1.000
	α=0.20	*red*	5.09	0.105	0.721	1.39	1.021
		blue	0.23	0.022	0.721	1.39	1.001
	α=0.40	*red*	7.58	0.312	0.752	1.31	1.074
		blue	0.44	0.119	0.752	1.31	1.005
	α=0.60	*red*	13.2	0.673	0.784	1.21	1.168
		blue	0.72	0.331	0.784	1.21	1.021
5 %	*α=0.05*	*red*	4.21	0.025	0.685	1.46	1,004
		blue	0.39	0.0001	0.685	1.46	1.000
	α=0.20	*red*	5.35	0.141	0.686	1.37	1.021
		blue	0.12	0.013	0.686	1.37	1.001
	α=0.40	*red*	8.01	0.357	0.732	1.29	1.074
		blue	0.16	0.067	0.732	1.29	1.003
	α=0.60	*red*	16.6	0.893	0.708	1.12	1.168
		blue	0.31	0.312	0.708	1.12	1.013

We apply this scaling equation to the systems with asperities. We have already observed that imposing a random distribution of stronger sites into the system promotes events of larger size in the system.

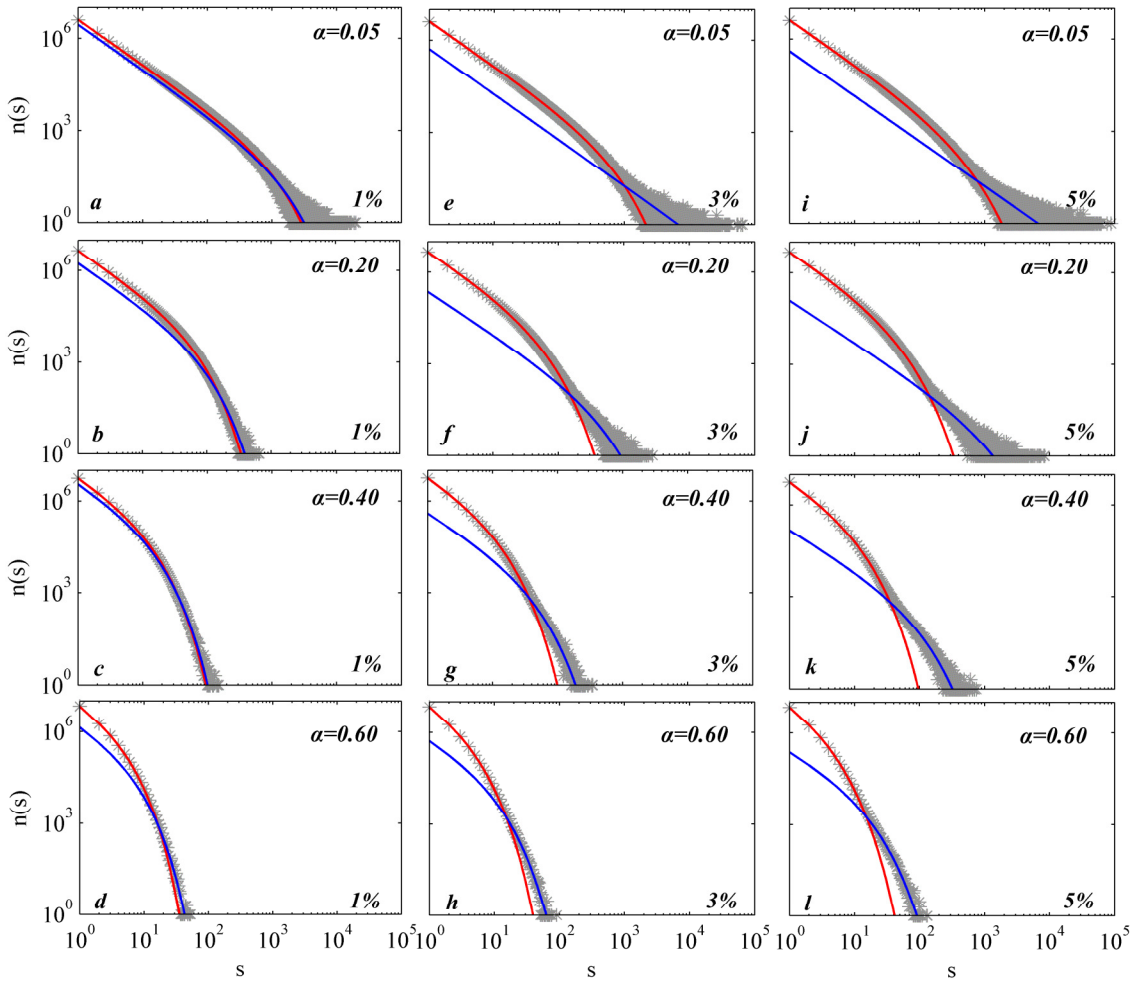

Figure 3-5 *Magnitude-frequency distribution of events of size "s". a) 1% asperity, α=0.05, b) 1% asperity, α=0.20 c) 1% asperity, α=0.40 d) 1% asperity, α=0.60 e) 3% asperity, α=0.05 f) 3% asperity, α=0.20 g) 3% asperity, α=0.40 h) 3% asperity, α=0.60 i) 5% asperity, α=0.05 j) 5% asperity, α=0.20 k) 5% asperity, α=0.30 l) 5% asperity, α=0.60. The red line of each graph shows the model that is used for the small size events and blue line shows the model for large size events. The exponents of each model are shown in Table 2.*

It appears that the magnitude-frequency distribution of events in systems with asperity sites is a combination of two different distributions; one for the small events and the second for the larger events. The second scaling form for larger events is difficult to observe in systems with only 1% of asperity sites, but increasing the number of asperities to 3% and 5% makes it easier to distinguish the second distribution in the tails of the distribution. In order to fit the two distributions, we choose a cross-over size which is the point on the magnitude-frequency distributions where two distributions separate. We then apply the scaling form of the Equation 1, above, only to those events smaller than the cross-over size. We then apply the same scaling model for larger events bigger than the cross-over size. Since the tail of the magnitude-frequency distributions for the large events is wide, we confined our model by fixing two of the four parameters to those values that we obtained from the small size model. This is based on the hypothesis that the two different distributions are the result of a single model with a constant percentage of asperities and stress dissipation and that σ and τ are related to both. As seen in Table 2, σ and τ for the larger events (blue line) are fixed to the corresponding values obtained from the smaller events (red line), and n_0 and Δh values are fit separately.

Figure 3-5 shows the results for several stress dissipation parameters in a system with different percentages of asperity sites. The exponents of the model are shown in Table 2. From these results, it appears that τ is a function of stress dissipation in the system while σ is function of both percentage of asperities and stress dissipation.

In Serino et al. (2011) Δh depends on damage, which was defined as the number of dead sites in the model. Our results also confirm the dependency of Δh on the damage in the system. However, we find that Δh depends both on the number and characteristics of asperities but it also is a function of the stress dissipation parameter. The stronger asperity sites in the system dissipate large amounts of stress during their failure, so here we define damage as a function of both the number of asperities and the stress dissipation parameter α. As described above, asperity triggering in this system means that the failure of one asperity site can trigger the other neighboring asperity sites to fail and results in the clustering of bigger events in the system. We also know that failure of an asperity site that has stored a large amount of stress dissipates a higher amount of stress from the

system (higher damage) and therefore imposes a time dependence on the model damage. On the other hand, larger events occur during asperity failure in this model. As discussed above, the maximum time-dependent stress release occurs during these time steps and is the most likely cause of the different values of Δh for the models in Table2.

3.4 Earthquake Clustering

The terms “earthquake cycle”, “seismic cycle” and “characteristic earthquake” have been used to describe the regularly occurring cycles of earthquake activity, including large events that are similar in magnitude and location. Temporal and spatial clustering is evident in seismicity data, including activation and quiescence, foreshock and aftershock sequences, repeating events, and variations in the rate of occurrence (see, e.g., Båth, 1965; Mogi, 1969; Swan et al., 1980; Habermann, 1981; Ogata, 1983; Bakun et al., 1986; Frohlich, 1987; Rundle, 1989; Keilis-Borok and Kossobokov, 1990; Kanamori, 1981; Pacheco et al., 1992; Bufe and Varnes, 1993; Romanowicz and Rundle, 1993; Gross and Kisslinger, 1994; King et al., 1994; Utsu et al., 1995; Dodge et al., 1996; Deng and Sykes, 1996; Gomberg, 1996; Wyss et al.,1996; Pollitz and Sacks, 1997; Ellsworth and Cole, 1997; Eneva and Ben-Zion, 1997; Jones and Hauksson, 1997; Nanjo et al., 1998; Bowman et al., 1998; Brehm and Braile, 1998; Jaume and Sykes, 1999; Tiampo et al., 2002; Shcherbakov and Turcotte, 2004; Tiampo et al., 2006a,b; Tiampo and Shcherbakov, 2012). This aspect of earthquake behavior is an essential characteristic of seismic sequences on different scales.

Most earthquake clusters consist of the mainshock and its following aftershocks. As noted above, aftershocks are the most easily identified clustering pattern in seismic catalogs. Aftershocks occur immediately after their triggering mainshocks and their rate usually decays with time, following the power law relation known as the modified Omori law (Ogata, 1983; Utsu et al., 1995). Alternatively, there is evidence of precursory earthquakes or foreshocks before a number of large events around the world, although they are more difficult to detect (Rikitake, 1976; Jones and Molnar, 1979; Ellsworth et al., 1981; Sykes and Jaumé, 1990; Bufe and Varnes, 1993; Bowman et al., 1998; Brehm and Braile, 1998; Jaumé and Sykes, 1999; Robinson, 2000; Bowman and King, 2001;

Ben-Zion and Lyakhovsky, 2002; Turcotte et al., 2003; Bakun et al., 2005; Mignan, 2008; Jordan and Jones, 2010; Shearer, 2012).

The ETAS (Epidemic Type Aftershock-Sequences) model (Ogata, 1999; Helmstetter and Sornette, 2002) is a triggering model based on the concept that every event, regardless of its size, increases the probability of later events. In ETAS, not only do mainshocks trigger aftershocks, they can trigger aftershocks with magnitudes larger than themselves. If the largest event is triggered by earlier, smaller events, these are classified as foreshocks. While ETAS can model many features of earthquake clustering seen in natural seismicity, recent work suggests that these triggering models may not fully explain the foreshock-mainshock-aftershock process and that other mechanisms may be important (Dodge et al., 1997; Enescu et al., 2009; Shearer, 2012). For example, Chen and Shearer (2013) studied foreshock sequences for M > 7 earthquakes in California and determined that they behaved more like swarms initiated by aseismic transients rather than triggered cascades or a nucleation process. These foreshock sequences occurred in areas of significant fault zone complexity, highlighting the importance of heterogeneity in the clustering process.

3.4.1 Temporal clustering of events

The concept of recurrent large events, or characteristic earthquakes, was first introduced by Schwartz et al. (1981) and Schwartz and Coppersmith (1984), based on the early work of Reid (1910). Based on elastic rebound theory, it hypothesizes that earthquakes repeatedly rupture the same fault segments with the similar magnitude and slip distribution (Ellsworth and Cole, 1997; Parsons and Geist, 2009; Schwartz and Coppersmith, 1984; Schwartz et al., 1981; Wesnousky, 1994).

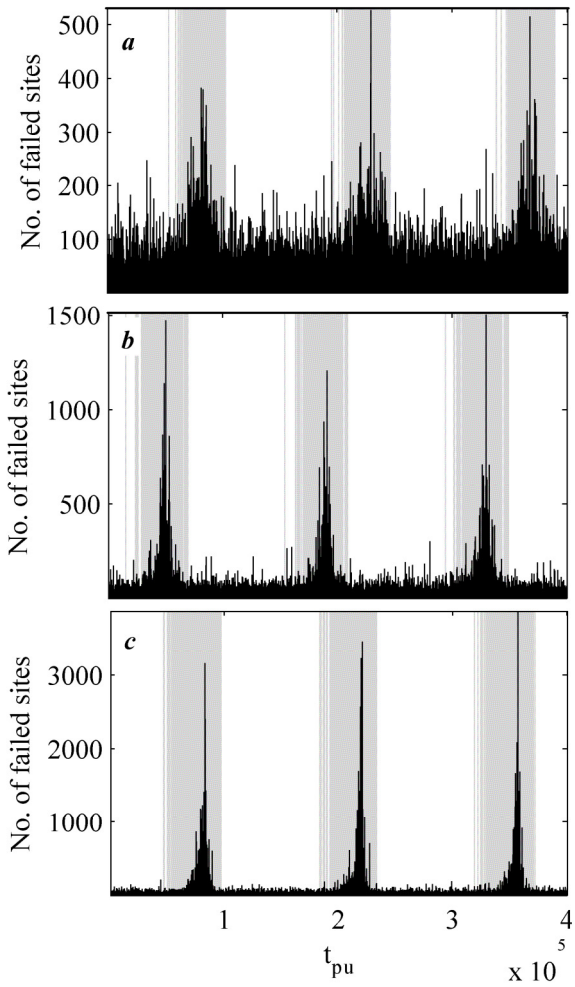

Figure 3-6 *Recurrence of the large events on the time series of events during a period of $4*10^5$ pu for three different amount of asperity sites (a-1%, b-3% and c-5%) and the stress dissipation parameter $\alpha = 0.2$.*

Here, we study the model described in Section 2 with 1%, 3% and 5% of randomly distributed asperity sites in a two-dimensional lattice of linear size L=256 with periodic boundary conditions. We considered a homogeneous failure threshold for the regular sites as σ^f=2.0, homogeneous residual stress for the entire lattice as σ^r=1.0, and temporal random distribution of noise as η=[-0.1,+0.1]. The failure threshold for asperity sites is also considered as $\sigma^f_{(asperity)} = \sigma^f + 10$. The system has the stress transfer range of R=16 and every site in the lattice is connected to z=1088 neighbors. Although the asperity sites have random spatial distributions, temporal clustering of events is clearly visible in Figure 3-6.

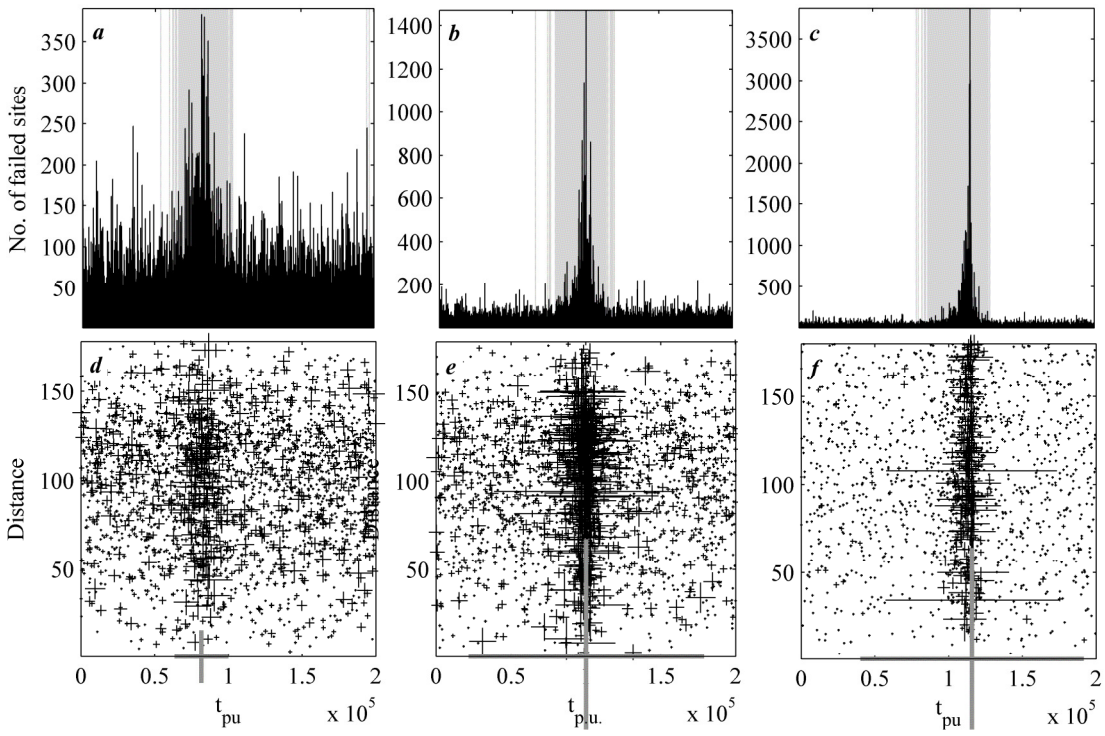

Figure 3-7 *Time series of events of a system with randomly distributed asperity sites and a) 1%, b) 3%, and c) 5% of asperity sites. (Shaded areas indicate the steps where an asperity site breaks.) The distance of each event from the biggest event in the sequence for the corresponding system d) 1%, e) 3%, and f) 5% of asperity sites (mainshock, shown by the larger grey cross). (All the above plots are for a model with α=0.2- low stress dissipation.)*

We observe the repeated occurrence of large events which starts with the gradually increasing number of bigger events (foreshocks) and ends with a tail of decreasing activity (aftershocks), similar to a characteristic earthquake. This is the first time that this complete set of phenomena has been observed in OFC models. Figure 3-7a, b and c show the time series ($2*10^5$ *pu*) of events (collected during 10^7 *pu*) for three different percentages of asperity sites (1%, 3% and 5%) and a fixed low stress dissipation system with α=0.2 (Figures 3-7-a,b and c). The time steps in which an asperity site breaks are shown with a grey background shade. In Figure 3-7d, e and f, we plot distance versus time for each event (foreshock or aftershock) relative to the largest event in the series

(mainshock). Figure 3-8 shows the same results but for a high stress dissipation system, α=0.6.

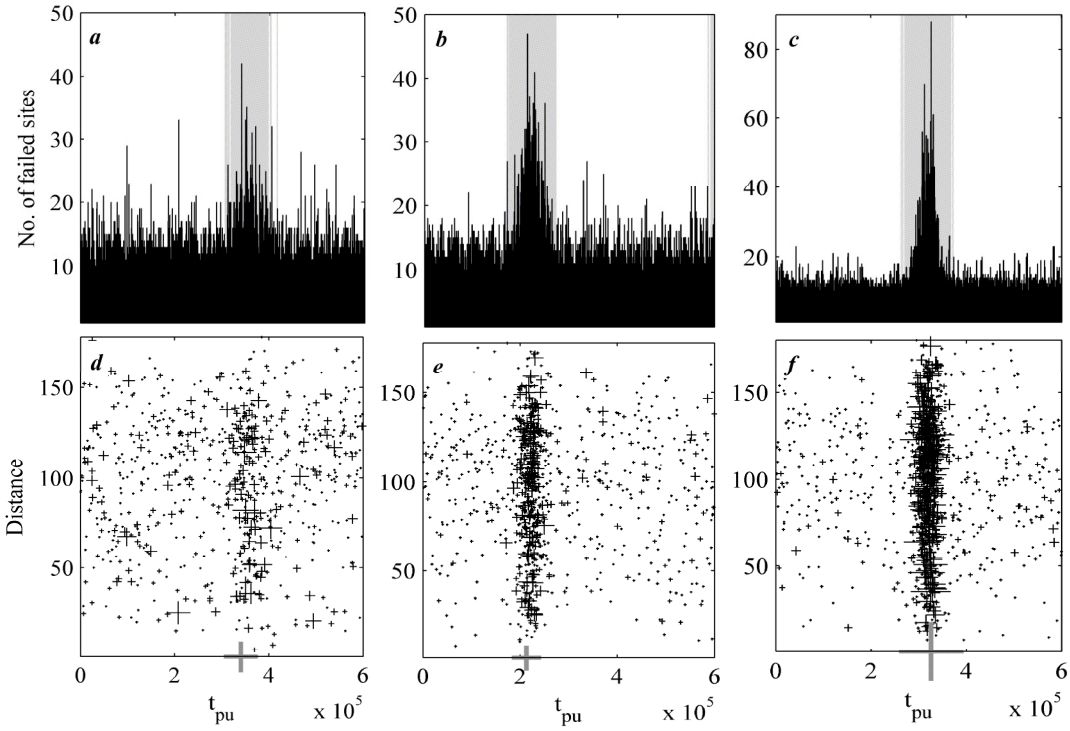

Figure 3-8 *Time series of events of a system with randomly distributed asperity sites and a) 1%, b) 3%, and c) 5% of asperity sites. (Shaded areas indicate the steps where an asperity site breaks.) The distance of each event from the biggest event in the sequence for the corresponding system d) 1%, e) 3%, and f) 5% of asperity sites (mainshock, shown by the larger grey cross). (All the above plots are for a model with α=0.6- high stress dissipation.)*

The inhomogeneities imposed on the system create a more realistic fault system. The failure of a strong asperity site distributes a large amount of stress into the system, triggering the remaining asperities and resulting in temporal clustering of the larger events. In an earlier work, we determined not only that the time between events and their magnitude are a function of the stress dissipation parameter, but that the relative length of the foreshock to aftershock sequences varies as a function of the amount of stress dissipation in the system (Kazemian et al., 2013). Here we investigate the behavior in more depth.

3.4.1.1 Accelerating Moment Release (AMR)

Mogi (1981) observed a regional increase in seismicity before great earthquakes, including an increase in the overall level of seismicity in the crust surrounding the future rupture zone, in conjunction with quiescence, or a relative shortage of events, along or near the fault. Ellsworth et al. (1981) also observed an increase in the rate of M5 events over a broad region in the years preceding the 1906 San Francisco earthquake. This particular pattern of precursory seismicity appears to accelerate with the approach of the mainshock (AMR) (Bowman and King, 2001; Bowman et al, 1998; Sornette and Sammis, 1995; Bufe and Varnes, 1993; Sykes and Jaumé, 1990) and is defined by the equation

$$\varepsilon(t) = A + B(t_f - t)^m, \tag{3.2}$$

$\varepsilon(t)$ has been interpreted as either the accumulated seismic moment, the energy release or the Benioff strain release within a specified region, from some origin time t_0, up to time t.

$$\varepsilon(t) = \sum_{1}^{N(t)} E_i^k, \tag{3.3}$$

is the number of events in the region between t_0 and t, E_i is the energy release from the ith event, and k=0, 1/2, 1. A is a constant that depends on the background level of activity, t_f is the time of the mainshock, B is negative and m is a value between 0.3 and 0.7. Ben-Zion and Lyakhovsky (2002) analyzed the deformation preceding large earthquakes and obtained a 1-D analytical power-law time-to-failure relation for AMR before big events. They found that phases of AMR exist when the seismicity occurring immediately before a large event has magnitude-frequency statistics over several ranges of magnitude. These and similar results of Turcotte et al. (2003) and Zoller et al. (2006) are consistent with observed seismic activation before some large earthquakes.

In this section, we investigate the AMR signal in the time series of the events in our model results. Because the dynamics of our model requires that there is at least one broken site in every time step, we binned time into coarse-grained units of Δt=500 *pu* and

counted the number of events greater than a predefined threshold in each bin. Then we calculate the number of events greater than a chosen threshold in each coarse-grained time unit.

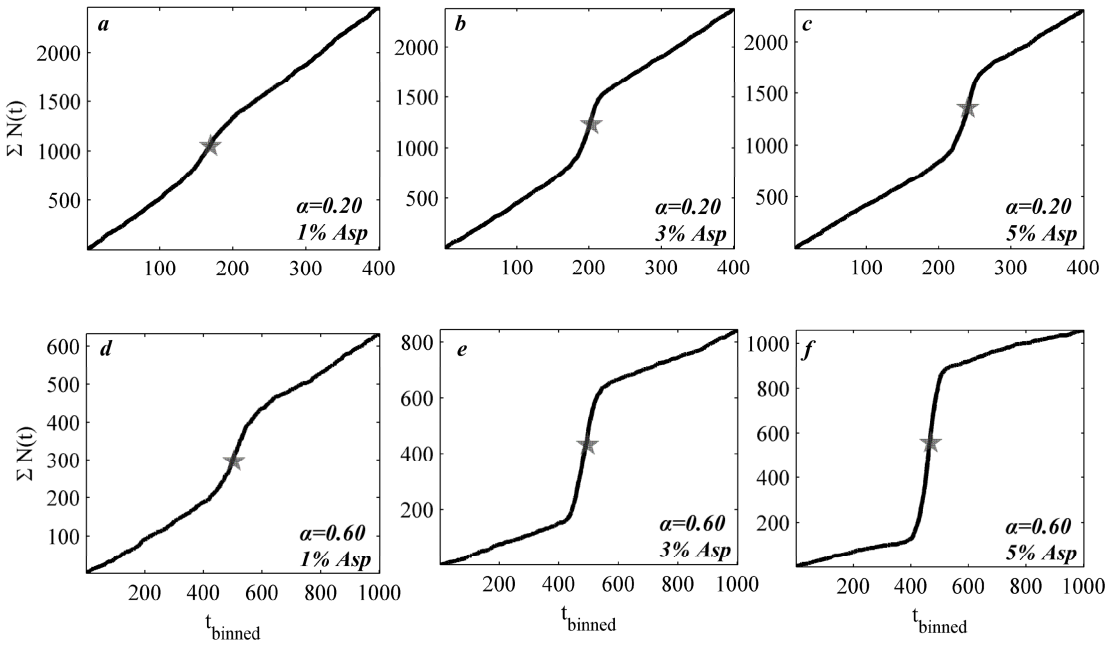

Figure 3-9 *The accumulated number of events bigger than the defined threshold versus coarse-grained time for a-1% and α=0.20, b-3% and α=0.20, c-5% and α=0.20, d-1% and α=0.60, 3% and α=0.60 and f-5% and α=0.60 of randomly distributed asperity sites for two different stress dissipation parameters. The grey star on each graph shows the time of the main shock.*

Figure 3-9 illustrates the cumulative number of events versus coarse-grained (binned) time for three different amounts of asperity sites in the models with different stress dissipation. The increasing number of larger events prior to the mainshock in all the subfigures also produces an increasing rate of activity similar to AMR behavior before large events. The results suggest that the AMR signal before the main event is more evident in those regions with more inhomogeneities and higher stress dissipation. This is also the first time this phenomenon has been observed in any simple model in conjunction with GR scaling. These results prompted investigation using the Thirumalai

and Mountain (TM) metric (Thirumalai and Mountain, 1989; Tiampo et al. 2003, 2007, 2010).

3.4.1.2 TM metric behaviour

In this section, we introduce the TM metric as a measure of event clustering. The TM metric was introduced in the field of statistical physics of fluids to study the time scales necessary to achieve effective ergodicity in models of liquids and supercooled liquids (Thirumalai and Mountain, 1989). This method was first applied to earthquake simulations (Ferguson et al., 1999) and later was applied to regional seismicity by Tiampo et al. (2003, 2007, 2010). They identified periods of metastable equilibrium in seismic activity, between large events, as well as the relationship between periods of effective ergodicity and certain types of seismicity patterns (Tiampo et al. 2003, 2007, and 2010).

The TM metric measures effective ergodicity, or the difference between the time average of an observable (e.g. energy or stress) at each site and the ensemble average of that time average (Thirumalai et al., 1989; Mountain and Thirumalai, 1992; Thirumalai and Mountain, 1993). A necessary but not sufficient condition for ergodicity is stationarity, so that regions of phase space identified as effectively ergodic are maintaining stationary statistics over a given period of time. In addition, it is a behavior generally limited to equilibrium states. The TM metric is defined as

$$\Omega_x(t) \equiv \frac{1}{N}\sum_{j=1}^{N}\left(f_j(t) - \overline{f}(t)\right)^2, \tag{3.4}$$

where j refers to lattice sites, N is the total number of sites in the system

$$f_j(t) \equiv \frac{1}{t}\int_0^t x_j(t')dt', \tag{3.5}$$

and

$$\overline{f}(\mathrm{t}) \equiv \frac{1}{N}\sum_{j=1}^{N} f_j(\mathrm{t}), \tag{3.6}$$

and x is an observable quantity (Thirumalai and Mountain, 1989). The TM metric is the spatial variance of the temporal mean and should disappear by the law of large numbers in ergodic systems. The system is "effectively ergodic" if

$$\Omega(t) \sim \frac{1}{t}, t \to \infty \tag{3.7}$$

and the TM metric is used to determine whether or not a system is in statistical equilibrium.

Here, we calculate the TM metric for our inhomogeneous fault model and use it to identify precursors, or foreshocks, of the mainshock in the associated time series. Figure 3-10 shows the inverse TM metric plot for 1%, 3% and 5% percent of randomly distributed asperity sites in the low dissipation model. The failure of the first asperity site in the series releases a large amount of stress into the system. Because the system has long-range stress interactions and low stress dissipation, the released stress can migrate farther and trigger other asperity cells.

Figure 3-10 clearly shows the deviation of the linear inverse TM metric in those time steps prior to the mainshock (grey star). By increasing the total number of asperity sites from 1% (Figure 3-10a) to 5% (Figure 3-10c), the probability of triggering and therefore the amount of released stress before the mainshock increases and we can see stronger fluctuations in the TM metric plot. Also, larger fluctuations in the TM metric plot occur prior to larger events in the time series. Figure 3-11 is similar to Figure 3-10, but for higher stress dissipation (α=0.6). In this case, the probability of asperity triggering is very low and, as a result, the model produces smaller events compared to the low dissipation model. The TM metric plot also shows smaller deviations for higher stress dissipation.

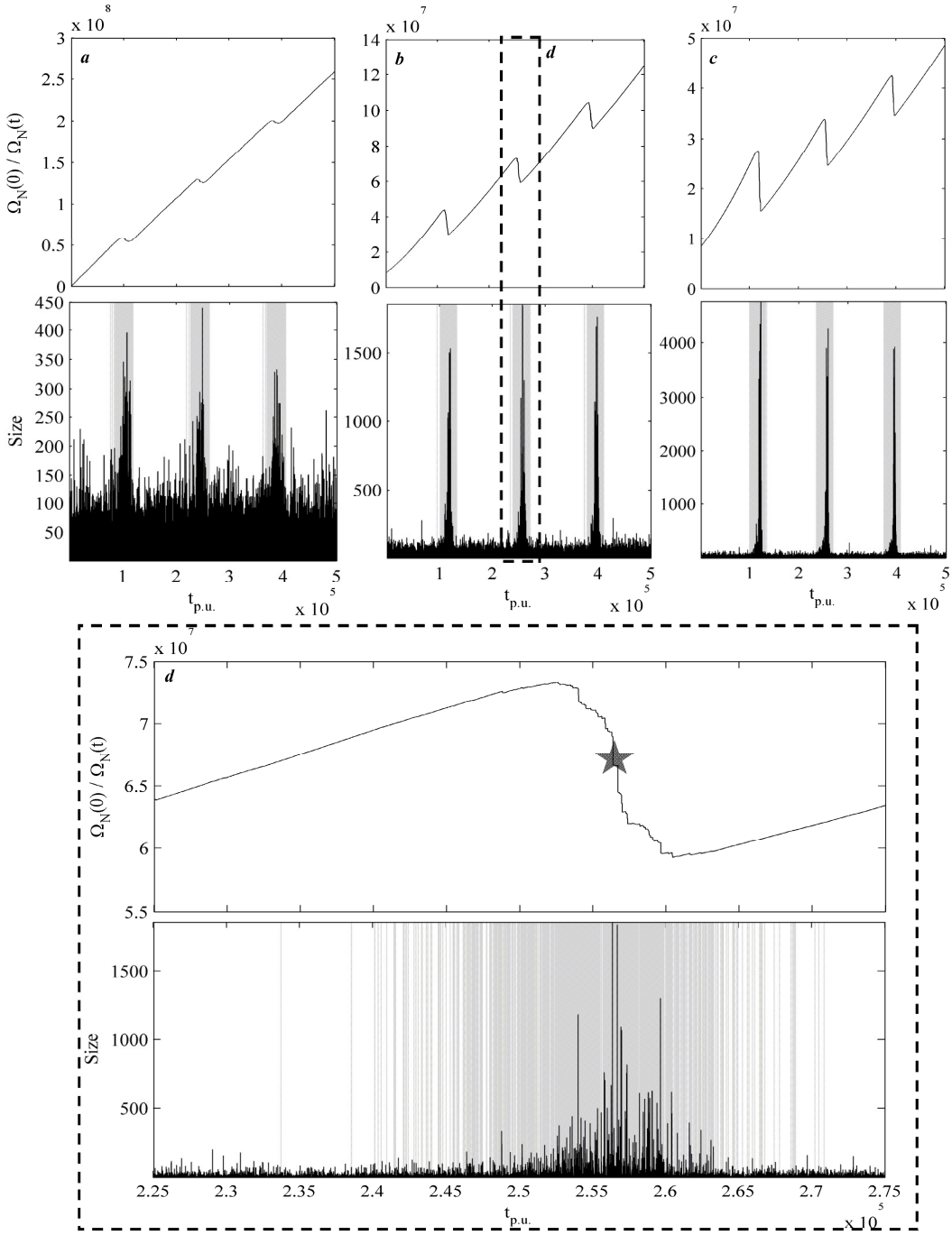

Figure 3-10 *Inverse TM metric of each event for a-1%, b-3% and c-5% of randomly distributed asperity sites. The grey star on the last graph shows the time of the main shock. (All the above plots are for a model with α=0.2- low stress dissipation.)*

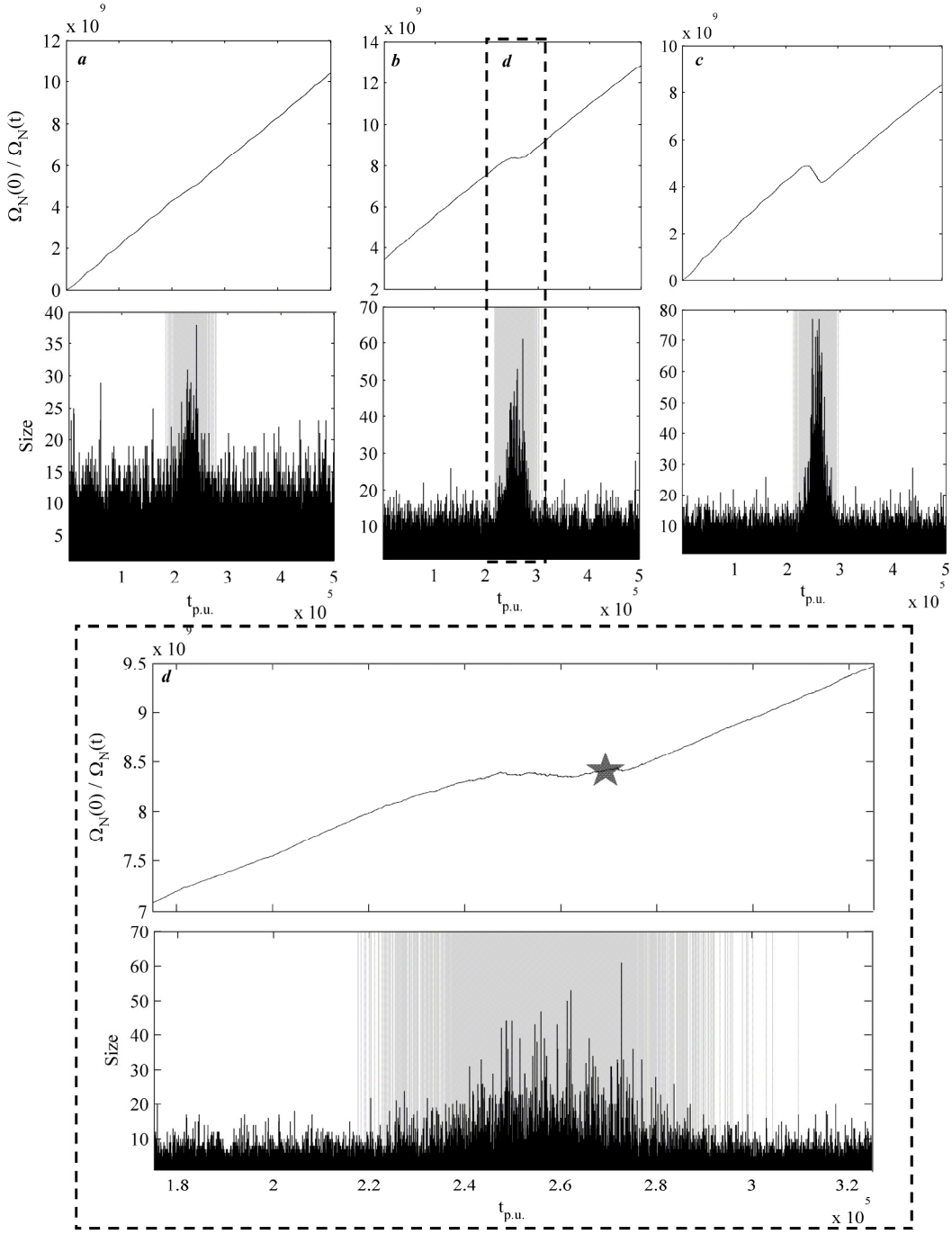

Figure 3-11 *Inverse TM metric of each event for a-1%, b-3% and c-5% of randomly distributed asperity sites. The grey star on the last graph shows the time of the main shock. (All the above plots are for a model with α=0.6- high stress dissipation.)*

3.4.1.3 Omori law

In this section we investigate the foreshock and aftershock statistics in our inhomogeneous model to see if the foreshocks are consistent with the observations of natural seismicity (Papazachos, 1975; Jones and Molnar 1979; Kagan and Knopoff, 1976) and the aftershocks with Omori's law (Omori, 1894; Utsu, 1961). The well-known modified Omori's law for aftershocks (Utsu, 1961) states that the rate of aftershocks is proportional to the inverse of time since the mainshock,

$$R_a \sim (t_M - t)^{-p_a}, \tag{3.8}$$

where R_a is the rate of aftershocks, t_M is the time of the mainshock, and p is the decay rate for aftershocks. It also has been suggested (Papazachos, 1975; Jones and Molnar 1979; Kagan and Knopoff, 1976) that there is an inverse Omori distribution for foreshocks with different exponents:

$$R_f \sim (t - t_M)^{-p_f}, \tag{3.9}$$

where R_f is the rate of foreshocks, t_M is the time of the mainshock, and p_f is the reverse decay (growth) rate for foreshocks.

In this section, we collect the statistics of 10^7 events for two different stress dissipation parameters (α=0.2 and 0.4) and three different amount of randomly distributed asperity sites (1%, 3% and 5%). The results for the Omori model for aftershocks and also the reverse Omori law for foreshocks are shown in Figures 3-12 and 3-13. In these figures we calculated the exponent of the Omori law based on the number of events counted on the coarse-grained bins of Δt=500 *pu*, and then averaged over many earthquake sequences.

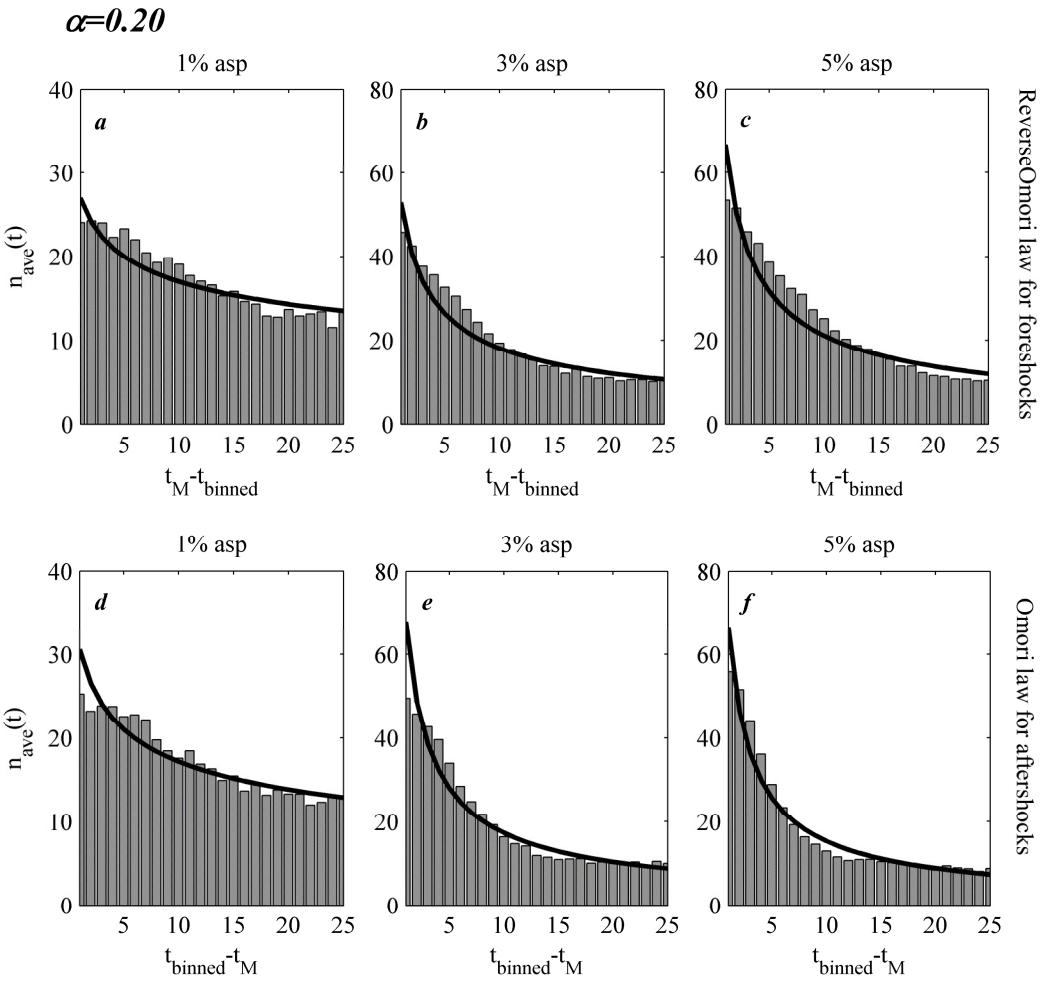

Figure 3-12 *(a, b and c) Number of event prior to the main shock (foreshocks) for α=0.2. (d, e and f) Number of events after the main shocks (aftershocks). Black line on each graph shows the Omori fit for each case (exponents in table 3).*

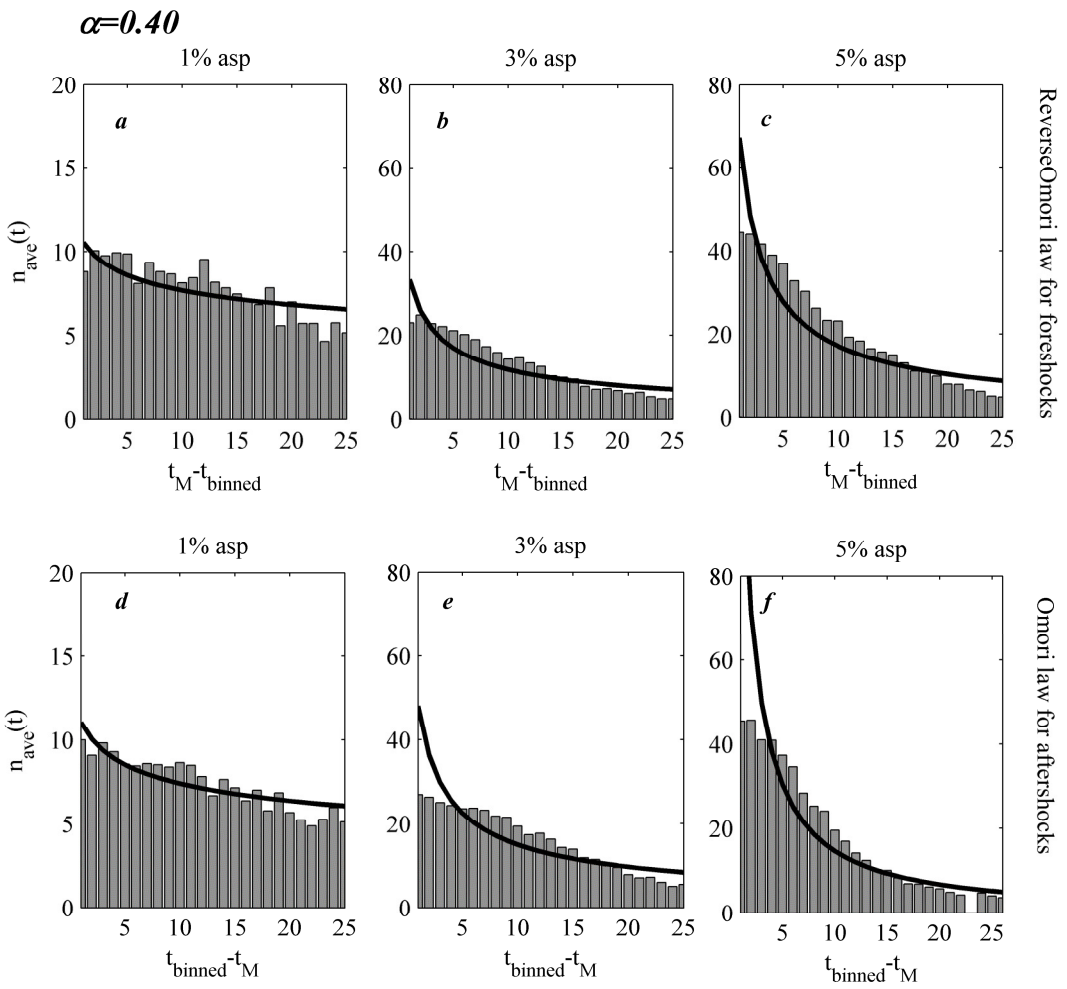

Figure 3-13 *(a, b and c) Number of event prior to the main shock (foreshocks) for α=0.4. (d, e and f) Number of events after the main shocks (aftershocks). Black line on each graph shows the Omori fit for each case (exponents in table 3).*

Table 3 records the exponents of the reverse Omori law for foreshocks in the form of

$$n_f(t) = \frac{K_f}{(\mathrm{t}+c)^{-p_f}}, \tag{3.10}$$

and the Omori law for aftershocks in the form of

$$n_a(t) = \frac{K_a}{(\mathrm{t}+c)^{-p_a}}. \tag{3.11}$$

Table 3-3 Exponents of the Omori law model for aftershocks and also reverse Omori law for foreshock.

Table 3.		***Aftershocks***		***Foreshocks***	
Asperity Percentage	Dissipation	K_a	p_a	K_f	p_f
1 %	***α=0.2***	38	0.331	32	0.264
	α=0.4	13	0.230	12	0.182
3 %	***α=0.2***	112	0.784	78	0.614
	α=0.4	74	0.669	49	0.594
5 %	***α=0.2***	114	0.843	102	0.659
	α=0.4	254	1.196	111	0.782

The results show that, in general, the decay rate is higher for aftershocks compared to the increase in the foreshocks rate, while the total number of aftershocks is higher than the total number of foreshocks in all cases. Increasing the number of asperities leads to a greater number of both foreshocks and aftershocks in the system. The decay rate is also higher in those systems with more asperity sites.

3.4.2 Spatial clustering of events

We studied the models with 1%, 3% and 5% percent of asperity sites for a different spatial configuration of asperity sites. Here, instead of randomly distributed asperity sites, we again aggregate all the asperity sites into a single block of asperities. Figures 3-14 and 3-15 present the time series of events for a low (α=0.2) and high (α=0.6) stress dissipation model. In the lower dissipation model (Figure 3-14), although the released stress of the failed asperity block can migrate farther and trigger the remainder of the

sites to fail, we can clearly see the quiescence in locations adjacent to the mainshock, both before and after its occurrence. In the high dissipation model (Figure 3-15) there is a very obvious temporal and spatial cluster of foreshocks and aftershock close to the biggest event (mainshock) in the series.

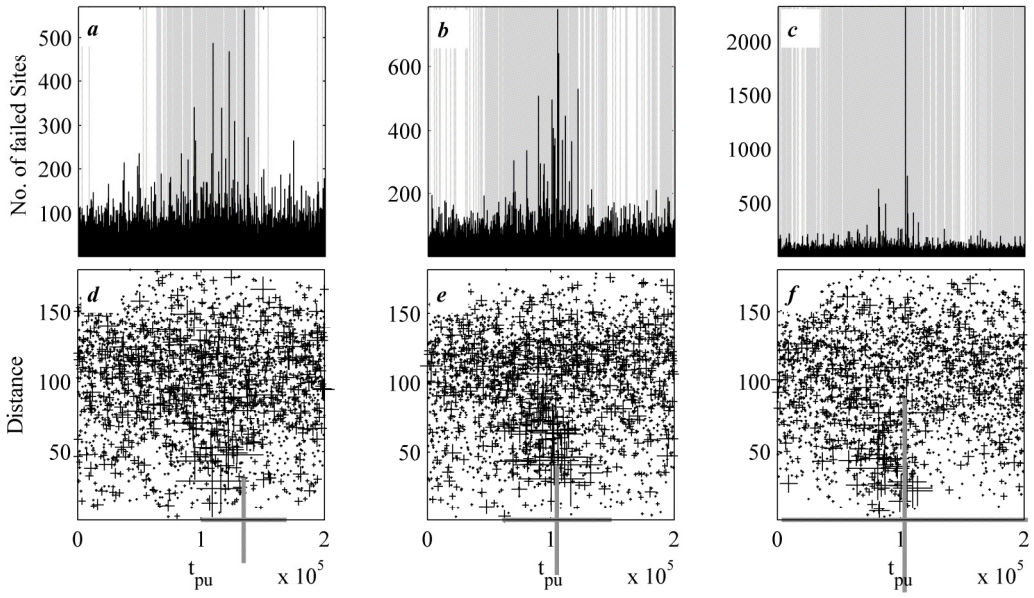

Figure 3-14 *Time series of events of a system with asperity sites aggregated in single large block and a) 1%, b) 3%, and c) 5% of asperity sites. (Shaded areas indicate the steps where an asperity site breaks.) The distance of each event from the biggest event in the sequence for the corresponding system d) 1%, e) 3%, and f) 5% of asperity sites (mainshock, shown by the larger grey cross). (All the above plots are for a model with α=0.2, low stress dissipation.)*

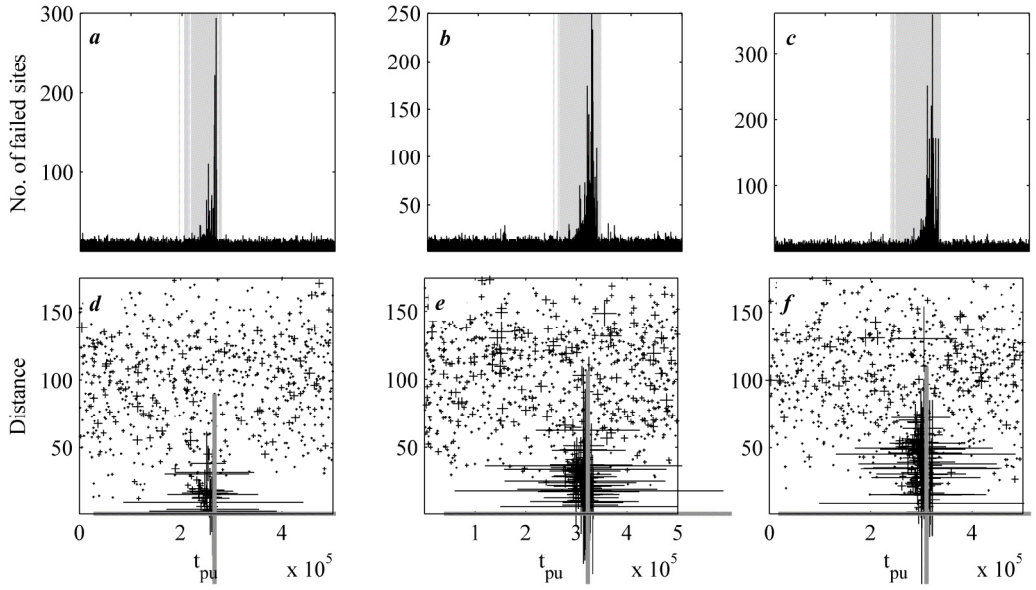

Figure 3-15 *Time series of events of a system with asperity sites aggregated in single large block and a) 1%, b) 3%, and c) 5% of asperity sites. (shaded areas indicate the steps where an asperity site breaks.) The distance of each event from the biggest event in the sequence for the corresponding system d) 1%, e) 3%, and f) 5% of asperity sites (mainshock, shown by the larger grey cross). (All the above plots are for a model with α=0.6- high stress dissipation.)*

Enescu et al. (2009) demonstrated that swarm-type seismic activity with higher foreshock rates occurred in areas of California with relatively high surface heat flow while more typical sequences occurred in regions with lower heat flow. McGuire et al. (2005) analyzed hydroacoustic data to mainshock along East Pacific Rise faults and identified sequences with higher foreshock rates and lower aftershock rates than previously observed in continental transform faults. The result is a relatively high ratio of foreshocks to aftershocks, similar to what is observed in the asperity-α combinations in Figures 3-3, 3-4, 3-14 and 3-15.

We performed a similar analysis for a swarm that began in the southern Eyjafjarðaráll graben off the north coast of Iceland in the late summer of 2012 (Figure 3-16). Data collected by the 55-station SIL seismic network was provided by the Icelandic Met Office (en.vedur.is). The bulk of the activity occurred between the Eyjafjarðaráll graben

and the Húsavík-Flatey fault. Fig. 15a shows a seismicity map of the events that occurred between Aug 20, 2012 and March 25, 2013, 66 and 66.75 degrees north latitude and -18 and -19.25 degrees longitude. We identified the fifteen largest events ($M \geq 2.5$) in the sequence. Eight of those events were associated with foreshock and/or aftershock clusters that could be distinguished from the background swarm activity. The spatial and temporal distribution of those foreshock and aftershock events, relative to their respective mainshocks, is plotted in Figure 3-16b. The pattern of spatial and temporal clustering is similar to Figure 3-15, although there is no distinct quiescent signal, providing further evidence for natural cases in which foreshock abundance is of the same order of magnitude and duration as aftershock sequences.

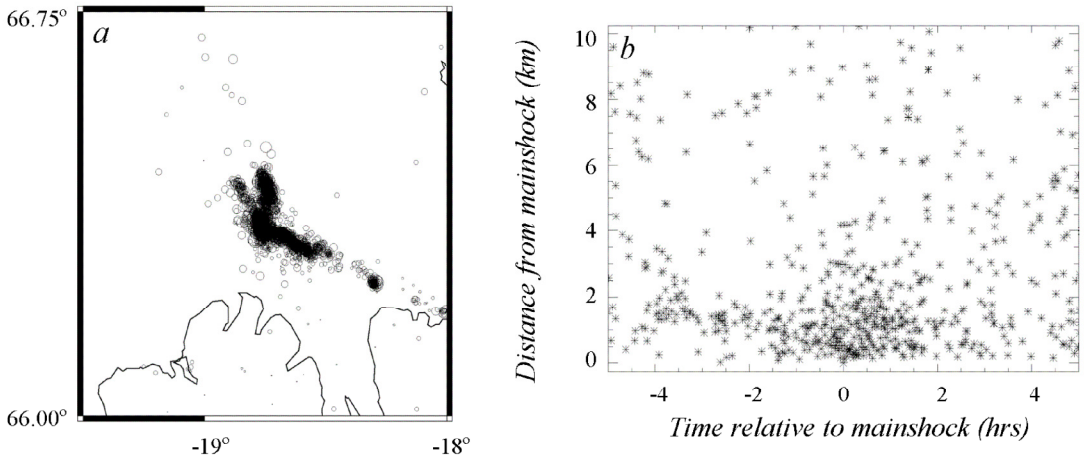

Figure 3-16 *(a) Swarm event, north Iceland, southern Eyjafjarðaráll graben, Aug 20, 2012 through March 25, 2013. (b) Spatiotemporal distribution of the seismicity associated with the twelve largest events in the sequence shown in (a).*

3.5 Summary and Discussion

The inhomogeneity of natural materials with different physical properties in the Earth motivated this investigation of the effect of spatial inhomogeneity on the macroscopic properties of a many-body system. The model studied here is a variation of the OFC and RJB cellular automata models of earthquake faults with long-range stress transfer. In order to reproduce the spatial inhomogeneities of real earthquake faults in the model we

have converted a percentage of selected locations in our lattice into local stress accumulators which have the ability to store and release a higher amount of stress than the surrounding lattice sites, similar to asperities on natural faults.

The initial results illustrate that increasing values of stress dissipation, regardless of the presence of inhomogeneity in the system, decrease the length of the scaling regime (Figure 3-1). In addition, the increasing number of asperity sites promotes the occurrence of larger events (Figure 3-2 and 3-3).

Results also demonstrate that imposing the stronger asperity sites does not change the MGR relation proposed by Klein et al. (2007). The spatial heterogeneity directly affects the size of the largest events, the length of the scaling regime and the upper bound of the MGR. However, it appears that the stronger lattice sites create a second distribution of the same form for the large events. As a result, the overall magnitude-frequency distribution is a combination of two distinct distributions of the same form for the smaller and larger events (Figure 3-5).

The proposed inhomogeneous model also introduces spatiotemporal clustering of events similar to that seen in natural earthquake fault systems. That spatiotemporal clustering is dependent on the size and spatial configuration of the asperities (Figures 3-7 and 3-8). Seismic sequences occur at regular time intervals, starting with a slow increase in the number and size of events (foreshocks) and ending with a tail of decreasing activity (aftershocks) after the mainshock, very similar to the concepts of both characteristic earthquakes and seismic sequences (Figure 3-6).

The increasing number of larger events in these recurrent time series follows a pattern of precursory AMR activity prior to the mainshock comparable to that observed in natural seismicity (Figure 3-9). Plots of the inverse TM metric also show a clear deviation from stationarity before the mainshock (Figures 3-10 and 3-11).

Finally, our results demonstrate that both the decay rate of the aftershock sequences and the growth rate of the foreshock sequences can vary, as observed in different tectonic regions. Our studies of the Omori law relation for both types of sequences confirm that

these rates are related to one or more of the controlling parameters of the model, including both the amount and complexity of the asperities as well as the stress dissipation (Figures 3-12 and 3-13).

This simple model supports the hypothesis that spatial heterogeneity has an impact on the primary features of both modeled and natural earthquake sequences and that the spatial and temporal patterns observed in natural seismicity may be controlled by the underlying physical properties. The model reproduces the MGR distribution and the size of the largest events and the length of the scaling regime on each fault are controlled by the amplitude of the stress dissipation of the system. The superposition of many faults, each with a different amount of damage, results in GR scaling in the larger fault network. Spatial features affect the critical point scaling behavior intrinsic to the earthquake fault process and the associated structure and geometry directly impacts the spatial and temporal nature of fault networks. These findings suggest that asperities could be responsible for much of the spatial and temporal behavior of real earthquake fault systems and support the hypothesis that the patterns observed in natural seismicity may be controlled by the underlying physical complexity, rather than simple triggering alone.

3.6 References

Alava, M. J., Nukala, P., and Zapperi, S. (2006). Statistical models of fracture, Adv. Phys. 55, 349.

Bach, M., Wissel F. and Dressel, B. (2008). Olami-Feder-Christensen model with quenched disorder. Phys. Rev. E77, 067101.

Bak, P., Tang, C. and Wiesenfeld K. (1987). Self-organized criticality: an explanation of 1/f noise. Phys. Rev. Lett., 59:381-384.

Bakun, W.H., King, G.C.P., Cockerham, R.S., (1986). Seismic slip, aseismic slip, and the mechanics of repeating earthquakes on the Calaveras fault, California, in Earthquake Source Mechanics. In: Das, S., Boatwright, J., Schlotz, C.H. (Eds.), Geophys. Monogr. Ser., vol. 37. AGU, Washington, D.C, pp. 195–208.

Bakun, W.H., Aagaard, B., Dost, B., Ellsworth, W.L., Hardebeck, J.L., Harris, R.A., Ji, C., Johnston, M.J.S., Langbein, J., Lienkaemper, J.J., Michael, A.J., Murray, J.R., Nadeau, R.M., Reasenberg, P.A., Reichle, M.S., Roeloffs, E.A., Shakal, A., Simpson, R.W., Waldhauser, F., (2005). Implications for prediction and hazard assessment from the 2004 Parkfield earthquake. Nature 437, 969–974.

Båth, M. (1965). Lateral inhomogeneities of the upper mantle, Tectonophysics, 2, 483–514.

Bell, A.F., Mark Naylor, M., Main, I.G. (2013). Convergence of the frequency-size distribution of global earthquakes, GRL, 40, 2585–2589, doi:10.1002/grl.50416.

Ben-Zion, Y. (2008). Collective Behavior of Earthquakes and Faults: Continuum-Discrete Transitions, Progressive Evolutionary Changes and Different Dynamic Regimes, Rev. Geophysics, 46, RG4006, doi:10.1029/2008RG000260.

Ben-Zion, Y., Lyakhovsky, V., (2002). Accelerated seismic release and related aspects of seismicity patterns on earthquake faults. Pure and Applied Geophysics 159, 2385–2412.

Bowman, D.D., Ouillon, G., Sammis, C.G., Sornette, A., Sornette, D., (1998). An observational test of the critical earthquake concept. Journal of Geophysical Research 103, 24,359–24,372.

Bowman, D.D., King, G.C.P., (2001). Accelerating seismicity and stress accumulation before large earthquakes. Geophysical Research Letters 28, 4039–4042.

Brehm, D.J., Braile, L.W., (1998). Intermediate-term earthquake prediction using precursory events in the New Madrid Seismic Zone. Bulletin of the Seismological Society of America 88, 564–580.

Bufe, C.G., Varnes, D.J., (1993). Predictive modeling of the seismic cycle of the greater San Francisco Bay region. Journal of Geophysical Research 98, 9871–9883.

Burridge, R., Knopoff, L. (1967). Model and theoretical seismicity, Bull. Seismol. Soc. Am. 57. 341–371.

Carlson, J. M. and Langer, J. S. (1989). Mechanical model of an earthquake fault. Phys. Rev. Lett. 62, 2632; Phys. Rev. A 40, 6470.

Ceva, H. (1995). Inhuence of defects in a coupled map lattice modeling earthquakes. Phys. Rev, E52, 154.

Chen X. and Shearer P. M. (2013). California foreshock sequences suggest aseismic triggering process, doi: 10.1002/grl.50444.

Dahmen, K., Ertas, D., and Ben-Zion, R. (1998). Gutenberg-Richter and Characteristic Earthquake Behavior in Simple Mean-field Models of Heterogeneous Faults, Phys. Rev. E 58, 1494–1501.

Deng, J.S., Sykes, L.R., (1996). Triggering of 1812 Santa Barbara earthquake by a great San Andreas shock: implications for future hazards in southern California. Geophysical Research Letters 23, 1155–1158.

Dodge, D.A., Beroza, G.C., Ellsworth, W.L., (1996). Detailed observations of California foreshock sequences: implications for the earthquake initiation process. Journal of Geophysical Research 101, 22,371–22,392.

Dodge D.A. and Beroza, G. C. (1997). Source array analysis of coda waves near the 1989 Loma Prieta, California, mainshock: Implications for the mechanism of coseismic velocity changes. J. Geophys. Res. 102, 24437–24458.

Dominguez, R., Tiampo, K., Serino, C. A. and Klein, W. (2012). Characterizing Large Events and Scaling in Earthquake Models with Inhomogeneous Damage. Geophysical Monograph Series. 196, 41-54. doi:10.1029/2011GM001082.

Dominguez, R., Tiampo, K.F., Serino, C.A. and Klein W. (2013). Scaling of earthquake models with inhomogeneous stress dissipation. Phys. Rev. E 87, 022809.

Ellsworth, W.L., Lindh, A.G., Prescott, W.H., Herd, D.J., (1981). The 1906 San Francisco Earthquake and the seismic cycle. In: Simpson, D.W., Richards, P.G. (Eds.), Earthquake Prediction: An Internation Review. Maurice Ewing Ser., vol. 44. AGU, Washington, D.C.

Ellsworth, W.I., Cole, A.T., (1997). A test of the characteristic earthquake hypothesis for the San Andreas Fault in central California. Seismological Research Letters 68, 298.

Eneva, M., Ben-Zion, Y., (1997). Techniques and parameters to analyze seismicity patterns associated with large earthquakes. Journal of Geophysical Research 102, 17,785–17,795.

Enescu, B., Hainzl S. and Ben-Zion Y. (2009). Correlations of seismicity patterns in southern California with surface heat flow data. BSSA, 99(6): 3114-3123.

Ferguson, C. D., Klein, W., and Rundle, J. B. (1999). Spinodals, scaling, and ergodicity in a threshold model with long-range stress transfer, Phys. Rev. E, 60, 1359–1373.

Fisher, D.S., Dahmen, K., Ramanathan, S. and Ben-Zion, Y. (1997). Statistics of Earthquakes in Simple Models of Heterogeneous Faults. Phys. Rev. Lett. 78, 4885.

Frohlich, C., (1987). Aftershocks and temporal clustering of deep earthquakes. Journal of Geophysical Research 92, 13,944–13,956.

Gomberg, J., (1996). Stress/strain changes and triggered seismicity following the Mw 7.3 Landers, California, earthquake. Journal of Geophysical Research 101, 751–764.

Gross, S.J., Kisslinger, C., (1994). Tests of models of aftershock rate decay. Bulletin of the Seismological Society of America 84, 1571–1579.

Gulbahce, N., Gould, H., Klein, W., (2004). Zeros of the partition function and pseudospinodals in long-range Ising models. Phys. Rev. E, 69, 036119.

Gutenberg, B. and Richter, C.F. (1956). Magnitude and energy of earthquakes. Annali di Geofisica, Vol. 9, n. 1.

Haberman, R.E., (1981). Precursory seismicity patterns: stalking the mature seismic gap. In: Simpson, D.W., Richards, P.G. (Eds.), Earthquake Prediction: An International Review. Maurice Ewing Ser., vol. 4. AGU, Washington, D.C, pp. 29–42.

Helmstetter, A., Sornette, D., (2002). Subcritical and supercritical regimes in epidemicmodels of earthquake aftershocks. Journal of Geophysical Research 107. doi:10.1029/2001JB001580.

Herz, A.V.M., and Hopfield, J.J. (1995). Earthquake Cycles and Neural Reverberations, Collective Oscillations in Systems with Pulse-Coupled Threshold Elements. Phys. Rev. Lett., 75, 1222-1225.

Jagla, E.A. (2010). Realistic spatial and temporal earthquake distributions in a modified Olami-Feder-Christensen model. Phys. Rev, E81, 046117.

Janosi, I.M. and Kertesz, J. (1994), Self-organized criticality with and without conservation. Physica A200, 0378.

Jaumé, S.C., Sykes, L.R., (1999). Evolving towards a critical point: a review of accelerating seismic moment/energy release prior to large and great earthquakes. Pure and Applied Geophysics 155, 279–306.

Jones L. M. and Molnar. P. (1979). Some characteristics of foreshocks and their possible relationship to earthquake prediction and premonitory slip on faults. J. Geophys. Res. 84 (1979), 3596.

Jones, L.M., Hauksson, E., (1997). The seismic cycle in southern California: precursor or response? Geophysical Research Letters 24, 469–472.

Jordan, T.H., Jones, L.M., (2010). Operational earthquake forecasting: some thoughts on why and how. Seismological Research Letters 81.

Kagan, Y. Y. and Knopoff, L. (1976). Statistical search for non-random features of the seismicity of strong earthquakes. Phys. Earth Planet. Inter. 12, 291.

Kagan, Y. Y. and Jackson, D.D (2000). Probabilistic forecasting of earthquakes, Geophys. J. Int., 143, 438-453.

Kanamori, H. (1981). The nature of seismicity patterns before large earthquakes, in Earthquake Prediction, Maurice Ewing Series, IV, 1–19, AGU, Washington D.C..

Kazemian, J., Tiampo, K.F., Klein, W., Dominguez, R. (2013). Foreshocks and aftershocks in simple earthquake models, Physical Review Letters, submitted.

Keilis-Borok, V.I., Kossobokov, V.G., (1990). Times of increased probability of strong earthquakes M≥7.5 diagnoes by algorithm M8 in Japan and adjacent territories. Journal of Geophysical Research 95, 12,413–12,422.

King, G.C.P., Stein, R.S., Lin, J., (1994). Static stress changes and the triggering of earthquakes. Bulletin of the Seismological Society of America 84, 935–953.

Klein, W. Rundle J. B. and Ferguson C. D. (1997). Scaling and Nucleation in Models of Earthquake Faults Phys. Rev. Lett. 78, 3793.

Klein, W., Anghel, M., Ferguson, C. D., Rundle, J. B. and Martins J. S. S. (2000). Geocomplexity and the Physics of Earthquakes (American Geophysical Union, Washington, DC), AGU Monograph 120.

Klein, W., Ferguson, C. and Rundle, J.B., (1996) in Reduction and Predictability of Natural Disasters, ed. by Rundle, J.B., Turcotte, D.L. and Klein W., SFI series in the science of complexity, XXV (Addison-Wesley, Reading, MA) p. 223.

Klein, W., Anghel, M., Ferguson, C.D., Rundle, J.B. and Sá Martins J.S., (2000) in Geocomplexity and the Physics of Earthquakes, ed. by Rundle, J.B., Turcotte, D.L. and Klein, W., Geophysical Monograph Vol. 120 (AGU, Washington D.C.) p. 43.

Klein, W., Gould, H., Gulbahce, N., Rundle, J. B. and Tiampo, K. (2007). Structure of fluctuations near mean-field critical points and spinodals and its implication for physical processes. Phys. Rev. E 75, 031114.

Lyakhovsky, V. and Ben-Zion, Y. (2009). Evolving geometrical and material properties of fault zones in a damage rheology model, Geochem. Geophys. Geosyst., 10, Q11011.

Main, I. (1996). Statistical physics, seismogenesis, and seismic hazard. Rev. Geophys. 34, 433–462.

Mignan, A., (2008). The Non-Critical Precursory Accelerating Seismicity Theory (NC PAST) and limits of the power-law fit methodology. Tectonophysics 452. doi:10.1016/j.tecto.2008.02.010.

Mogi, K., (1969). Some features of recent seismic activity in and near Japan 2, Activity before and after large earthquakes. Bulletin of the Earthquake Research Institute, Tokyo University 47, 395–417.

Mogi, K. (1981). Seismicity in western Japan and long term earthquake forecasting, in Earthquake Prediction: An International Review, Maurice Ewing Ser., vol. 4, edited by D. W. Simpson, and P. G. Richards, pp. 43 – 51, AGU, Washington, D. C.

Mori, T., and H. Kawamura (2008a). Simulation study of the two-dimensional Burridge-Knopoff model of earthquakes, J. Geophys. Res., 113, B06301, doi:10.1029/2007JB005219.

Mori, T., and H. Kawamura (2008b). Spatiotemporal correlations of earthquakes in the continuum limit of the one-dimensional Burridge-Knopoff model, J. Geophys. Res., 113, B11305, doi:10.1029/2008JB005725.

Mountain, R. M. and Thirumalai, D. (1992), Ergodicity and loss of dynamics in supercooled liquids, Phys. Rev. A 45, 3380–3383.

Mousseau, N. (1996). Synchronization by Disorder in Coupled Systems. Phys. Rev. Lett. 77, 968.

Nakanishi, H. (1990). Cellular-automaton model of earthquakes with deterministic dynamics. Phys. Rev. A 41, 7086.

Nanjo, K., Nagahama, H., Satomura, M., 1998. Rates of aftershock decay and the fractal structure of active fault systems. Tectonophysics 287, 173–186.

Ogata, Y. (1983). Estimation of the parameters in the modified Omori formula for aftershock frequencies by the maximum likelihood procedure, Journal of Physics of the Earth, Vol.31, 115-124.

Ogata, Y. (1999). Seismicity analysis through point-process modeling: A review, Pure Appl. Geophys., 155, 471–507.

Olami, Z., Feder, HJS., Christensen, K. (1992). Self-organized criticality in a continuous, nonconservative cellular automaton modelling earthquakes. Phys Rev Lett 68(8):1244–1247.

Omori. F. (1984). On the aftershocks of earthquakes. J. Coll. Sci. Imp. Univ. Tokyo 7, 111.

Otsuka, M. (1972). A Simulation of earthquake occurrence. Phys Earth Planet Inter. 6-311.

Pacheco, J.F., Scholz, C.H., Sykes, L.R., (1992). Changes in frequency–size relationship from small to large earthquakes. Nature 3557, 1–73.

Papazachos, B. C. (1975). Foreshocks and earthquake prediction. Tectonophysics 28 213.

Parsons, T., Geist, E.L., 2009. Is there a basis for preferring characteristic earthquakes over a Gutenberg–Richter distribution in probabilistic earthquake forecasting? Bulletin of the Seismological Society of America 99, 2012–2019. doi:10.1785/0120080069

Pollitz, F.F., Sacks, I.S., 1997. The 1995 Kobe, Japan, earthquake: a long-delayed aftershock of the offshore 1944 Tonankai and 1946 Nankaido earthquakes. Bulletin of the Seismological Society of America 87, 1–10.

Ramos, O., Altshuler, E. and Maloy K.J. (2006). Quasiperiodic Events in an Earthquake Model. Phys. Rev. Lett. 96, 098501.

Reid, H.F., (1910). The mechanics of the earthquake, the California earthquake of April 18, 1906. Report State Investig. Comm., vol. 2. Carnegie Inst., Washington.

Richter C.F. (1935). An instrumental earthquake magnitude scale Bull. Seismol. Soc. Am. 25, 1.

Rikitake, T., (1976). Earthquake Prediction. Elsevier, Amsterdam, Netherlands, pp. 7–26.

Robinson, R., (2000). A test of the precursory accelerating moment release model on some recent New Zealand earthquakes. Geophysical Journal International 140, 568–576.

Romanowicz, B., Rundle, J.B., (1993). On scaling relations for large earthquakes. Bulletin of the Seismological Society of America 83, 1294–1297.

Rundle, J. B. (1988). A physical model for earthquakes, J. Geophys. Res. 93-6237.

Rundle, J.B., (1989). Derivation of the complete Gutenberg–Richter magnitude–frequency relation using the principle of scale invariance. Journal of Geophysical Research 94, 12,337–12,342.

Rundle, J. B. and Jackson, D. D. (1977). Numerical simulation of earthquake sequences, Bull. Seismol. Soc. Am. 67.

Rundle, J. B. and Brown, S. R. (1991). Origin of Rate Dependence in Frictional Sliding, J. Stat. Phys. 65, 403.

Rundle, JB, Klein W. and Gross S. (1999). Physical basis for statistical patterns in complex earthquake populations: Models, predictions, and tests, PAGEOPH, 155, 575-607.

Rundle, J. B., Klein, W., Tiampo, K. and Gross S., (2000). Linear pattern dynamics in nonlinear threshold systems, Phys. Rev. E, 61 (3), 2418–2431.

Rundle, J.B., Klein, W., Gross, S. and Turcotte, D.L., (1995). Boltzmann Fluctuations in Numerical Simulations of Nonequilibrium Lattice Threshold Systems. Phys. Rev. Lett. 75, 1658.

Rundle, J.B., Turcotte, D.L., Shcherbakov, R., Klein, W., Sammis, C., (2003). Statistical physics approach to understanding the multiscale dynamics of earthquake fault systems. Review of Geophysics, 41, 1019.

Serino, C. A., Tiampo, K. F. and Klein W. (2011). New Approach to Gutenberg-Richter Scaling, Phys. Rev. Lett. 106, 108501.

Scholz, C.H. (2002). The mechanics of earthquakes and faulting, Cambridge University Press, p. 471.

Schorlemmer, D., and Gerstenberger, M. C. (2007). RELM testing center, Seismol. Res. Lett. 78, 1, 30-36.

Schwartz, D.P., Coppersmith, K.J., Swan III, F.H., Somerville, P., Savage, W.U., (1981). Characteristic earthquakes on intraplate normal faults. Earthquake Notes 52, 71.

Schwartz, D.P., Coppersmith, K.J., (1984). Fault behavior and characteristic earthquakes: examples from Wasatch and San Andreas fault zones. Journal of Geophysical Research 89, 5681–5698.

Shcherbakov, R., Turcotte, D.L., Rundle, J.B., Tiampo, K.F., Holliday, J.R., (2010). Forecasting the locations of future large earthquakes: an analysis and verification. Pure and Applied Geophysics 167, 743–749.

Shearer, P. M. (2012). Self-similar earthquake triggering, Båth's law, and foreshock / aftershock magnitudes: Simulations, theory, and results for southern California, J. Geophys. Res., 117, B06310.

Sornette D. and Sammis, C. G. (1995). Complex critical exponents from renormalization group theory of earthquakes: Implications for earthquake predictions, J.Phys.I France 5, 607-619.

Stanley H. E. (1999). Scaling, universality, and renormalization: Three pillars of modern critical phenomena. Rev. Mod. Phys. 71, S358.

Swan, F.H., Schwartz, D.P., Cluff, L.S., (1980). Recurrence of moderate to large magnitude earthquakes produced by surface faulting on the Wasatch fault zone, Utah. Bulletin of the Seismological Society of America 70, 1431–1462.

Sykes, L.R., Jaumé, S.C., (1990). Seismic activity on neighbouring faults as a long-term precursor to large earthquakes in the San Francisco Bay area. Nature 348, 595–599.

Thirumalai, D., Mountain, R.D., Kirkpatrick, T.R., (1989). Ergodic behavior in supercooled liquids and in glasses. Physical Review A 39, 3563–3574.

Thirumalai, D. and Mountain, R. D. (1993), Activated dynamics, loss of ergodicity, and transport in supercooled liquids, Phys. Rev. E 47, 479–489.

Tiampo, K.F., Rundle, J.B., Gross, S.J., McGinnis, S., Klein, W. (2002). Eigenpatterns in southern California seismicity, Journal of Geophysical Research, 107.

Tiampo, K.F., Rundle J.B., Klein, W. Sá Martins, J.S. and Ferguson C.D. (2003). Ergodic dynamics in a natural threshold system. Phys. Rev. Lett., 91, p. 238501

Tiampo, K.F., Rundle, J.B., Klein, W, Holliday, J. (2006). Forecasting rupture dimension using the Pattern Informatics technique, Tectonophysics, 424/3-4, pp. 367–376.

Tiampo, K.F., Rundle, J.B., Klein, W., (2006a). Premonitory seismicity changes prior to the Parkfield and Coalinga earthquakes in southern California. Tectonophysics 413, 77–86.

Tiampo, K.F., Rundle, Klein, W., (2006b). Stress shadows determined from a phase dynamicalmeasure of historic seismicity. Pure and Applied Geophysics. doi:10.1007/200024-006-0134-y.

Tiampo, K. F., Rundle, J. B., Klein, W., Holliday, J., S´aMartins, J. S. and Ferguson, C. D. (2007). Ergodicity in natural earthquake fault networks. Phys. Rev. E 75, 066107.

Tiampo, K.F., Klein, W., Li, H.-C., Mignan, A., Toya, Y., Rundle, J.B., Chen, C.-C., (2010). Ergodicity and earthquake catalogs: forecast testing and resulting implications. Pure and Applied Geophysics 167. doi:10.1007/s00024-010-0076-2.

Tiampo, K.F., Shcherbakov, R., (2012). Seismicity-based earthquake forecasting techniques: Ten years of progress, Tectonophysics, doi:10.1016/j.tecto.2011.08.019.

Turcotte, D. L. (1997). Fractals and chaos in geology and geophysics, 2nd edn. Cambridge, UK: Cambridge University Press.

Turcotte, D.L., Newman, W.I., Shcherbakov, R. (2003). Micro and macroscopic models of rock fracture. Geophysical Journal International 152, 718–728.

Torvund F., and Froyland, J. (1995). Strong ordering by non-uniformity of thresholds in a coupled map lattice. Physica Scripta 52, 624.

Utsu, T. (1961). A statistical study on the occurrence of aftershocks. Geophys. Mag. 30, 521.

Utsu, T., Ogata, Y. and Matsu'ura, R. S. (1995). The centenary of the Omori formula for a decay law of aftershock activity, Journal of Physics of the Earth, Vol.43, pp.1-33.

Vere-Jones, D. (2006). The development of statistical seismology, A personal experience. Tectonophysics 413, 5–12.

Wesnousky, S., (1994). The Gutenberg–Richter or characteristic earthquake distribution, which is it? Bulletin of the Seismological Society of America 84, 1940–1959.

Wyss, M., Shimaziki, K., Urabe, T., (1996). Quantitative mapping of a precursory seismic quiescence to the Izu-Oshima 1990 M6.5 earthquake, Japan. Geophysical Journal International 127, 735–743.

Zechar, J.D., Jordan, T.H. (2010). Simple smoothed seismicity earthquake forecasts for Italy. Annals of Geophysics 53.

Zoller, G., Hainzl, S., Ben-Zion Y., and Holschneider, M. (2006). Earthquake activity related to seismic cycles in a model for a heterogeneous strike-slip fault, Tectonophys., 423, 137–145.

Zoller G., Holschneider M., Hainzl S. (2013). The maximum earthquake magnitude in a time horizon: theory and case studies. Bull. seism. Soc. Am. 2013; 103 (2A) : 860-875.

Chapter 4

4 Spatial heterogeneity in earthquake fault-like systems

Various aspects of the spatial heterogeneities are studied in the long-range stress interaction earthquake fault model. As described earlier, localized stress accumulators are added into the system by converting a percentage of randomly selected sites into stronger sites which are called 'asperity cells'. These asperity cells support much higher failure stresses than the surrounding regular lattice sites but eventually rupture when the applied stress reaches their threshold stress. Here we investigate the scaling in these systems for different percentages of asperity sites and different asperity configurations, comparing those results with the simple homogeneous system with no asperities. We see that the addition of spatial heterogeneity into the lattice increases the length of the scaling regime and the size of the largest events as the randomness of the spatial pattern decreases. We also find that the total percentage of asperities can affect the capability of the system to produce larger events. In addition, we observe an increasing number of larger events associated with the total number of asperities in the lattice.

4.1 Introduction

Despite the multitude of space-time patterns of activity observed in natural earthquake fault systems, the bulk of the research associated with these patterns has focused on a relatively small fraction of the events, those associated with either larger magnitudes or persistent, localized signals such as aftershock sequences (Kanamori, 1981; Ogata, 1983; Utsu et al., 1995]. One significant problem associated with studies of the earthquake fault network is that the underlying dynamics of the system are not observable (Herz and Hopfield, 1995; Rundle et al., 2000]. A second is that the nonlinear earthquake dynamics are strongly coupled across a wide range of spatial and temporal scales (Kanamori, 1981; Main, 1996; Turcotte, 1997; Rundle et al., 1999; Scholz, 2002]. Finally, the relatively small number of extreme events occur very rarely, impacting our ability to evaluate the significance of the associated local and regional patterns in the instrumental and historic data (Schorlemmer and Gerstenberger, 2007; Vere-Jones, 1995, 2006; Zechar et al., 2010]. As a result, computational simulations are critical to enhancing our understanding of the dynamics of the earthquake system and the occurrence of its largest events (see, e.g., Rundle et al., 2003].

Although simple models cannot replicate the complete spectrum of earthquake phenomenology, these models can provide insights into the important patterns and features associated with the earthquake process and improve our understanding of the dynamics and underlying physics of earthquake fault networks. As a result, simple models of statistical fracture have been used to test some of the typical assumptions and parameters and their possible outcomes (Burridge and Knopoff, 1967; Otsuka, 1972; Rundle and Jackson, 1977; Rundle, 1988; Carlson and Langer, 1989; Nakanishi, 1990, Rundle and Brown, 1991; Olami et al., 1992; Alava et al. 2006). Most of these models assumed a spatially homogeneous earthquake fault, despite the fact that numerical and experimental models of rock fracture suggest that spatial inhomogeneities play an important role in the occurrence of large events and the associated spatial and temporal phenomenology (Dahmen et al., 1998; Turcotte et al., 2003; Tiampo et al., 2002, 2007; Lyakhovsky and Ben-Zion, 2009]. One argument for this approach has been that earthquake faults have long-range stress transfer (Klein et al., 2007]. For long-range

stress transfer without inhomogeneities, or randomly distributed inhomogeneities, these models have been found to produce scaling similar to the Gutenberg-Richter (GR) scaling found in real earthquake systems (Gutenberg and Richter, 1956; Serino et al., 2011]. When the stress transfer range is longer than the length scales associated with the inhomogeneities in the system, the dynamics appear to be unaffected by the inhomogeneities. However, recent work by Dominguez et al., (2013] shows that the ratio of the stress transfer range to the length scale of the inhomogeneities affects the GR scaling distribution and the ability of the system to produce large events.

The spatial arrangement of fault inhomogeneities is dependent on the geologic history of the fault. This history is typically quite complex and, as a result, the spatial distribution of the various inhomogeneities occurs on many length scales. Because spatial inhomogeneity plays an important role in the seismicity of an earthquake fault, here we extend the homogeneous OFC model with long-range stress transfer to inhomogeneous models, where particular parameters might vary from site to site.

There have been some earlier studies of the inhomogeneous OFC model (Janosi and Kertesz, 1993; Torvund and Froyland, 1995; Ceva, 1995; Mousseau, 1996; Ramos et al. 2006; Bach et al., 2008; Jagla, 2010). Although, these models considered a number of different ways to impose inhomogeneity on the system, most only investigated systems with nearest neighbor or short-range stress transfer. For example, Janosi and Kertesz (1993) introduced spatial inhomogeneity into the lattice by imposing random site-dependent stress thresholds. Torvund and Froyland (1995) imposed inhomogeneity by changing the uniform distribution of threshold stresses to a Gaussian distribution. Ceva (1995) introduced defects associated with the stress transmission parameter. Ramos (2006) and Jagla (2010) considered varying levels of randomness in the stress threshold.

Serino et al. (2011) studied OFC models with long-range stress transfer in which random damage was incorporated into the lattice. Dominguez et al. (2013) studied the various spatial configurations of damage in a long-range stress transfer model with varying amounts of stress dissipation, α ($0 < \alpha \leq 1$) which describe the portion of stress dissipated from the failed sites. Both models represented damage by imposing live and dead sites in

the lattice framework. The live sites can hold an internal stress that is a function of time. Dead sites cannot hold any stress and therefore all the stress that is passed to them during an event is dissipated from the system. The amount of stress dissipated by damage sites at each location can be characterized by the percentage of dead sites in a given neighborhood, φ_i. Serino et al. (2011) established a connection between the two types of dissipation, stress dissipation and damage dissipation, and Dominguez et al (2013) showed that they can be characterized together in one parameter, γ_i, herein called site dissipation, $\gamma_i = 1 - \varphi_i(1 - \alpha_i)$. Results showed that both stress dissipation and damage dissipation reduces the length of the scaling regime in their magnitude-frequency distributions and reduces the size of the largest events.

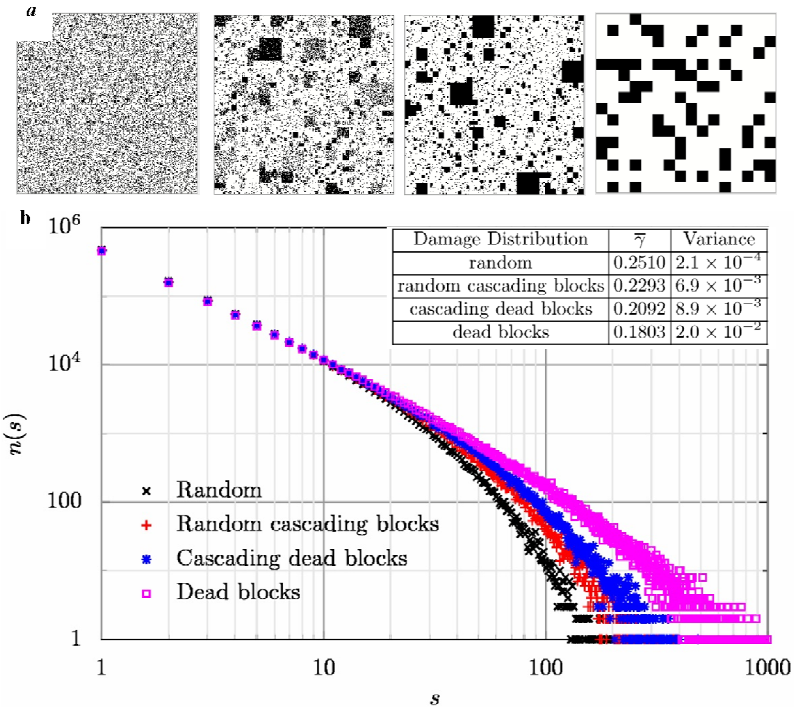

Figure 4-1 *a) Various configurations of 25% dead sites (in black) for a lattice with $\alpha = 0$ and a linear size $L = 256$. From left to right, lattices contain dead sites distributed randomly (random), blocks of various sizes, where each block has varying values of randomly distributed dead sites (random cascading blocks), completely dead blocks of various sizes (cascading dead blocks), and dead blocks of a uniform size (dead blocks); b) Numerical distribution of avalanche events of size s for the various spatial*

distributions of dead sites shown in (a) with stress transfer range R = 16. $\overline{\gamma}$ *is the average dissipation for each lattice.*

Dominguez et al. (2013) imposed various spatial patterns for the dead sites and compared the behavior with simpler systems with uniformly distributed stress dissipation. Figure 4-1 shows four different configurations of 25% dead sites for a lattice with linear size L=256, stress dissipation α=0, and a stress transfer range of R = 16. These include one case with randomly distributed dead sites (random); a second with blocks of various sizes, where each block has varying values of randomly distributed dead sites (random cascading blocks); a third with completely dead blocks of various sizes (cascading dead blocks); and a fourth with dead blocks of a uniform size (dead blocks). The resulting numerical distribution of events of size s for the various spatial distributions of dead sites shown is shown in Figure 4-1b. Here we see that the addition of spatial heterogeneity into the lattice increases the length of the scaling regime and the size of the largest events as the randomness of the spatial pattern decreases.

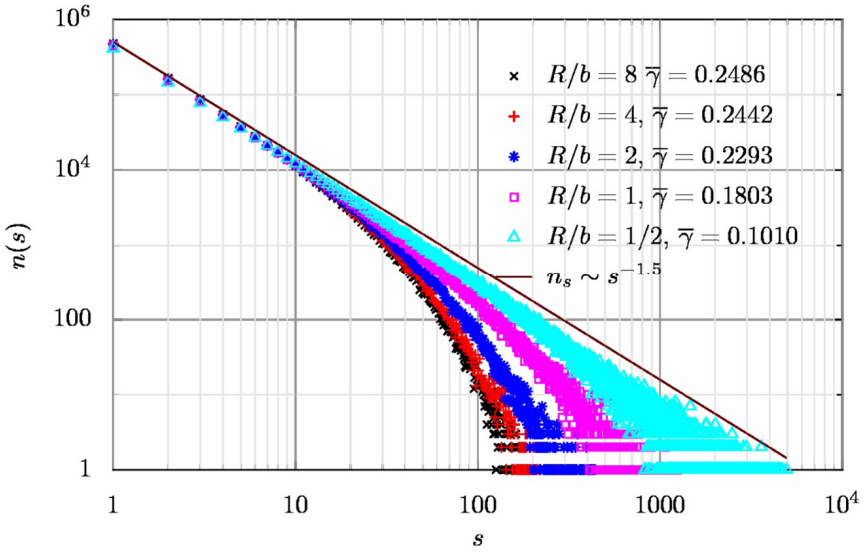

Figure 4-2 *Numerical distribution of avalanche events of size s for blocks of dead sites of linear size b. Systems are characterized by the dimensionless parameter R/b. (the inset corresponds to R/b = 1.) The size of the systems shown here is L = 256, α = 0, and the stress transfer range is R = 16.*

Figure 4-2 investigates the effect of the size of the damage blocks. Again, results are for a lattice with 25% dead sites, a linear size $L = 256$, stress dissipation $\alpha = 0$, and a stress transfer range of $R = 16$. The dead block size, b, is varied while the interaction length, R, remains constant. In this case, the scaling regime and maximum event size increases as the ratio R/b decreases. The spatial distribution of γ_i affects the potential for a large event because failing sites with low values of γ_i pass along a high percentage of excess stress to neighboring sites, encouraging additional failures. In the damage only system, site dissipation is determined by spatial locality only, so we require large clumps of sites with low values of γ_i in order to allow for a large event.

In this work, the focus is also on the spatial heterogeneity in OFC models with long-range stress transfer. The model is a cellular automata version of earthquake faults based on the OFC (Olami et al., 1992) and RJB (Rundle and Jackson, 1977; Rundle and Brown, 1991) models with some minor variations. Here, inhomogeneities are imposed in the model by allowing a percentage of randomly selected locations that accumulate higher levels of stress, similar to asperities on natural faults. These sites are incorporated by varying the ability of individual sites to support much higher stress for different spatial configurations. We find that the scaling relationship for the heterogeneous systems depends on the amount of the asperity sites as well as the spatial distribution of those asperities and the ratio of the size of the asperities to the stress transfer range. Investigation of the effects of a variety of spatial configurations for asperity sites provides insights into the construction of practical models of an earthquake fault system which is consistent with GR scaling.

4.2 The Model

Our model is a two-dimensional cellular automaton model with periodic boundary conditions. In this model every site in the lattice is connected to z neighbors, which are defined as sites within a certain distance or stress interaction range, R. A homogeneous residual stress σ^r is assigned to all the sites in the lattice. To impose spatial inhomogeneity on the lattice, two sets of failure thresholds are introduced; 'regular sites' with a constant failure threshold of σ^f and 'asperity sites' with a much higher failure

threshold ($\sigma^f_{(asperity)}=\sigma^f+\Delta\sigma^f$). These asperity sites are imposed in order to incorporate some percentage of stronger sites into the lattice which will bear higher stress before failure.

Initially, the internal stress variable, $\sigma_j(t)$, is randomly distributed on each site in such a way that the stress on all sites lies between the residual and failure stress thresholds ($\sigma^r < \sigma_i(t=0) < \sigma^f$). At t=0 no sites will have $\sigma_i > \sigma^f$. There are several ways to simulate the increase in stress associated with the dynamics of plate tectonics. Here we use the so-called zero velocity limit (Olami et al., 1992). The entire lattice is searched for the site that minimizes ($\sigma^f - \sigma_i$) and that amount of stress is added to each site such that the stress on at least one site is now equal to its failure threshold. That site fails and some fraction of its stress, given by α [$\sigma^f-(\sigma^r\pm\eta)$], is dissipated from the system. α is a dissipation parameter ($0 < \alpha \leq 1$) which describes the portion of stress dissipated from the failed site and η is randomly distributed noise. The failed site's stress is lowered to ($\sigma^r\pm\eta$) and the remaining stress is distributed to its neighbors. After the first site failure, all neighbors are searched to determine if the stress change from the failed site caused any of others to reach their failure stress. If so, the described procedure repeats for those neighbors and if not, the time step (known as the plate update) increases by unity and the lattice is searched again for the next site which minimizes ($\sigma^f - \sigma_i$). The size of the event is calculated from the total number of failures that expand from the first failed site. Stress is dissipated from the system both at the regular lattice sites and through asperity sites which are placed inhomogeneously throughout the lattice. However, because the asperity sites release much higher stress at the time of their failure, the amount of stress dissipated by these sites is different from the bulk of the system and results in inhomogeneous stress dissipation in this model.

Initial results for two different sized large asperity blocks are shown in Figure 4-3 (a-5% and b-10% of the total lattice sites are considered as asperity sites), with their associated magnitude-frequency relation plotted for varying values of α. Both plots support previous results that increasing values of stress dissipation decrease the length of the scaling regime and the time of the largest events, and that larger asperity, or damage, regions promote the occurrence of larger events.

In this study we want to investigate the scaling in these systems for different percentages of asperity sites and different asperity configurations, comparing those results with the simple homogeneous system with no asperities.

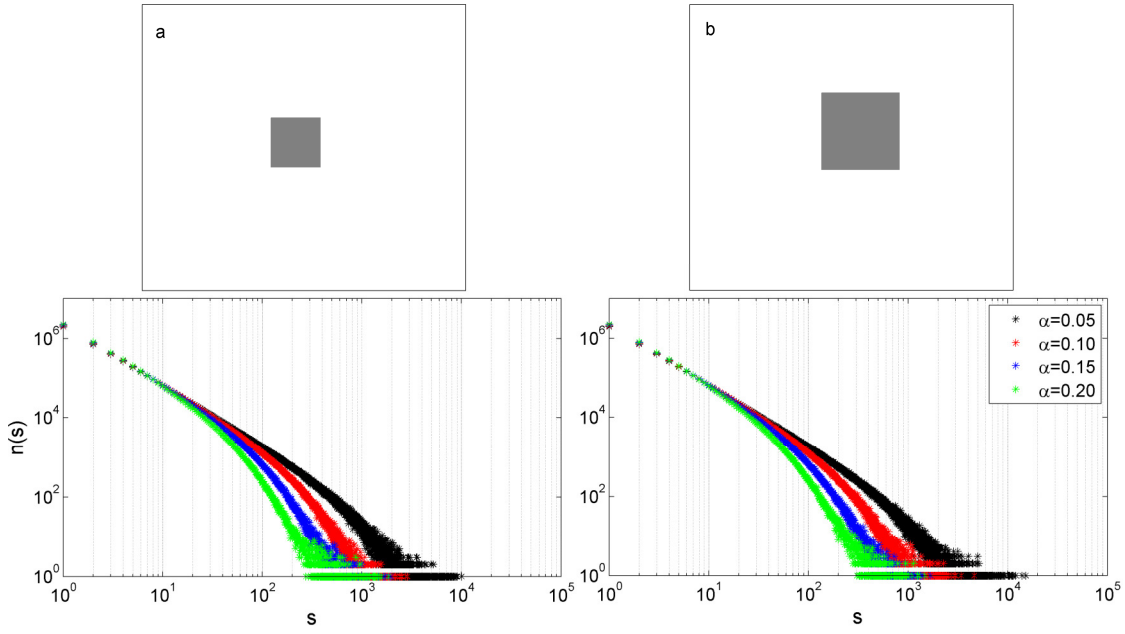

Figure 4-3 *a) Schematic depicting the size and location of a smaller set (5% of the total lattice sites) of grouped asperities (top). Numerical distribution of event sizes for varying values of stress dissipation, α, for the layout shown above. b) Schematic depicting the size and location of the larger set (10% of the total lattice sites) of grouped asperities (top). Numerical distribution of event sizes for varying values of stress dissipation, α, for the layout shown above.*

4.3 Percentage of asperity blocks

A system with different percentage of randomly distributed asperity sites in a two dimensional cellular automaton lattice of linear size L=256 with periodic boundary conditions and long range of interaction (R=16) is studied here. In this model we consider a homogeneous failure threshold for the regular sites of σ^f=2.0, a homogeneous residual stress for the entire lattice of σ^r=1.0, and a random distribution of noise as η=[-0.1,+0.1]. The failure threshold for the asperity sites is $\sigma^f_{(asperity)}=\sigma^f+10$. Figure 4-4 shows the distribution of event sizes for different cases where α is equal to 0.2. This study begins

with smaller percentages of asperities and increase the number of randomly distributed stronger sites in the lattice (no asperities in black, 1% in blue, 3% in green and 5% in red). As the percentage of asperities increases, the system produces significantly larger events. However, the relative number of moderate-sized events decreases as the number of asperities in the lattice is increased. By increasing the number of asperities in the lattice some of the moderate events appear to grow into a larger event. This migration from the moderate to large sizes could be consequence of two effects. When an asperity site breaks a greater amount of stress is released into the system and that amount of released stress can cause the failure of more sites and result in larger events, especially in a system with long range stress transfer.

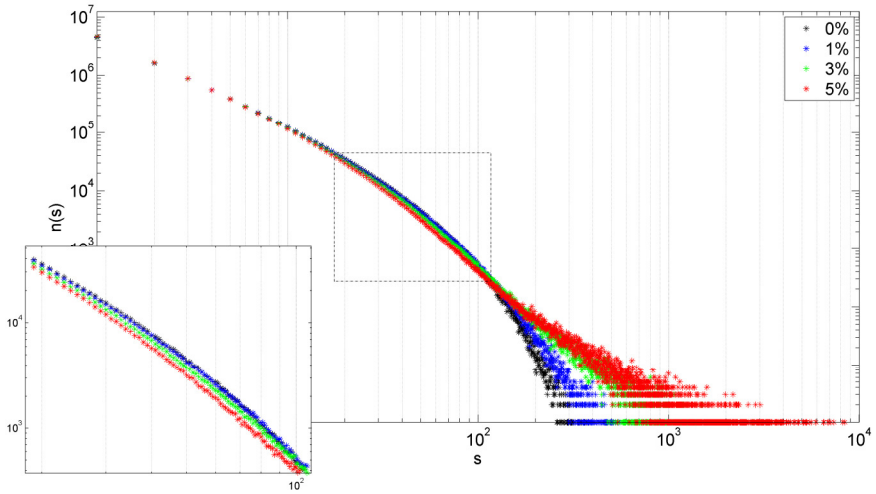

Figure 4-4 *Numerical distribution of events of size "s" for various amounts of randomly distributed asperity sites, α=0.2.*

In addition, a greater number of randomly distributed asperity sites in the lattice increases the probability of asperity sites triggering. In other words, a system with a higher density of asperities increases the chance of asperity blocks to be in the stress transfer range of another asperity. So, failure of one asperity site can results in a cascade behavior and a greater likelihood for a medium size event to grow and become an extreme event.

4.4 Configuration of spatial heterogeneity

Dominguez et al. (2013) studied the scaling behavior of systems with damage and showed that event distribution depends not only on the total amount of damaged sites in the system but also on the spatial distribution of damage. They noticed that lattices with more homogeneously distributed dead sites suppress large events. Here, we study the effect of different spatial configurations of the asperity blocks in the system.

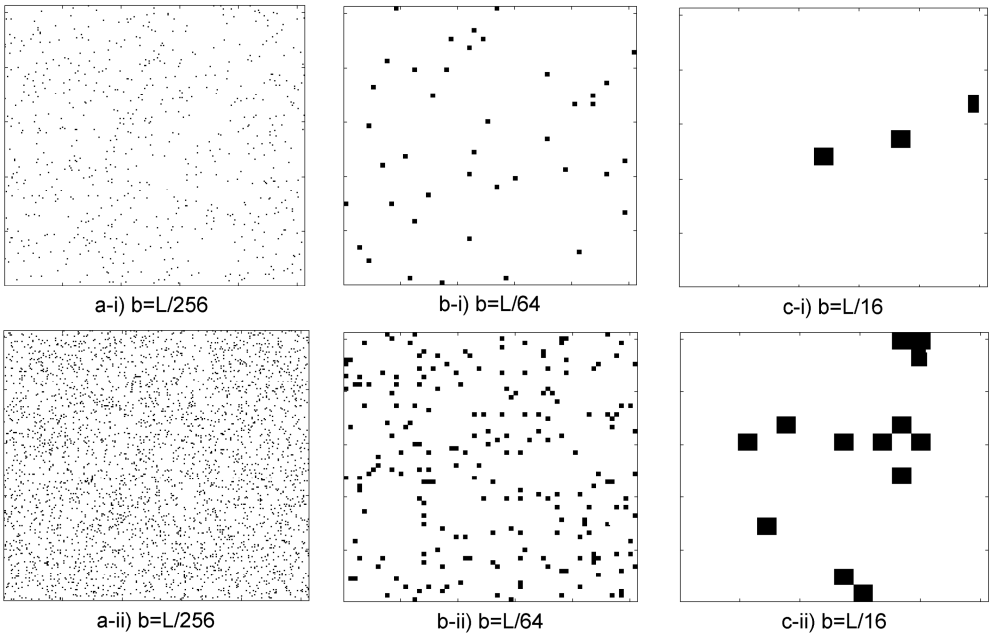

Figure 4-5 *Four different configurations of 1 percent asperity sites (upper row) and 5 percent asperity sites (lower row) (in black) for lattices with linear size L=256. Each lattice has asperity blocks of a single size b. For each a) b=L/256, b) b=L/64, c) b=L/32, and d) b=L/16.*

In this model, the lattices have the same size (256 × 256), a constant percentage of asperity sites (1% and 5% for each case), and a constant stress transfer range (R = 16). As a result, any differences in the large event behavior are not caused by the finite size of the lattice. Figure 4-5 presents two-dimensional lattices of linear size L = 256 and asperity blocks with a linear size of b which are randomly distributed throughout the system and two cases of 1% (top) and 5% (bottom) of asperity sites (note that the stress dissipation parameter is constant in all cases, α = 0.2). To highlight the distinction between the different configurations of asperities, logarithmic bins are used in the distributions and they are normalized to the total number of events in each case. Figure 4-6 shows the probability density function of event sizes for the various arrangements of asperity blocks in Figure 4-5.

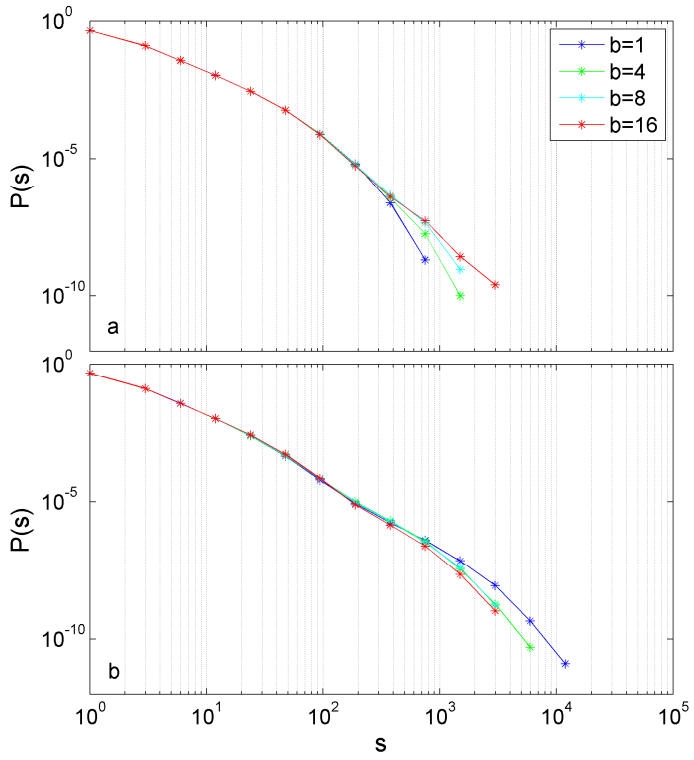

Figure 4-6 *Normalized probability density function of events of size "s" for various sizes of asperity blocks which are randomly distributed in the system for R=16 and a) 1% and b) 5% of asperity sites.*

By changing the linear size of the asperity blocks, we ensure that at least some of the asperity sites which are inside a larger asperity block are in the stress transfer range of others and will certainly interact with each other. On the other hand, we decrease the probability of interaction between two large blocks of asperity sites. Although the number of asperity sites is constant, changing the linear size of the asperity sites has a significant effect on the event distributions. For 1% of asperities, b=1 (Figure 4-5a-i) has the lowest spatial separation among the different size of asperity blocks. But since there are fewer of asperities in the lattice, the probability of interaction between the asperity sites is still very low and big events do not occur even with the failure of an asperity site. For b=4, there are 16 asperity sites in a 4 by 4 block that are adjacent to each other. Failing a site in the asperity block can easily trigger the rest of the block and create larger events than for b=1 (Figure 4-6a). The numerical distributions for b=8 and b=16 confirms that there is triggering of asperity sites inside the block, but because the distance between the blocks is higher than the stress transfer range they cannot affect each other directly. Again, in this case the largest events occur for smaller values of R/b.

The biggest event for 5% of asperity sites falls between different configurations of asperity blocks and occurs for the smallest block size (Figure 4-6b, b=1). Because the percentage of asperities is much higher, the shortest spatial separation between the asperities occurs in the case of b=1 and there is a higher probability of asperity triggering. In this case, the number of triggered asperity sites increases and a much bigger event occurs. However, increasing the linear size of asperity blocks (b=4, 8 and 16) increases the probability of triggering inside a block, but it also increases the spatial separation between the blocks, resulting in a decrease in the probability of triggering between asperity blocks.

4.5 Range of interaction

To further investigate the effect of block size and asperity triggering on event size for larger numbers of asperities, we focus on the stress transfer range. Here, 5% of asperity sites are randomly distributed in the system in the blocks with four different linear sizes (b=1, 4, 8 and 16, Figure 4-5a-ii, b-ii, c-ii and d-ii) and the system is run for three

different stress transfer ranges, R=16, R=8 and R=1. Figure 4-7 shows the comparison between the event distributions for different stress transfer ranges and different asperity block sizes. By reducing the stress transfer range, the likelihood that an asperity site will be affected by a neighboring asperity site decreases. This results in a lower probability of asperity triggering in the model. The absence of triggering asperities makes the system unable to produce big events. Figure 4-7 confirms that, for lower percentages of asperities, the size of the biggest event occurs in systems with long range interactions (R=16), regardless of the asperity block size, and that event is much larger than the size of the biggest event in system with short stress transfer range. In addition, for short range stress transfer (R=1), the size of the largest events does not change with increasing asperity block size. For longer range stress transfer, the size of the asperity blocks affects the size of the biggest event.

4.6 Stress dissipation

We also compare the effect of stress dissipation parameters on different asperity configurations in a system with long stress transfer range, R=16. As discussed earlier, upon failure, some fraction of a site's stress, given by $\alpha\ [\sigma^f-(\sigma^r \pm \eta)]$, is dissipated from the system ($0 < \alpha \leq 1$). In general, lower stress dissipation models produce more larger events and higher stress dissipation suppresses large events.

This also should be true in the system with asperity sites. In higher dissipation models, less stress is transferred to neighboring sites, even when asperities fail. As a result, there is lower probability of asperity triggering in the model. This implies smaller events and more plate update steps to fail all of the asperities. In Figure 4-8 the event distribution for four different stress dissipation parameters and 1% of asperity sites in the lattice is compared for three different configuration of asperity blocks (b=1, b=4 and b=16). This figure shows the results for four stress dissipation parameters, α=0.2, 0.3, 0.4 and 0.5, in each 20%, 30%, 40% and 50% of the failed site stress dissipates at the time of failure and the remaining stress is distributed to its z=1088 neighbors.

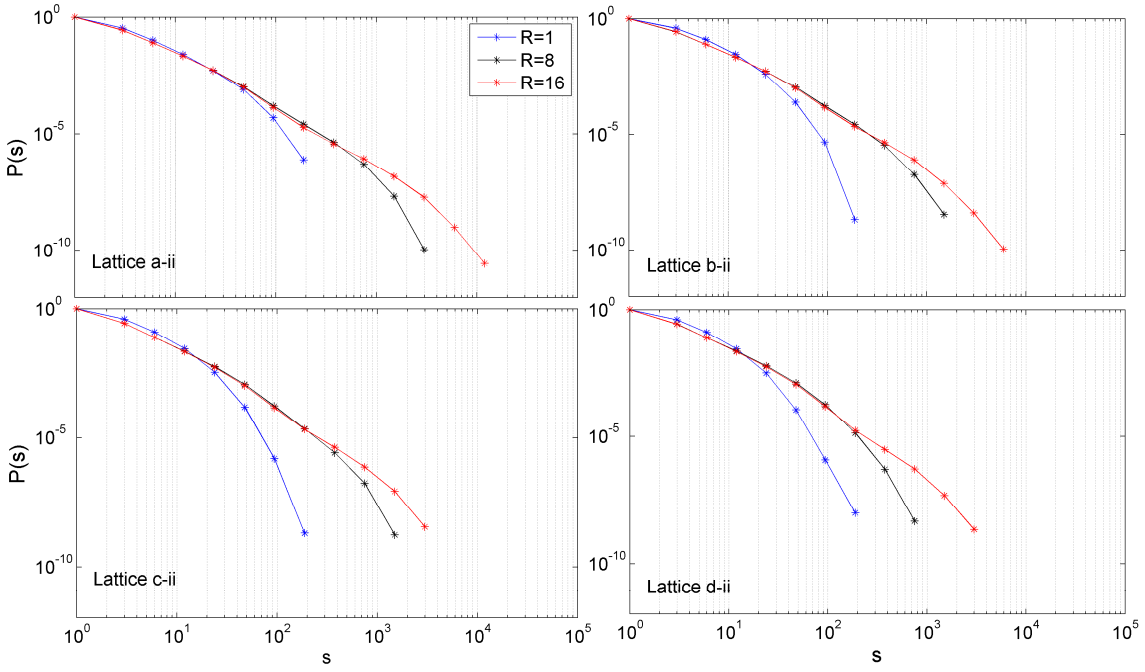

Figure 4-7 *Normalized probability density function of events of size s for various stress transfer range in a system with 5% of asperity sites for four different linear sizes of asperity blocks shown in Figure 2 and a) b=1, b) b=4, c) b=8 and d) b=16.*

For all three asperity configurations (Figure 4-8 a, b and c), lower values of stress dissipation leads to a higher number of big events. On the other hand, in systems with a high amount of stress dissipation, the released stress from a small asperity block is not enough to offset the greater dissipation and cannot trigger any of the neighboring asperity blocks. As a result, the change in the asperity block size from b=1 to b=4 (Figure 4-8a and 4-8b) does not significantly affect the distributions of events, especially for higher stress dissipation. However, the released stress from bigger asperity blocks of b=16 is high enough to trigger another asperity block. We again observe larger events in the tail of the distributions, even for higher stress dissipation models (Figure 4-8c).

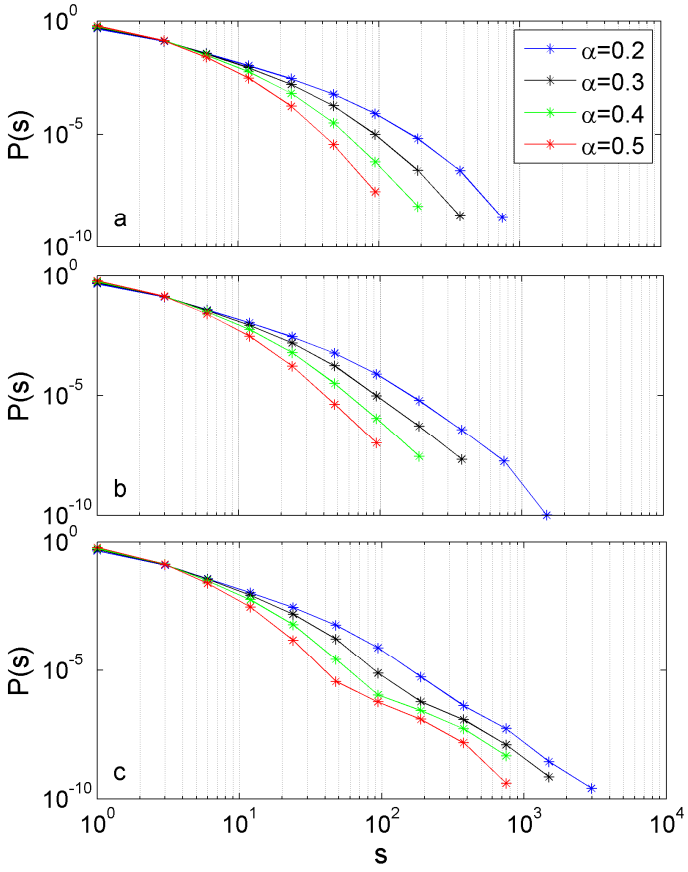

Figure 4-8 *Normalized probability density function of events of size s for various amount of stress dissipation parameter and for 1% of three different sizes of asperity blocks randomly distributed in the system for a) b=1, b) b=4 and c) b=16.*

4.7 Discussions

Here we investigated a variation of the OFC model in which localized stress accumulators were added to the system by converting a small percentage of the lattice site into stronger sites. We studied different spatial configurations of the stronger asperity sites and observed the effect of asperity patterns on the distribution of event sizes in the systems for a selected stress transfer range. In particular, we observed an increasing number of larger events associated with the total number of asperities in the lattice (Figure 4-4). We also found that imposing a fixed number of asperity sites with different spatial distributions strongly affects the capability of the fault system to generate extreme events, but that the total percentage of asperities is important as well. The event

distributions shown in Figure 4-6 confirm the sensitivity of the system to different configurations of inhomogeneities. In addition, we studied the role of the interaction range on triggering asperities and observed that the probability of asperity triggering and the occurrence of larger events is much higher in the in those systems with a longer stress transfer range (Figure 4-7). However, in models with higher dissipation it is the asperities are less sensitive to other failures and therefore the probability of asperity triggering decreases in high dissipation models. This implies that higher dissipation results in a lower probability of smaller events regardless of the number and spatial distribution of asperities.

4.8 References

Alava, M. J., Nukala, P., and Zapperi, S. (2006), Statistical models of fracture, Adv. Phys. 55, 349.

Bach, M., Wissel F. and Dressel, B. (2008), Olami-Feder-Christensen model with quenched disorder. Phys. Rev. E77, 067101.

Burridge, R., Knopoff, L. (1967), Model and theoretical seismicity, Bull. Seismol. Soc. Am. 57. 341–371.

Carlson, J. M. and Langer, J. S. (1989), Mechanical model of an earthquake fault. Phys. Rev. Lett. 62, 2632; Phys. Rev. A 40, 6470.

Ceva, H. (1995), Inhuence of defects in a coupled map lattice modelling earthquakes. Phys. Rev, E52, 154.

Dahmen, K., Ertas, D., and Ben-Zion, R. (1998), Gutenberg-Richter and Characteristic Earthquake Behavior in Simple Mean-field Models of Heterogeneous Faults, Phys. Rev. E 58, 1494–1501.

Dominguez, R., Tiampo, K.F., Serino, C.A. and Klein W. (2013), Scaling of earthquake models with inhomogeneous stress dissipation. Phys. Rev. E 87, 022809.

Gutenberg, B. and Richter, C.F. (1956), Magnitude and energy of earthquakes. Annali di Geofisica, Vol. 9, n. 1.

Herz, A.V.M., and Hopfield, J.J. (1995), Earthquake Cycles and Neural Reverberations, Collective Oscillations in Systems with Pulse-Coupled Threshold Elements. Phys. Rev. Lett., 75, 1222-1225.

Jagla, E.A. (2010), Realistic spatial and temporal earthquake distributions in a modified Olami-Feder-Christensen model. Phys. Rev, E81, 046117.

Janosi, I.M. and Kertesz, J. (1994), Self-organized criticality with and without conservation. Physica A200, 0378.

Kanamori, H. (1981), The nature of seismicity patterns before large earthquakes, in Earthquake Prediction, Maurice Ewing Series, IV, 1–19, AGU, Washington D.C..

Klein, W., Gould, H., Gulbahce, N., Rundle, J. B. and Tiampo, K. (2007), Structure of fluctuations near mean-field critical points and spinodals and its implication for physical processes. Phys. Rev. E 75, 031114.

Lyakhovsky, V. and Ben-Zion, Y. (2009), Evolving geometrical and material properties of fault zones in a damage rheology model, Geochem. Geophys. Geosyst., 10, Q11011.

Main, I. (1996), Statistical physics, seismogenesis, and seismic hazard. Rev. Geophys. 34, 433–462.

Mousseau, N. (1996), Synchronization by Disorder in Coupled Systems. Phys. Rev. Lett. 77, 968.

Nakanishi, H. (1990), Cellular-automaton model of earthquakes with deterministic dynamics. Phys. Rev. A 41, 7086.

Olami, Z., Feder, HJS., Christensen, K. (1992), Self-organized criticality in a continuous, nonconservative cellular automaton modelling earthquakes. Phys Rev Lett 68(8):1244–1247.

Ogata, Y. (1983), Estimation of the parameters in the modified Omori formula for aftershock frequencies by the maximum likelihood procedure, Journal of Physics of the Earth, Vol.31, 115-124.

Otsuka, M. (1972), Phys Earth Planet Inter. 6-311.

Ramos, O., Altshuler, E. and Maloy K.J. (2006), Quasiperiodic Events in an Earthquake Model. Phys. Rev. Lett. 96, 098501.

Rundle, J.B., Turcotte, D.L., Shcherbakov, R., Klein, W., Sammis, C.,(2003), Statistical physics approach to understanding the multiscale dynamics of earthquake fault systems. Review of Geophysics, 41, 1019.

Rundle, J. B., Klein, W., Tiampo, K. and Gross S., (2000), Linear pattern dynamics in nonlinear threshold systems, Phys. Rev. E, 61 (3), 2418–2431.

Rundle, JB, Klein W. and Gross S. (1999), Physical basis for statistical patterns in complex earthquake populations: Models, predictions, and tests, PAGEOPH, 155, 575-607.

Rundle, J. B. and Brown, S. R. (1991), Origin of Rate Dependence in Frictional Sliding, J. Stat. Phys. 65, 403.

Rundle, J. B. (1988), A physical model for earthquakes, J. Geophys. Res. 93-6237.

Rundle, J. B. and Jackson, D. D. (1997), Numerical simulation of earthquake sequences, Bull. Seismol. Soc. Am. 67.

Serino, C. A., Tiampo, K. F. and Klein W. (2011), New Approach to Gutenberg-Richter Scaling, Phys. Rev. Lett. 106, 108501.

Scholz, C.H. (2002), The mechanics of earthquakes and faulting, Cambridge University Press, p. 471.

Schorlemmer, D., and Gerstenberger, M. C. (2007), RELM testing center, Seismol. Res. Lett. 78, 1, 30-36.

Tiampo, K. F., Rundle, J. B., Klein, W., Holliday, J., S´aMartins, J. S. and Ferguson, C. D. (2007), Ergodicity in natural earthquake fault networks. Phys. Rev. E 75, 066107.

Tiampo, K.F., Rundle, J.B., McGinnis, S., Gross, S., Klein, W. (2002), Mean-field threshold systems and phase dynamics: an application to earthquake fault systems. Eur. Phys. Lett. 60, 481–487.

Torvund F., and Froyland, J. (1995), Strong ordering by non-uniformity of thresholds in a coupled map lattice. Physica Scripta 52, 624.

Turcotte, D.L., Newman, W.I., Shcherbakov, R. (2003), Micro and macroscopic models of rock fracture. Geophysical Journal International 152, 718–728.

Turcotte, D. L. (1997), Fractals and chaos in geology and geophysics, 2nd edn. Cambridge, UK: Cambridge University Press.

Utsu, T., Ogata, Y. and Matsu'ura, R. S. (1995), The centenary of the Omori formula for a decay law of aftershock activity, Journal of Physics of the Earth, Vol.43, pp.1-33.

Vere-Jones, D. (2006), The development of statistical seismology, A personal experience. Tectonophysics 413, 5–12.

Vere-Jones, D. (1995), Forecasting earthquakes and earthquake risk. International Journal of Forecasting 11, 503–538.

Zechar, J.D., Jordan, T.H. (2010), Simple smoothed seismicity earthquake forecasts for Italy. Annals of Geophysics 53.

Chapter 5

5 General discussion and conclusions

5.1 Summary and Conclusions

The goal of this work is to study the role of inhomogeneities in an earthquake fault-like system with long-range interactions by imposing different amount of spatial inhomogeneities in different sizes and configurations in a cellular automaton model of earthquakes.

The proposed model is a two-dimensional cellular automata model with periodic boundary conditions that is variation of the well-known Rundle, Jackson and Brown (RJB) and Olami-Feder-Christensen (OFC) earthquake fault models. In this model every site in the lattice is connected to z=1088 neighbors which are defined as sites within a certain distance or stress interaction range, R=16. Spatial inhomogeneity is imposed on the lattice by introducing two sets of different failure thresholds. The stronger sites, designated “asperity sites”, are significantly stronger than the surrounding lattice sites but eventually rupture when the applied stress reaches their higher failure threshold. A higher amount of stress is released into the system at the time of their failure.

In the first study, 1% randomly distributed asperity sites are included in the long-range stress transfer model. The findings illustrate that although the asperities do not change the modified GR relation proposed in (Serino, et al., 2011), this type of inhomogeneity introduces temporal clustering of events which is very similar to that seen in real earthquake fault systems. Characteristic earthquake sequences are observed which are associated with periods of higher activity that start with gradually increasing numbers of larger events, or foreshocks, that display AMR-like behavior, and end with a tail of decreasing activity, or aftershocks (Fig. 2-2). Similar to activity observed in different tectonic regions (Fig. 2-3), the relative length of the foreshock and aftershock sequences

varies and the length of the foreshock and aftershock activation period is shown to be related to one or more controlling parameters of the model, including the stress dissipation (Fig. 2-4). These results provide a potential explanation for the observation that certain tectonic regimes, such as mid-ocean ridges, produce measurable foreshock sequences, while others, such as crustal transform faults, produce very few foreshocks. These initial results also suggest that asperities are responsible for the time-dependent behavior observed in natural earthquake fault systems and support the hypothesis that spatial and temporal patterns observed in natural seismicity are controlled by the underlying physical properties, rather than simple triggering alone.

The second stage of this study investigates the effect of variations in the total number of asperity sites (1%, 3% and 5%), both in systems with random spatial distributions of asperities and those with a single large block of asperities. The effect on the magnitude-frequency distribution of events as well as the spatial and temporal clustering of events is studied in greater detail and with respect to different stress dissipation regimes in the system. It was found that regardless of the presence of inhomogeneity in the system, higher stress dissipation systems suppress the ability of the system to produce larger events (Figure 3-1). Also, increasing the number of asperity sites in the systems with a constant stress dissipation parameter promotes the occurrence of larger events (Figure 3-2 and 3-3). Results confirm that although the incidence of inhomogeneities does not change the form of the modified GR relation proposed by Klein et al. (2007), it does affect the size of the largest events, the length of the scaling regime and the upper bound of the modified GR. In addition, it appears that the stronger lattice sites create a second distribution of the same form as the smaller events, but for the large events. Therefore the overall magnitude-frequency distribution becomes a combination of two distinct distributions of the same form for the smaller and larger events (Figure 3-5).

The clustering of events seen in Chapter 2 is investigated in more detail for systems with higher percentages of inhomogeneities. The spatiotemporal clustering of events is dependent on the size and spatial configuration of the asperities (Figures 3-7 and 3-8). These results show that the presence of inhomogeneities in terms of the asperity sites in the system results in the occurrence of seismic sequences at regular time intervals which

starts with a slow increase in the number and size of events and ends with a tail of decreasing activity after the mainshock. This behaviour is very similar to the concepts of both characteristic earthquakes and seismic sequences (Figure 3-6). The increasing number of larger events in these recurrent time series follows a pattern of precursory AMR activity prior to the mainshock comparable to that observed in natural seismicity (Figure 3-9). Results from the inverse TM metric plots also highlighted a clear deviation from stationarity at the time steps prior to the mainshock (Figures 3-10 and 3-11). In addition, the decay rate of the aftershock sequences and the growth rate of the foreshock sequences can vary, as observed in different tectonic regions. Analysis of the Omori law relation for both types of sequences confirms that these rates are related to one or more of the controlling parameters of the model, including both the amount and complexity of the asperities as well as the stress dissipation (Figures 3-12 and 3-13).

In the final stage of this study, different spatial configurations of the stronger asperity sites in the systems were investigated for selected stress transfer ranges in order to observe the effect of asperity patterns on the event distribution. In particular, it was shown that imposing a fixed number of asperity sites with different spatial distributions on the lattice strongly affects the capability of the fault system to generate extreme events, but that the total percentage of asperities is important as well. The event distributions shown in Figure 4-6 confirm the sensitivity of the system to different configurations of inhomogeneities.

In addition, the role of the interaction range on triggering asperities was studied and it was observed that the probability of asperity triggering and consequently the occurrence of larger events is much higher in systems with longer stress transfer range (Figure 4-7). However, in models with higher dissipation the asperities are less sensitive to the failure of their neighboring asperity sites and therefore the probability of asperity triggering is much lower in such systems. This implies that higher dissipation results in a lower probability of smaller events regardless of the number and spatial distribution of asperities.

Finally, results from this simple earthquake fault model support the hypothesis that spatial heterogeneities play an important role on the primary features of both modeled and natural earthquake sequences and that the spatial and temporal patterns observed in natural seismicity may be controlled by the underlying physical properties. Our model reproduced the modified GR distribution and the size of the largest events and the length of the scaling regime on each fault are controlled by the amplitude of the stress dissipation of the system. The superposition of many faults, each with a different amount of damage, results in GR scaling in the larger fault network. Spatial features affect the critical point scaling behavior intrinsic to the earthquake fault process and the associated structure and geometry directly impacts the spatial and temporal nature of fault networks. These findings suggest that asperities could be responsible for much of the spatial and temporal behavior of real earthquake fault systems and support the hypothesis that the patterns observed in natural seismicity may be controlled by the underlying physical complexity, rather than simple triggering alone.

5.2 Suggestions for future studies

This study on a simple inhomogeneous cellular automata model of earthquake fault systems provides insights into the important aspect of heterogeneities in natural fault systems. The effect of the total number and the configuration of the inhomogeneities in such systems are studied. The research presented in this thesis also raises additional questions that should be pursued.

First of all, the next step toward understanding a more realistic fault model should include investigating the effect of the asperity strength and effects of different configurations of asperities with different failure threshold on the spatiotemporal clustering of events.

The second step is to study the role of the stress transfer range on the asperity triggering of a fault. In particular, associating a dependent range of interactions with the strength of the asperities will likely ensure that the simulations are closer to those of a real fault system.

Third, understanding the interaction between the numbers of asperity sites in the systems with different stress dissipation and stress transfer ranges, and how they affect the triggering of the asperities, could provide a better understanding of the effects of inhomogeneities in natural fault systems.

Fourth, more detailed comparison of the model results for various parameter ranges with historic earthquake seismicity from a variety of regions, including swarms, induced seismicity and tectonic sequences, can help to both narrow the applicability of the associated parameter (stress dissipation and percent asperities) as well as provide potential insights into natural fault structure.

Finally, it also is possible to establish a fault network of individual interacting fault models with different internal parameters, using the presented model as a basis, in order to model a more realistic fault system of interacting faults.

5.3 References

Klein, W., Gould, H., Gulbahce, N., Rundle, J. B. and Tiampo, K. (2007). Structure of fluctuations near mean-field critical points and spinodals and its implication for physical processes. Phys. Rev. E 75, 031114.

Serino, C. A., Tiampo, K. F. and Klein W. (2011), New Approach to Gutenberg-Richter Scaling, Phys. Rev. Lett. 106, 108501.

Appendices

Appendix A: The computer code

This appendix contains the computer code that is used to model the earthquake fault system. The code is written in the FORTRAN language.

```
      Program Inhomogeneous OFC Model
! The code is written by Javad Kazemian to model an inhomogeneous fault based on the homogeneous OFC Model
! Last revision November 2013
      implicit none
!*************************************************************************************
! DEFINING THE INTERNAL VARIABLES OF THE CODE

      integer*1 tempi1,syo,wri,asp(20000000)
      integer*2 L,minl(2),x,y,xf(20000000),yf(20000000),tempi,neib
      integer*4 timeArray(3),t,ta,i,j,tsel,tlen,i1,aval(20000000)
      real:: alpha,rand,minv,sr,dsigmaf,noise,stressr(20000000),stressi(20000000)
      integer,allocatable:: st(:,:),stat(:,:)
      real,allocatable:: sigma(:,:),sigmar(:,:),sigmac(:,:),fmin(:,:)
      character filename*45,yes*1

!*************************************************************************************
! Defining the input parameters

      L=256          ! Linear size of the Lattice
      alpha=0.05     ! Stress dissipation Parameter
```

```
neib=16          ! Defining the Radius of the neighborhood
dsigmaf=10.0     ! Δσ_f
noise=0.10       ! Amplitude of the Noise η
syo=0            ! Selecting the boundary condition, 0 for periodic and 1 for open boundary
tsel=10000000    ! The time step in which the code starts to collect the statistics
tlen=10000000    ! Length of the window for collecting the statistics

!*****************************************************************************
! ALLOCATING THE INTERNAL VARIABLES WICH ARE DEPENDENT TO THE INPUT PARAMETERS

allocate(sigma(L,L),sigmar(L,L),sigmac(L,L),st(L,L),fmin(L,L),stat(L,L))
st=0;sigma=0.0;sigmar=0.0;sigmac=0.0;fmin=0.0;t=1;ta=1
tempi=0;i=0;j=0;wri=0;xf=0;yf=0;asp=0;aval=0;i1=1

!*****************************************************************************
! Reading the time of the system to use as a seed for "Rand" function

call itime(timeArray)
write(*,'(/,a13,2x,i2,a1,i2,a1,i2)')" Start time",timearray(1),":",timearray(2),":",timearray(3)
j= rand (timeArray(1)+timeArray(2)+timeArray(3))
!*****************************************************************************
! Selecting the asperity sites regions by calling different subroutines for different configurations
! BR: Random distributions
! B16: 16 by 16 randomly distributed blocks
! B16C: Cascading distribution
! B16RC: Random Cascading distribution
call br(L,st)
```

```
! Single block of asperity sites in desired size
!       do i=1,44
!       do j=1,45
!               st(i+100,j+100)=1
!       enddo
!       enddo
!*************************************************************************
! Assigning the residual and failure threshold to all the sites in the lattice containing the asperity sites as
well as assigning white random noise with the predefined amplitude

        do i=1,L
                do j=1,L
                        sigmar(i,j)=1.0+noise*(2*rand(0)-1)
                        sigmac(i,j)=2.0
                        sigma(i,j)=sigmar(i,j)+(sigmac(i,j)-sigmar(i,j))*rand(0)
                        if (st(i,j)==1) then
                                sigmac(i,j)=sigmac(i,j)+dsigmaf
                                tempi=tempi+1
                        endif
                        if (sigmac(i,j)<sigma(i,j).or.sigmar(i,j)>sigma(i,j)) then
                                print*,sigmar(i,j),sigmac(i,j),sigma(i,j)
                        endif
                enddo
        enddo
!*************************************************************************
! Printing the input parameters of the model to verify
        print*, "Number of asperity sites", tempi
```

```
        if(syo==1)write(*,'(1x,a13)')'Closed system'
        if(syo==0)write(*,'(1x,a11)')'Open system'
        write(*,'(1x,a3,1x,i3)')'L= ',L
        write(*,'(1x,a3,1x,i5)')'n= ',(2*neib+1)**2-1
        !write(*,'(1x,a3,1x,i3)')'R= ',neib
        write(*,'(1x,a7,1x,f3.2)')'alpha= ',alpha
        write(*,'(1x,a15,1x,f6.2)')'Delta sigma F= ',dsigmaf
        write(*,'(1x,a7,1x,f5.2)')'Noise= ',noise
        write(*,'(1x,f5.2,1x,a50)')(1.*tempi/L**2)*100,"percent of the sites are considered as asperities"
! Check to see if the user wants to start from an existing file of the state of the system or not
        print*,"Load stress values from an existing file? (y/n)"
        read*,yes
        if(yes=='y')then
                open(99,file=filename,status='old')
                read(99,'(i3,1x,i3,1x,f6.3)')((x,y,sigma(x,y),j=1,L),i=1,L)
                close(99)
                print*,'loads the inputs'
        endif
        print*,'Start'
        x=0;y=0
!*********************************************************************************
! MAIN BODY OF THE CODE
        do
                stat=0
!****************************************
! Finding the minimum value of sigma(i)-sigmar and adding that amount to all lattice
                fmin=sigmac-sigma
```

```
                minv=minval(fmin)
                minl=minloc(fmin)
                xf(i1)=minl(1)
                yf(i1)=minl(2)
                sigma=sigma+minv
                stressi(i1)=minv
                do i=1,L
                        do j=1,L
                                if (sigma(i,j)>=sigmac(i,j)) stat(i,j)=1
                        enddo
                enddo
                tempi=1
                do while (tempi==1)
                        tempi=0
!*****************************************
! Failing of the site and distributing its stress to the predefined neighbours

                        if (st(minl(1),minl(2))==1) asp(i1)=1
                        sr=(1-alpha)*(sigma(minl(1),minl(2))-sigmar(minl(1),minl(2)))
                        aval(i1)=aval(i1)+1
                        stressr(i1)=stressr(i1)+sr
                        minv=0
                        sigma(minl(1),minl(2))=sigmar(minl(1),minl(2))
                        stat(minl(1),minl(2))=0
                        sigmar(minl(1),minl(2))=1.0+noise*(2*rand(0)-1)

! ****    Choosing different versions of neighborhood
```

```
! ****    Nearest neighbour open boundary
! ****
!                       do i=1,4
!                               selectcase (i)
!                                       case(1)
!                                               x=minl(1)-1
!                                               y=minl(2)
!                                       case (2)
!                                               x=minl(1)+1
!                                               y=minl(2)
!                                       case (3)
!                                               x=minl(1)
!                                               y=minl(2)-1
!                                       case (4)
!                                               x=minl(1)
!                                               y=minl(2)+1
!                               endselect
!                               if(x>0.and.x<=L.and.y>0.and.y<=L) sigma(x,y)=sigma(x,y)+(sr/4.0)
!                       enddo
!*********************************************
!****    Nearest neighbour Close boundary
!                       do i=1,4
!                               selectcase (i)
!                                       case(1)
!                                               x=minl(1)-1
!                                               if (x<=0) x=x+L
!                                               y=minl(2)
```

```
!                                       case (2)
!                                               x=minl(1)+1
!                                               if (x>L) x=x-L
!                                               y=minl(2)
!                                   case (3)
!                                               x=minl(1)
!                                               y=minl(2)-1
!                                               if (y<=0) y=y+L
!                                       case (4)
!                                               x=minl(1)
!                                               y=minl(2)+1
!                                               if (y>L)  y=y-L
!                                   endselect
!                                   sigma(x,y)=sigma(x,y)+(sr/4.0)
!                           enddo
!***********************************************
! ****   Next nearest neighbour close boundary
                            do i=minl(1)-neib,minl(1)+neib
                                    do j=minl(2)-neib,minl(2)+neib
                                            x=i
                                            y=j
                                            !if(syo==1)then
                                                    if (i<=0) x=x+L
                                                    if (i>L)  x=x-L
                                                    if (j<=0) y=y+L
                                                    if (j>L)  y=y-L
                                                    if (x/=minl(1).or.y/=minl(2)) then
```

```
                                        sigma(x,y)=sigma(x,y)+(sr/((2.*neib+1)**2-1))
                                        endif
! ****  Next nearest neighbour open boundary
                                    !elseif(syo==0)then
!                                       if(x>0.and.x<=L.and.y>0.and.y<=L)then
!                                           if (x/=minl(1).or.y/=minl(2)) then
!                                       sigma(x,y)=sigma(x,y)+(sr/((2.*neib+1)**2-1))
!                                           endif
!                                       endif
                                    !endif
                                enddo
                            enddo
!****************************************
! Check to see if there was another site ready to fail before redistribution of stresses
                            tempi1=0
                            do i=1,L
                                do j=1,L
                                    if (stat(i,j)==1)then
                                        tempi1=1
                                        tempi=1
                                        minl(1)=i
                                        minl(2)=j
                                    endif
                                enddo
                            enddo
! ****************************************
! When there is no site before redistribution of stresses check to find the minimum sigma-sigmar again
```

```
                if (tempi1==0) then
                    do i=1,L
                        do j=1,L
                            if (sigma(i,j)>=sigmac(i,j))then
                                tempi=1
                                stat(i,j)=1
                                minl(1)=i
                                minl(2)=j
                            endif
                        enddo
                    enddo
                    ta=ta+1
                endif
                tempi1=0
            enddo
            ta=1
            i1=i1+wri
            t=t+1
            if(mod(t,100000)==0) print*,t
! Check to see if the system has reached to the time step to start collecting the statistics
            if (t==tsel+1) then
! Open a file for saving the state of the system at the desired time step
                i1=1;xf=0;yf=0;aval=0;asp=0;wri=1;stressr=0.;stressi=0.
                open(11,file='S1-L256-a05br-sd005-n1088-sf10-noi010-c.dat', action='write')
                write(11,'(i3,1x,i3,1x,f6.3)')((i,j,sigma(i,j),j=1,L),i=1,L)
                close(11)
            endif
```

```
! Check to see if the system has reached to the last time step to finish collecting the statistics and exiting
the loop and start to writing the results inside the output file

                if (t==tsel+tlen+1) then

                        print*,'1 ',i1

                        open(22,file='L256-a05br-sd005-n1088-sf10-noi010-c.dat',action='write')

                        write(22,'(i9,1x,i3,1x,i3,1x,i1,1x,f10.5,1x,f10.8)')
                        (aval(j),xf(j),yf(j),asp(j),stressr(j), stressi(j), j=1,tlen)

                        i1=1;xf=0;yf=0;aval=0;asp=0;wri=0;stressr=0.;stressi=0.

                        close(22)

                        print*,'2 ',i1

                endif

                if (t==tsel+tlen+1) exit

        enddo

!*******************************************************************************

! PRINTING RESULTS

        print*, “last time step”,t

! Writing the time that program stops

        call itime(timeArray)

        write(*,'(a13,2x,i2,a1,i2,a1,i2)')" End time",timearray(1),":",timearray(2),":",timearray(3)

        print*,'done'

        end


!*******************************************************************************

! Subroutines for different distributions of asperity sites

! Random distributions

subroutine Br(L,status1)

integer*2 L

integer n0,dummy,i,j,k,status1(L,L)
```

```
real rand
integer*4 timeArray(3)
call itime(timeArray)
print*,"**RANDOM DISTRIBUTION**"
dummy= rand (timeArray(1)+timeArray(2)+timeArray(3))
Status1=0;n0=L**2;k=0
do
        i=L*rand(0)+1
        j=L*rand(0)+1
        do while (status1(i,j)==1)
                i=L*rand(0)+1
                j=L*rand(0)+1
        enddo
        if (status1(i,j)==0) then
                status1(i,j)=1
                k=k+1
                if (1.*k/n0>0.05) goto 55 ! Specifying the percentage of asperities
        endif
enddo
55 continue
endsubroutine
!*****************************************************************************
! B16: 16 by 16 randomly distributed blocks
 subroutine B16(L,status1)
integer L,n0,dummy,i,j,k,m1,n1,m2,n2 ,status1(L,L),ll,temp
real rand
integer*4 timeArray(3)
```

```
call itime(timeArray)
dummy= rand (timeArray(1)+timeArray(2)+timeArray(3))
Status1=0;n0=L**2;k=0;ll=L/256;
print*,"**FIXED ",ll," by ", ll," BLOCK DISTRIBUTION**"
do
        temp=1
        do while (temp==1)
                i=L*rand(0)+1
                j=L*rand(0)+1
                m=i/ll
                n=j/ll
                m1=m*ll
                n1=n*ll
                temp=0
                do m2=m1+1,m1+ll
                        do n2=n1+1,n1+ll
                                if (status1(m2,n2)==1) temp=1
                        enddo
                enddo
        enddo
        do m2=m1+1,m1+ll
                do n2=n1+1,n1+ll
                        status1(m2,n2)=1
                        k=k+1
                        if (1.*k/n0>0.01) goto 55  ! Specifying the percentage of asperities
                enddo
        enddo
```

```
enddo
55 continue
endsubroutine
!*****************************************************************************
! B16C: Cascading distribution
subroutine B16c(L,status1)
integer L,n0,dummy,i,j,k,m1,n1,m2,n2 ,status1(L,L),jj
real rand
integer*4 timeArray(3)
call itime(timeArray)
print*,"**CASCADING DISTRIBUTION**"
dummy= rand (timeArray(1)+timeArray(2)+timeArray(3))
Status1=0;n0=L**2;k=0
do
        i=L*rand(0)+1
        j=L*rand(0)+1
        do while (status1(i,j)==1)
                i=L*rand(0)+1
                j=L*rand(0)+1
        enddo
        jj=8*rand(0)+1
        do m2=i+1,i+jj
                do n2=j+1,j+jj
                        m1=m2
                        n1=n2
                        if (m1>L) m1=m1-L
                        if (n1>L) n1=n1-L
```

```
                    if (status1(m1,n1)==0) then
                        status1(m1,n1)=1
                        k=k+1
                    endif
                    if (1.*k/n0>0.01) goto 55 ! Specifying the percentage of asperities
                enddo
            enddo
        enddo
        55 continue
        endsubroutine
        !*****************************************************************************
        ! B16RC: Random Cascading distribution
        subroutine B16rc(L,status1)
        integer L,n0,dummy,i,j,k,m1,n1,m2,n2 ,status1(L,L),jj,nn
        real rand,rr
        integer*4 timeArray(3)
        call itime(timeArray)
        print*,"**RANDOM CASCADING DISTRIBUTION**"
        dummy= rand (timeArray(1)+timeArray(2)+timeArray(3))
        Status1=0;n0=L**2;k=0
        do
            i=L*rand(0)+1
            j=L*rand(0)+1
            do while (status1(i,j)==1)
                i=L*rand(0)+1
                j=L*rand(0)+1
            enddo
```

```
        nn=0
        rr=rand(0)
        jj=8*rand(0)+1
        do m2=i+1,i+jj
                do n2=j+1,j+jj
                        m1=m2
                        n1=n2
                        if (m1>L) m1=m1-L
                        if (n1>L) n1=n1-L
                        if(m1<0.or.n1<0)print*,'Error'
                        if (status1(m1,n1)==0.and.(nn/(jj**2.)<rr).and.rand(0)<0.5) then
                                status1(m1,n1)=1
                                k=k+1
                                nn=nn+1
                                if (1.*k/n0>0.01) goto 55 ! Specifying the percentage of asperities
                        endif
                enddo
        enddo
enddo
55  continue
Endsubroutine
```

Curriculum Vitae

Name: Javad Kazemian

Post-secondary Education and Degrees:
- The Ferdowsi University of Mashhad
Mashhad, Iran
2000-2005 B.Sc.
- The University of Tehran
Tehran, Iran
2005-2008 M.Sc.
- The University of Western Ontario
London, Ontario, Canada
2009-2013 Ph.D.

Honours and Awards: Western Graduate Research Scholarship
2009-2013

Related Work Experience Teaching Assistant
The University of Western Ontario
2009-2013

Publications:

Kazemian, J., Tiampo, K.F., Klein W. and Dominguez, R. (2013), Foreshock and aftershocks in simple earthquake models. Physical Review Letters. (in review)

Kazemian, J., Dominguez, R., Tiampo, K.F. and Klein W. (2013), spatial heterogeneity in earthquake fault-like systems. Pure and Applied Geophysics. (in review)

Kazemian, R., Tiampo, K.F., Klein, W., Dominguez, R. and Serino, C.A. (2013),. Spatiotemporal clustering in simple earthquake fault models. Journal of Geophysical Research. (in review)